UNIVERSITA' DEGLI STUDI DI PARMA

Dottorato di ricerca in

Scienza e Tecnologia dei Materiali Innovativi

Ciclo XXVII (2012-2014)

Synthesis and characterization of novel nanosystems for biomedical applications

Coordinatore:

Chiar.mo Prof. Enrico Dalcanale

Tutor:

Chiar.ma Prof. Franca Bigi

Dottoranda: **Elena Bedogni**

2015

A mia mamma

e mio nonno

Contents

Introduction

1.1 Nanomedicine

Nanoscience and nanotechnology are now well established scientific and engineering disciplines. This is evidenced by the investments of government funding programs specifically targeting nano-research and development, the proliferation of research journals devoted to *nano* and the massive investment by worldwide research institutions in nanotechnology facilities, infrastructure and personnel.

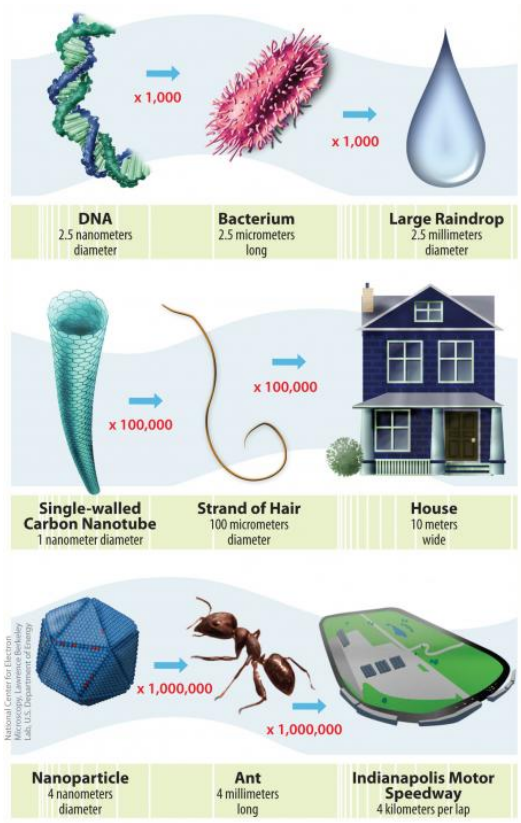

Figure 1 . *Correlation between visual objects and micro- and nano-compounds. Nano is the prefix for the unit that are 10^{-9} m in size. Nanometer is a billionth of a meter (a millionth of a millimeter).* [1,2]

Nanotechnology requires the ability to understand and to precisely manipulate and control nanoscale materials in a useful way. Nanomedicine is emerging as one of the most important sub-disciplines under the nanotechnology umbrella.

Nanomedicine was definite (by the European Science Foundation, ESF) as "the science and technology of diagnostic treating and preventing disease and traumatic injury, of relieving pain, and of preserving and improving human health, using molecular tools and molecular knowledge of the human body". Nanomedicine is defined as the application of nanometer technologies in medical areas (from biomedical imaging to drug delivery and therapeutics). This is a new and fast expanding medical field. The overall goal of nanomedicine is the same as it is for traditional medicine: early and accurate diagnosis, effective treatments that are free of side effects, and *non*-invasive evaluation of the efficacy of the treatment. Nanotechnology is a very broad interdisciplinary research field that involves various areas of science and chemistry. Physics and engineering properties of nanomaterial can change completely if you compare the nanosystem with bulk phenomena. Some of these nanosystems are already appearing in the market place or as clinical trials.

In the world and also in Italy, the interest in nanodevices and nanosystems for biomedical applications is growing rapidly.

1.2 Nanoparticles

Nanoparticles are characterized by an high surface to volume ratio, and the large percentage of surface atoms compared with bulk materials are the results of the small size. Due to their size, the nanodevices (like nanoparticles) can possess properties useful in biomedical field, being in the same range of dimension like nucleus, protein and so on.

There are numerous journals publishing papers dealing with nanoparticles for various applications and many of them are specifically devoted to nanomaterials. Researchers at Rice University have demonstrated that cerium oxide nanoparticles act as an antioxidant to remove oxygen free radicals that are present in a patient's bloodstream following a traumatic injury.[3] The nanoparticles absorb the oxygen free radicals and then release the oxygen in a less dangerous state, leaving free the nanoparticles to absorb more free radicals. Another example is reported by MIT, where nanoparticles are used to deliver vaccine. The nanoparticles protect the vaccine, allowing the vaccine time to trigger a stronger immune response.[4] Other groups are developing ways to use carbon nanoparticles called nano-diamonds in medical applications.[5] For example, nano-diamonds with attached protein molecules can be used to increase bone growth around dental or joint implants. Some other researchers are testing the use of chemotherapy drugs attached to nanoparticles to destroy the cancer cells. [6]

In according with the chemical composition, the nanoparticles can have powerful properties like imaging for in vivo analysis or in vitro test. The presence of receptors or smart molecules makes possible to use this nanosystems for obtaining diagnostic responses as well as the presence of specific drugs, makes possible to apply the therapy in a local and specific area. In recent years a new generation of very efficient nanoparticles allowed to create multifunctional systems that have bonded together different functional groups. For *in vitro* and *in vivo*

applications in biomedical field, nanoparticles have to possess the following features:

- small overall size,
- high surface area for a specific functionalization,
- high colloidal stability,
- capacity to cross the cell walls in order to enter the cells and then perform their function
- *non* toxicity,
- *non* immunogenicity,
- capable to stay in solution for long time.

Therefore, we can conclude that for biomedical application the aim is to obtain multifunctional nanoparticles with a narrow size distribution, non-aggregated and stable for long time in biological media.

Nanoparticles can have different applications[7] according with the crystal structure, the shell composition, the shape and size. The performance as drug delivery system has been improved enormously because of the development of controlled release of drugs under some specific stimulation (changing pH, light, temperature, presence of specific substances…).

The development of targeted delivery possible to release the drug just inside the specific area of the body). In order to further improve the drug delivery process, some crucial properties of the free drugs such as solubility, *in vivo* stability, pharmacokinetic, and bio distribution must be considered. The overall efficacy can be improved by using suitable nanoparticles carrying drug with increasing selectivity toward the targeted tissue.

Different types of molecular imaging techniques, such as optical imaging (OI), magnetic resonance imaging (MRI), ultrasound imaging, positron emission tomography (PET), and others are used for the imaging of both *in vivo* and *in vitro* biological specimens. However, optical and magnetic resonance imaging techniques are the most acceptable because they utilize the inherent luminescent and magnetic properties of nanoparticles. Some other applications are in sensor field. Sensor is a device that measure a physical quantity and converts it into an analog or digital signal that can be read by an instrument. In *in vivo* applications, nanoparticles are also used like a sensor for the detection of damaged cells, DNA, RNA, glucose, cholesterol …

A magnetic material coated with a fluorescence material can also be used as sensor. Here the fluorescence dye tracks the particle location, whereas the magnetic core serves to transfer heat at that position via magnetic excitation.

Nanoparticles coated with a functional material such as a noble metal, semiconductor, or appropriate oxide have increased the physical properties (optical, catalytic activity, electrical, magnetic and thermal) of the combine particles compared with the pure core particles.

Among the nanoparticles, superparamagnetic ones properties have been intensively developed not only for their fundamental scientific interest

but also for many technological applications, such as target in drug delivery[8], as contrast agent in magnetic resonance imaging (MRI)[9] and also as magnetic inks for jet printing[10]. The control of the size and dispersal is very important since the properties of the nanocrystals strongly depend upon the dimension of the nanoparticles.[11] Superparamagnetic iron oxide nanoparticles depending on the surface modification can be used for numerous in vivo applications, such as MRI contrast enhancement, tissue repair, detoxification of biological fluid, immunoassay, cell separation, hyperthermia and drug delivery. All these techniques require magnetic nanoparticles with large magnetization value, size smaller than 100 nm and narrow size distribution. These applications also need peculiar surface coating of the magnetic particles, which as to be *non* toxic and biocompatible, allowing also a targetable delivery with particle localization in a specific area. Magnetic nanoparticles binding drugs, proteins, enzymes, can be directed toward an organ, tissue, or tumor using an external magnetic field.

Another sector of application is the environmental field. Besides treatment of exhausts mono particulate catalysts are employed in waste water treatment. For example Pd-Fe_3O_4 composite catalyst was used for environmentally friendly treatment of AOX polluted substance (AOX: absorbable organically bound halogens). In China Feng et al.[12] are studying the adsorption of ions in exhaust water using magnetic nanoparticles coated with specific functional groups. Among the various superparamagnetic nanoparticles, magnetite displays the best magnetic properties.

In particular, the project developed in the present work is combine the hyperthermia properties of Fe_3O_4 nanoparticles with the photodynamic properties of a photosensitizer for a bimodal treatment of cancer. Aiming to prepare a single nanosystem able to display both properties for deep cancer treatment, the functionalization of cubic SiC/SiO_2 nanowires with Fe_3O_4 nanoparticles and with porphyrins was studied.

There are different ways to synthesize Fe_3O_4 nanoparticles. The first one was the co-precipitation method described by Massart et al.[13] , that

starts from salts of iron (III) and iron (II) in a stoichiometric ratio and heated under basic condition. The nanoparticles obtained by this method are not well stabilized, since the stabilization come only from the OH ion on the surface.

Indeed usually they form aggregates (Fig. 2) that for biomedical application are unwanted.

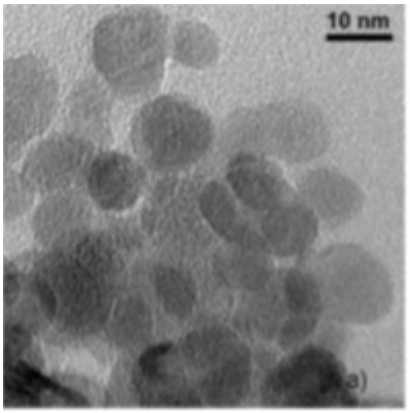

Figure 2. *TEM picture shows the magnetic nanoparticles obtained by co-precipitation method.*

Other two synthetic routes are microwave and thermal decomposition method. The last one is the method that I used, and it will be described in details in the second chapter.
Microwave method is a new and efficient method that starts from the same precursors, such as $Fe(ac)_x$ or $Fe(acac)_x$ employed in thermal decomposition. Being very energetic conditions, the reaction takes a very short time. The critical point could be the very fast reaction which often determines a *non*-good crystallinity.
Magnetite has the following composition Fe_3O_4 and has an inverse spinel crystal structure. The 32 O^{2-} ions have a cubic close packing (ccp) with an ABCABC stacking. The anions packing gives rise to two different interstitial sites: tetragonal and octahedral sites. The spatial crystal group is Fd3m and the unit cell dimension is 0.8369 Å (Fig. 3).

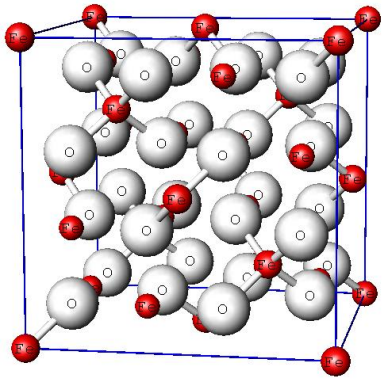

Figure 3. Magnetite crystal structure: ccp of oxygen anions (white balls) with Fe^{2+} Fe^{3+} (red balls).

The tetrahedral sites are occupied by Fe^{3+} cations while the octahedral are occupied by both Fe^{2+} and Fe^{3+} randomly distributed. The inverse spinel structure can be written as **Y [XY]O_4** where X = Fe^{2+} Y = Fe^{3+} and the brackets indicate octahedral sites.

Below the Curie temperature T_C= 850 K, magnetite is ferromagnetic material

This material is also characterized by a structural transition (**Verwey transition**) as a function of temperature. The first observation of this phase transition was observed by Renger in 1913 on a synthetic polycrystal, measuring the initial susceptibility as a function of temperature. The first electric measurements as a function of temperature, in which the evidence of a change in resistivity was observed, were done by Okamura[14] and Verwey[15]. They observed a variation of resistivity by about a factor of 100 at the critical temperature $T_V \approx 125K$ (Verwey transition temperature). At the beginning no structural transition was identified by XRD and only later the crystal structure was solved[16]. Verwey explained the variation of all the structural parameters considering that

1. above T_V, the Fe^{2+} and Fe^{3+} ions are randomly distributed over the B-sites, permitting relatively easy valance exchange by means of thermally activated fast electron hopping

$$Fe^{2+} - e \rightleftharpoons Fe^{3+}$$

2. below the critical temperature, there is a reduction of the crystal symmetry from cubic to tetragonal and the charges order in a way that successive, a/4-spaced (100) lattice planes would be occupied, alternatively, by ferric and ferrous ions.

In this way, above the Verwey transitions the electronic conduction is described by a thermally activated hopping process between the ferrous and ferric ions in the octahedral lattice sites, and their random distribution gives rise to an isotropic conductivity[17].

Superparamagnetism of nanostructured material

The magnetic properties of nanomaterials strongly depend on the size as show in *figure 4*.

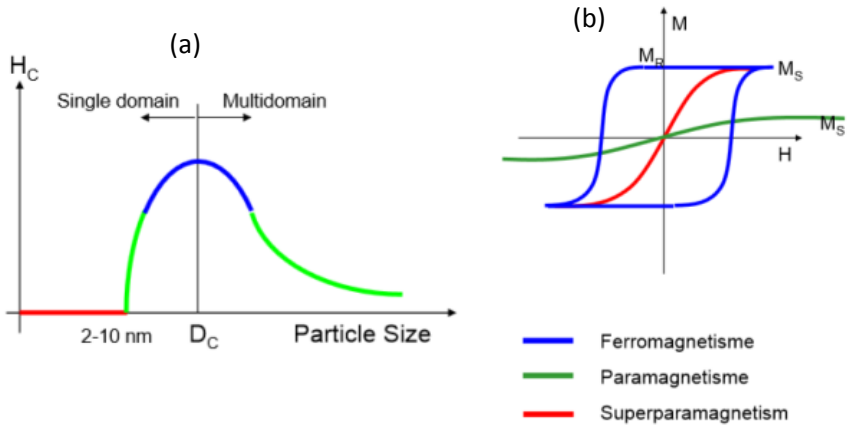

Figure 4. *(a) Coercivity as a function of the particle sizes and (b) typical hysteresis loop shape for systems showing superparamagnetic (red), paramagnetic (green) and ferromagnetic (blue) properties.*

For our purpose, we need nanoparticles in the superparamagnetic state. Superparamagnetism arises only in systems constituted by very small nanoparticle sizes, smaller than 20 nm in the case of Fe_3O_4. In this regime, the magnetic moments are randomly distributed and can randomly flip their direction under the influence of temperature. The

typical time between two flips is called the Néel relaxation time. In the absence of external magnetic field, when the time used to measure the magnetization of the nanoparticles is much longer than the Néel relaxation time, their magnetization appears to be in average zero. In this state, an external magnetic field is able to magnetize the nanoparticles, similarly to a paramagnet. However, their magnetic susceptibility is much larger than the one of paramagnets. Only below a critical temperature called blocking temperature TB, the magnetic moments are blocked, and the thermal energy becomes unable to affect the system. A magnetic order establishes giving rise to ferromagnetic properties.

The equation that describes the relation between magnetization and magnetic field is:

$$\vec{M} = Xm \cdot \vec{H}$$

where $\vec{M}$ is the magnetization, $\vec{H}$ the magnetic field and Xm the magnetic susceptibility, a positive number which increases decreasing the temperature.

Another relation is:

$$\vec{H} = \frac{\vec{B} - \mu_0 \vec{M}}{\mu_0}$$

$$\vec{B} = \mu_0 \vec{H}\,(1 + Xm) = \mu \vec{H}$$

Where μ is the magnetic permeability.
Superparamagnetic materials are characterized by two important properties:

- high saturation magnetization M_S
- no remanence M_R (value of the magnetization in sero applied magnetic field).

The superparamagnetic property depends from the size of nanoparticles. This property is manifested in magnetite nanoparticles only under the limit of 20 nm. Over this critical size, the magnetization curves show an hysteresis, with a non-zero remanence and coercivity .
On the other hand, for size much lower than this critical size the magnetization becomes too low and in some case it is almost impossible to catch up. In our case the goal is to achieve a high value for saturation magnetization remaining below the limit imposed by superparamagnetism.

Magnetic hyperthermia

One of the most interesting application of superparamagnetic nanoparticles (MNPs) is the magnetic hyperthermia. MNPs are mediator of heat transfer when a radio-frequency magnetic field is applied. When an alternate magnetic field is applied many phenomena occur:

(i) the spins rotate inside the nanoparticle, and this internal friction generates heat which is transferred outside by way of thermal conductivity,
(ii) because of the coupling between the magnetic moment and the particle, the particle itself starts to rotate with respect to the matrix, generating a deformation around the particle and heat is produced as a consequence of viscous dissipation..

The local tissue temperature has to be higher than 42°C but lower than 47°C for almost 30 min., to destroy cancer cells, while the healthy cells are less affected. The product of applied field and frequency has to be lower than 4.85 10^8 A/ms.[18] These parameters have to be controlled because of peripheral and skeletal muscles, possible cardiac stimulation and arrhythmia and *non*-specific inductive heating of tissue. Therefore frequencies and amplitudes must be f = 0.05-1.2 MHz and H=0-15 kAm^{-1}.[19] The nanoparticles can be directly injected in tumor or can be injected through intravascular administration or antibody targeting. This method isn't efficient enough when applied alone[20], even if for certain types of cancer, it is more suitable than the conventional treatments of radiotherapy and chemotherapy; in particular when the tumor is located close to vital organs or is drug resistant. Sometimes it is used together with chemotherapy, in fact below 42°C, it doesn't directly cause cell death but can increase the effect of certain chemotherapy drugs that are more active at higher temperatures, and in this way a lower dose is required.

Radiotherapy can also be used with hyperthermia[21]. The ability of a magnetic material to be a hyperthermic mediator depends on many different parameters and the mechanism of heating is not well understood it can be due to losses in a hysteresis cycle, susceptibility loss, or frictional heating due to particle rotation in a liquid environment.

When a magnetic moment is exposed to a field there exists a magneto static energy and in order to reduce its magneto static energy it rotates to align with the field. If low field strength is applied at a high frequency the moment can't follow the field and heat is generated due to this phase lag and also to frictional effects.

If we consider multi domains MNPs, the effects of heat transfer are related to the mechanism of hysteresis loop, as well movement. The amount of heat generated per unit volume P_{FM} is given by frequency of multiplied by area of hysteresis loop:

$$P_{FM} = \mu_0 f \oint H \, dM$$

For ferromagnetic particles well above the super-paramagnetic size limit the P_{FM} can be approximately determined from *quasi* static measurements of the hysteresis loop. The orientation and growth of spontaneously magnetized domains within a given ferromagnetic particle depends on both microstructural features such as vacancies, impurities or grain boundaries, and intrinsic features such a magneto-crystalline-anisotropy as well as the shape and size of particles. If we consider instead single domain nanoparticles near to super-paramagnetic size we can identify two mechanisms: hysteresis loses, relaxation of magnetization when an alternating field is applied leads to a frequency dependence of hysteresis loss. The remanence and the coercivity increase at high sweep-rate, increasing loop squarenes [222324] and the hysteresis losses are proportional to the square of the frequency. At high frequency, in fact, some nanoparticles are not in super-paramagnetic state. Therefore we can conclude that frequency of the alternating applied field is an important parameter in controlling the amount of heat produced from hysteresis losses. Another mechanism of

release of heat is the physically rotation of particles in order to align their moments with an applied field. It is called Brownian relaxation and depends on hydrodynamic volume of nanoparticles, V_H, on the solvent viscosity η and on temperature T:

$$\tau_B = \frac{3\eta\, V_H}{K_B \Gamma}$$

Where $\Gamma = KV_M/(kT)$. The other mechanism of relaxation of magnetization is the Nèel relaxation that is due to the thermal fluctuation of magnetization at a given temperature. [25]

$$\tau B = \frac{\sqrt{\pi}}{2}\tau_0 (expT)/T^{\frac{1}{2}}$$

For both relaxation times there is a dependence from volume and therefore from of the MNPs size. The particles suspended in a colloidal Ferrofluid have a reduced heating when Brownian relaxation is prevented, but when injected into a tumor the ability of the particles to move freely will be reduced and Brownian losses are unable to contribute to the heating. For non-interacting magnetic nanoparticles in a single domain state, we can describe the power dissipation through the model of Rosensweig). An optimum particle size exists at which corresponds the maximum power heating, independently from the applied field intensity. The critical size strongly depends on the material of nanoparticles, being due mainly to the anisotropy constant, an intrinsic property. Another mechanism of heating is the presence of eddy currents. The electrical conductivity of the particles induces eddy currents at the surface of the particles when an alternating field is applied, producing heat due to the resistance of the material. . The eddy currents have been shown to be negligible for small particles (less the 100 nm in diameter) if the frequency of the alternating field is also less the 10 GHz.

Other characteristics influence the heat rate, i.e. MNPs size distribution, the surface functionalization[26,27,28,29], the anisotropy and the

interactions, the ferrofluid parameters as well as the concentration of nanoparticles in solution and the solvent properties.[30]

The heating capacity of a magnetic material is quantified through the specific absorption power rate (SAR), defined as the amount of energy converted into heat per time and per mass. The following equation describe SAR:

$$SAR = Cs\frac{\Delta T}{\Delta t}$$

where Cs is the sample heat capacity (that is specific for each sample).

1.3 Nanowires

In the last decade nanowires became really important in different fields, such as mechanics, electronics and in nanomedicine. Several nanosystem are being studied. Such as carbon nanotubes (single-walled and multi-walled). Metal nanowires (e.g. based on gold, iron and silver), semiconducting nanowires (e.g. silicon, GaN and other III-V nanowires), and oxide nanowires (e.g. ZnO, SiO_2, and TiO_2). Further, SiC nanowires are being studied as neuronal probes for their cytocompatibility and better performances respect to other materials.[31]
During my PhD thesis work I developed some methods to functionalize core-shell SiC/SiO_x nanowires, supplied by the IMEM-CNR Institute of Parma, where they were grown and characterized. These nanowires are composed by core of cubic silicon carbide and shell of silica, as well evidenced in Figure 5.
The technique employed for the preparation of the nanowires is called chemical vapour deposition (CVD) and consists in the growth of the nanowires on a silicon substrate, without removing the native oxide and in the presence of metal catalysts. In this technique, the substrate is pre-treated with an iron salt, then exposed to a stream of CO mixed with N_2 and Ar as carrier gas. The growth of the nanowires is catalyzed by the iron and occurs at temperatures between 1050-1100 °C. During this time, the carbon monoxide diffuses across silica and at the interface between SiO_2 and Si. Where the following carbothermic reaction between CO and Si occurs:

$$4\ CO\ (g) + 6\ Si\ (s) = 4\ SiC(s) + 2\ SiO_2$$

In agreement with the preferential mechanism of nucleation at the interface vapor-liquid (VLS), the formation of a dense forest of nanowires SiC/SiO_2 can be observed. The nanowires obtained were characterized by various analytical techniques, including transmission electron microscope, cathodoluminescence, X-Ray and Raman spectroscopy. The results confirm that the nanowires actually have a structure “core-shell”, with a core of about 15-20 nm and a coating of approximately equal thickness, for total diameter of about 60 nm.

In our project, I developed methods of functionalization, , of core-shell nanowires, exploiting different materials. The system produced at the IMEM-CNR of Parma is composed by a core of silicon carbide SiC and a shell of silica SiO_2 as reported in Figure 5.

As reported by Fabbri et al.[32], SiC is biocompatible[33],[34] and can be of great interest for biomedical applications, in particular if functionalized with specific organic macromolecules like porphyrins (described later). This core-shell inorganic-organic system can create an active anticancer device when excited by energetic X-Ray radiation. The energy associated to this radiation activates the green emission of SiC in its cubic phase, which in turn determines the production by phorphyrins of the singlet oxygen, the best cytotoxic agent produced in photodynamic therapy (see next paragraph)[35],[36].

Fabbri et al.[37] observed that the silica shell improved the emission of the SiC core.

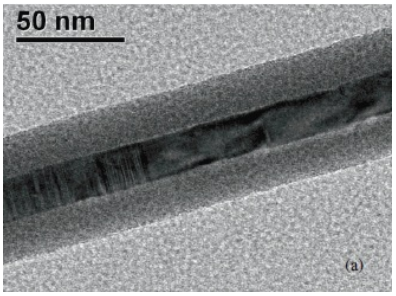

Figure 5. *Zero-loss image of core-shell nanowire by TEM*

They proposed a model to explain why the presence of the silicon dioxide shell increases the radiative recombination in the silicon carbide core. A type I band alignment of 3C-SiC and SiO_2 can be hypothesized. The conduction and valence band offsets have been experimentally found in the case of bulk material[29] and they are equal to ΔE_c= 3.6 eV and ΔE_v= 2.9 eV, respectively as reported in *Figure 6*. The carriers generate by the electron beam in the shell diffuse into the core, where it can recombine according to the allowed transitions in

3C-SiC. No effects are observed in the energy transfer from the shell to the core.

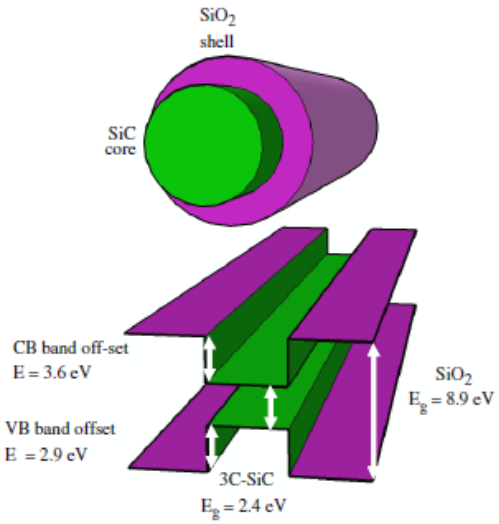

Figure 6. *Sketch of the type I band alignment between 3C-SiC and SiO_2. Fabbri et al. model*

The diffusion of the carriers could be considered as an energy transfer from the shell to the core (it was the first time that this effect was observed in NWs).

In this type of NWs the shell is beneficial in enhancing the luminescence intensity of the crystalline core, preferentially the SiC NBE radiative recombination. In the model's figure (*Figure 6*) the quantum confinement effect depends from the size core of SiC.

1.4 Porphyrins and photodynamic therapy

Porphyrins and related macrocycles provide an extremely versatile synthetic base for a variety of material applications. The exploration of metal porphyrins assemblies as building blocks for tailored material properties has grown rapidly during the past decade. The *non*linear optical properties of these materials are of special interest, also for potential applications in optical communications, data storage, and electro-optical signal processing. Porphyrins are extensively employed as photosensitizers in photodynamic therapy for the treatment of superficial tumors, and new structures of porphyrin are being proposed to improve their properties and to use more penetrating radiation. During my thesis I synthesize porphyrins as photosensitizers and prepared new hybrid nanosystems conjugated with porphyrins for possible photodynamic therapy.

It's due a briefly explanation of the activity of this type of molecules. Singlet oxygen generated by the photosensitizer from molecular triplet oxygen is the principal toxic species formed during PDT, although the extent to which these species are responsible for the photodynamic effect is under debate. Nevertheless, the generation of singlet oxygen is extremely crucial to the success of PDT, and one of the first tests performed on new PDT drugs is to probe their ability for singlet oxygen generation.[38,39] Figure 7 shows the modified Jablonski's diagram for a typical photosensitizer.

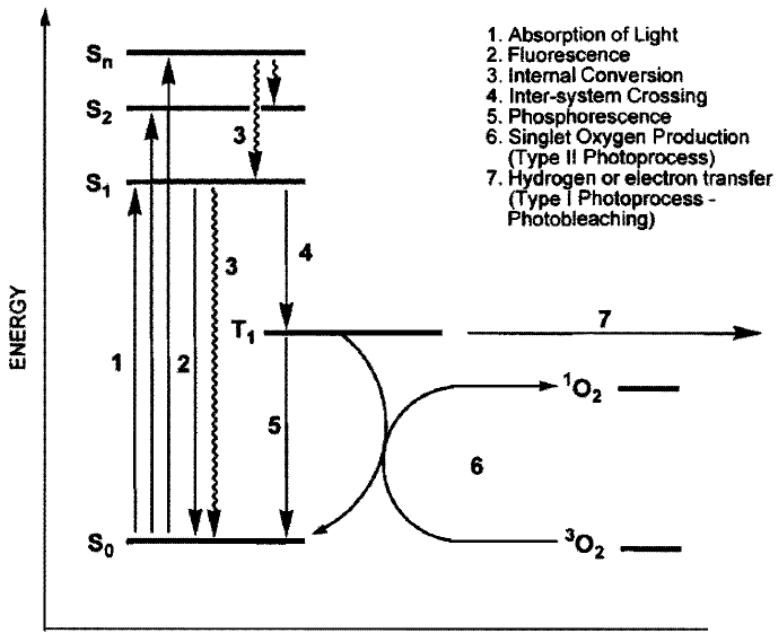

Figure 7. *Modified Jablonski diagram for a typical photosensitizer*

Of particular importance with regard to PDT is that the excited photosensitizer can undergo the *non*-radiative process of inter-system crossing. This is a spin-forbidden process which requires spin inversion, thereby converting the photosensitizer to a triplet state.

Any "forbidden" pathway is less likely than an "allowed" process, but a good photosensitizer undergoes the "forbidden" ISC pathway with very high efficiency. The molecule can relax from the triplet via at least two pathway: radioactively by fluorescence, and non-radioactively by spin exchange with another triplet state molecule.

Fluorescence involves a spin-inversion which is also spin-forbidden, and imposes a relatively long lifetime of the triplet state, on the microsecond time scale. This allows the interaction between molecules close to the excited photosensitizer. One interaction is spin exchange (also corresponding to energy transfer) with triplet oxygen, which generates the highly reactive singlet oxygen species, one of the most

reactive species having a lifetime in water of roughly four microseconds. It undergoes several reactions with biological substrates such as oxidation or cycloaddition or a kind of reactions that are disruptive to biological processes. An important photophysical property is represented by the efficiency of transferring the energy of the absorbed light from the triplet state of the photosensitizer to the triplet oxygen with the consequent generation of singlet oxygen, defined also as the singlet oxygen quantum yield.

There is only an indirect evidence for the production of singlet oxygen in a biological system since the lifetime of singlet oxygen is so short that cannot be observe directly. The application of light is of primary importance to the efficacy of PDT. Like the number and the types of photosensitizer compounds have been increasing over recent years, also the variety of light sources were considerably increased.

The basis of the structure of porphyrins skeleton is formed by four pyrroles linked with four methine bridges (Fig. 8).

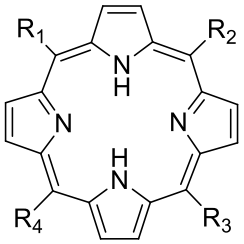

Figure 8. *Porphyrin ring*

Porphyrins (from the Greek means purple, scarlet) are based on 16 – atom rings containing four nitrogen atoms. They are macro cycles that contain only sp^2-hybridized bridging meso carbon atoms within their framework. The structure is fully aromatic, contains 18 π-electrons. They are in a perfect size to bind nearly all metal ions.[40]

By substitution of hydrogens in the *meso*-position with some substituents, complex porphyrins can be obtained. Depending on the synthesis, the substituents in the *meso*-position can either be the same or different. The basic porphyrin skeleton can be synthesized by several routes based on condensation reactions between aldehydes, pyrroles,

dipyrromethanes or similar precursor under acidic conditions and subsequent oxidation. Symmetric porphyrins are more easily synthetized than asymmetrical ones. Their synthesis is based on a condensation of pyrrol and aldehyde with different reaction conditions (like *Adler-Longo conditions*).[41] The first prepared symmetrical porphyrin had four phenyl substituents in meso-positions.

On the other hand, the asymmetrical porphyrins are much less synthetically accessible. Their preparation is based on various approaches (like a Adler-Longo conditions or 2+2 approach, 3+1 approach and so on). The first time that the activity of porphyrins was found to be useful in the photodynamic therapy was in 1913, when Meyer Betz injected himself with 200 mg of hematoporphyrin and registered no ill effects until he exposed himself to sunlight, whereupon for several months he suffered extreme swelling. The most recent photoactive based drug therapy utilizes phorphyrin-based chromophores in combination with visible light. Phototherapy was dormant for several decades, although the idea that light could be a therapeutic modality was well explored. Photodynamic therapy (PDT), a new treatment modality, involves administration of a tumor-localizing photosensitizing agent (PS) followed by activations of the agent by light of a specific wavelength. This result in a sequence of photochemical and photobiological processes that cause irreversible photodamage in tumor tissues. The hallmark of PDT is intracellular oxidative stress mediated by reactive oxygen species. In order to achieve the most efficient photosensitizer effect in tumor cells, two are the possibilities, the sensitizer must enter the cells or it has to become closely associated with the subcellular structure. Photosensitizer may enter cells either directly through the plasma membrane or by endocytosis. Uptake over the plasma membrane may occur by simple or facilitated diffusion or by an active transport mechanism. Cancer cells, in common with other rapidly proliferating cells, may have an increased requirement of cholesterol for membrane biosynthesis. They may therefore upregulate the expression of the low-density lipoprotein (LDL) receptor. It is know that lipoproteins are major carriers of

lipophilic porphyrins in the bloodstream and may therefore be a means of entry of these compounds into cells.
A decreased intra tumor pH may affect the ionization of porphyrin species, reducing in this way the activity of PDT.
Tumors contain increased numbers of lipid bodies and particularly neutral lipid droplets; in addition their cell membranes may be more hydrophobic than those of normal cells.
A combination of "leaky" tumor vasculature and reduced lymphatic drainage might encourage the build-up of porphyrins in the interstitial space. In tumors cells can increase capabilities for phagocytosis or pinocytosis, this effect can became dangerous for porphyrin aggregates and nanosystem.
The porphyrin can have different R-groups (F*igure 8*). In my case I worked with *meso* porphyrin and asymmetric ones in order to examine different rings and different symmetry.
Figure 10 I explains the steps of photodynamic therapy starting from the transport of sensitizer inside the human body, then the distribution inside the specific tissue, and the differential clearance tissue. After that there is the excitation to the photosensitizer and consequently the chemical and biological damage with cells and tissue necrosis.

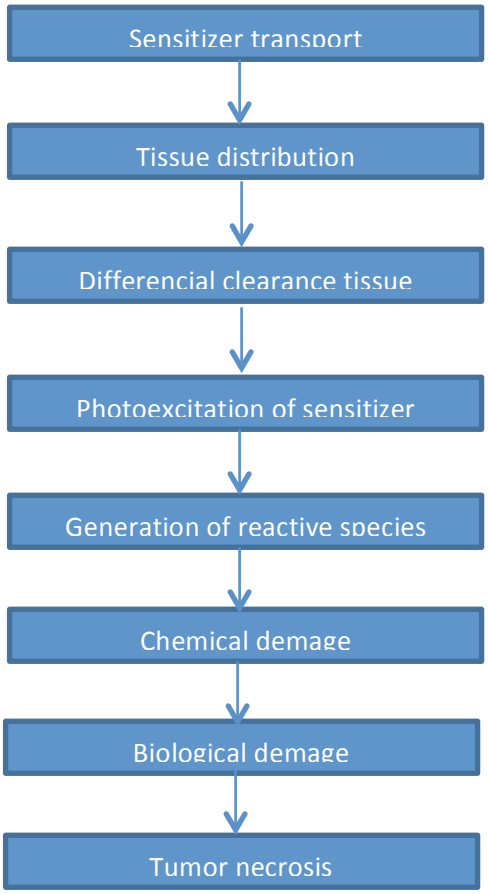
Sensitizer transport
Tissue distribution
Differencial clearance tissue
Photoexcitation of sensitizer
Generation of reactive species
Chemical demage
Biological demage
Tumor necrosis

Figure 10.

1.5 BioNiMed

The aim of my thesis is to synthetize nanosystems for biomedical applications, in particular for anticancer therapy.

The idea and research funding come from a project called BioNiMed, written by Dott. G. Salviati of the IMEM-CNR Parma. The final aim is the synthesis of nanosystems constitued by core shell SiC@SiO_x nanowires decorated with porphyrins and Fe_3O_4 nanoparticles and. The final system, combining the properties of the MNPs and porphyrins, could be suitable both for the photodynamic and the hyperthermia therapy.
The aim of my PhD thesis was the preparation and characterization of hybrid nanosystems for application in nanomedicine, with particular interest to the possible anticancer therapies. The anticancer effect can be induce by the magnetic hyperthermia therapy using magnetite nanoparticles and the photodynamic therapy induced by a irradiation of a specific system by X-rays. For increasing the efficiency of the hyperthermia therapy, we developed also core shell nanoparticles, able to encapsulate and release drug thanks to the mesoporous shell. This part of the work was done in Functional Nano Meterial (FNM) group in Stockholm (Sweden) under the supervision of Professor M. Toprak and Professor M. Mohamed at KTH, Royal Institute of Technology.
Thanks to the collaboration with Mutti's and Petronini's group at University of Parma, the systems were also characterized from the biological point of view, we perform *in vitro* study for the evaluation of the activity and biocompatibility of the system.

References

[1] http://www.nano.gov/nanotech-101/what/nano-size

[2] Charles R M., Welcome to Nanomedicine, *Nanomedicine* 1 (1), 5-5(**2006**)

[3] S. S. Lee, W. Song, M Cho, H. L. Puppala, P. Nguyen, H. Zhu, L. Segatori, and V. L. Colvin *ACS Nano*, **2013**, *7* (11), 9693–9703

[4] D. J. Irvine, M. A. Swartz, and G. L. Szeto; *Nat Mater*.; 12(11): 978–990 (**2013**)

[5] L. Moore, M. Gatica,H. Kim, E. Osawa, and D. Ho; *J Dent Res*.; 92(11): 976–981. (**2013**)

[6] I. Rivkin, K. Cohen, J. Koffler, D. Melikhov, D. Peer, R. Margalit. *Biomaterials*, 31 (27): 7106 (**2010**)

[7] C. R. Ghosh , S. Paria *Chem. Rev*., 112, 2373-2433 (**2012**)

[8] T.K Jain, M.A. Morales, S. F. Cheng, S. Bounnak, *Appl. Phys. Lett*., 81, 2211 (**2002**); I. Chourpa, L. Douziech-Eyrolles, J.F. Ngaboni-Okassa. S. Cohen-Jonathan, M. Source, H. Marchais, P. Dubois, *Analyst* 130(10), 1395 (**2005)**

[9] J. W. Bultè, *Methods Mol. Med*. 124, 419 (**2006**), M. Modo, J. W. Bultè, *Mol. Imaging* 4 (3), 143 (**2005)**

[10] S. W. Charles, J. Popplewell, *J. Endeavour*, 6, 153 (**1982**)

[11] S. Laurent, D. Forge, M. Port A. Roch, C. Robic, L. Vander Elst, and R. N. Muller Chem. Rev., 108, 2064-2110, (**2008**)

[12] L Feng, M Cao, X Ma, Y. Zhu, C. Hu*; Journal of Hazardous materials* 217-218 439-446, (**2012**)

[13] Massart, R. J., "Preparation of magnetite nanoparticles", *IEEE Trans Magn*., 17, 11247-11250 (**1981**)

Bee, A., Massart, R., Neveu, S., *J. Magn. Magn. Mater*., 149, 6-9 (**1995**)

[14] B.S. Ellefson, N.W: Taylor *J.Chem. Phys*., 2:58, (**1934)**.

[15] E.J.W. Verwey. *Nature*, 144:327, (**1939)**

[16] W.H. Bragg. *Nature*, 95:561, (**1915)**

[17] F. Walz. *J. Phys.: Condens. Matter*, 14:R285, (**2002**)

[18] W.J. Atkinson, I. A. Brezovich, D. P. Charaborty IEEE Trans. *Biomed. Eng*., 31:70, (**1984**)

[19] Q. A. Pankhurst**,** J. Connolly, S. K. Jones, and J. Dobson. *J. Physic. D: Appl. Phys.,* 36:R167, (**2003**)

[20] B. Hildebrandt, P. Wust, O. Ahlens *Crit. Rew. Oncol. Hematol.*, 43:33, (**2002)**

[21]K. Maier-Huff et al. *Int. J. Neuroncol.* , 241;317, (**2011**)

[22] R. W. Chantrell, G. N. Coverdale, and K. O'Grady *J. Phys. D: Appl. Phys.*, 21:1469, (**1988**)

[23] **M. El-Hilo,** A. M. de Writte, K. O'Grady, and R. W. Chantrell,. *J. Magn. Magn. Mater.*, 117:307, (**1992**)

[24] A. M. de Witte, M. El-Hilo, K. O'Grady, R. W. Chantrell, *J. Magn. Mater.*, 120: 184, (**1993**)

[25] Nedelcu G. Mangetic nanoparticles impact on tumoral cells in the treat- ment by magnetic fluid hyperthermia. Digest Journal of Nanomaterials and Biostructures Vol. 3, No. 3, (**2008)**

[26] R. Hergt; S. Dutz, M. Roder *J. Phys.: Condens. Matter,* 20:385214, (**2008**)

[27] G. Goya, Jr. E Lima, A.D. Arelaro, T. Torres, H. R. Rechenberg, L. Rossi, et all *EEE Trans. On Mag.*, 44:4444, (**2008**)

[28] M. A. Gonzalez-Fernandez, T.E. Torres, M. Andre ´s-Verge ´s, R. Costo, P. de la Presa, C.J. Serna, et al. J. *Sol. State Chem.*, 182:2779, (**2009)**

[29] G. F. Goya, R. Fernandez-Pacheco , M. Arruebo , N. Cassinelli and M. R. Ibarra, *J. Magn. Magn. Mater.*, 316, 132 -135 (**2007**)

[30] E. Lima Jr, E. De Biasi, R. D. Zysler, M. V. Mansilla, M. L. Mojica-Pisciotti, T. E. Torres, M. P. Calatayud , C. Marquina • M. R. Ibarra • G.F. Goya, *J Nanopart Res* 16:2791 (**2014**)

[31] C.L. Frewin, C. Locke, S.E. Saddow,E:J: Weeber; *Silicon Carbide Biotechnology*, Inc. E., Ed., 209-256 (**2012**)

[32] F. Fabbri, F. Rossi, G. Attolini, G. Salviati, S. Iannotta, L. Aversa, R. Verucchi, M. Nardi, N.Fukata, B. Dierre and Takashi Sekiguchi Nanotechnology 21 345702 (**2010**)

[33]G. Colletti, M J Jaroszeski, A. Pallaoro, A.M. Hoff, S. Iannotta and S. E. Saddow, Proc. 29th Annu. Int. Conf. IEEE EMBS vol 5849 (**2007**)

[34] G. Cicero, A. Catellani and G. Galli. **93** 016102 *Phys. Rev.Lett* (**2004**)

[35] R. R. Allison, G. H. Downie, R. Cuenca, X. H. Hu, C.J.H. Childs, C.H. Sibata, *Photodiag. Photodyn. Therapy* 1 27-42 (**2004**)

[36] Chen W. and Zhang J., *J. Nanosci. Nanotechnol.* 6 1159-66 (**2006**)

[37] F. Fabbri, F. Rossi, G. Attolini, G. Salviati, S. Iannotta, L. Aversa, R. Verucchi, M. Nardi, N.Fukata, B. Dierre and Takashi Sekiguchi Nanotechnology 21 345702 (**2010**)

[38] Ethan D. Stenberg, David Dolphin, *Tetrahedron* 54 4151-4202 (**1998**)

[39] Van Lier, J. E. in *Photobiological Techniques*, 216, 85-98 (**1991**)

[40] V. Kral, J. Kralova, R. Kaplanek, t. Briza, P. Martasek, *Physiol. Res.* 55, S3-S26, (**2006**)

[41] H.I. Adler, W.D. Fischer, A. Cohen, A.A. Hardigree *Proc.Natl.Acad.Sci.USA* 57:321-326 (**1967**)

Synthesis and characterization of superparamagnetic Fe_3O_4 nanoparticles

Introduction

Small magnetic nanoparticles (MNPs) in the super-paramagnetic state are suitable for both the diagnostic and the therapeutic approaches. In the field of diagnostics, they have been proposed as a contrast agent to enhance the magnetic resonance imaging (MRI) signal while in the field of therapeutics they can be used as magnetic vector in drug delivery and/or as heat mediators in hyperthermia treatment.
Hyperthermia properties and drug delivery are of particular interest. In order to be superparamagnetic the particles need to be small (diameter minor than 20 nm), but hyperthermia increase with the size.
The magnetic hyperthermia can be effective on cancer cells, as a consequence of their increased sensitivity to temperature higher than 41°C in comparison to healthy ones. Hyperthermia consists in the application of a magnetic radiofrequency field to the magnetic nanoparticles. The ability of a material to be a good hyperthermic mediator is measured by the specific absorption rate (SAR) that represents the thermic power developed by the MNPs per mass unit. In order to increase the efficiency of the hyperthermia treatment, the SAR value has to be maximized leading to a desired increment of temperature at low doses of MNPs and at lower frequencies and fields. The actual work of scientific community for the achievement of this aim is being developed in three different ways: the choice of material, the optimization of the size and the change of shape. The choice of the material is driven by the requirements on the magnetic crystalline anisotropy, an intrinsic parameter tunable by composition and structure, which influences the hysteresis loop shape and consequently the SAR value. In MNPs, the maximization of hyperthermia effect is observed in proximity of the critical size for the super paramagnetic to the ferromagnetic transition. This value depends on the crystalline anisotropy: higher is the anisotropy value, smaller is the critical size.
At the same time, also the variation of the shape can produce an increase of the magnetic anisotropy by adding two *non*-negligible terms, the shape anisotropy directly related to the shape of MNPs and

the surface anisotropy, due to the dead layer of surface spins aligned perpendicular to the surface, which is influenced by the faceting of the MNPs.

Another factor that influence the hyperthermia is the nature of the NP stabilizers and coating. In the present chapter, I report the synthesis of magnetite nanoparticles obtained using different methods.

I tried different synthetic procedures in order to find the better result in term of homogeneous size distributions, crystal structure and ending functional groups in surfactants chains.

I started with the most famous procedure the co-precipitation (Massart's procedure). This method started from a solution of iron (III) and iron (II) in stoichiometric ratio in basic condition, heated under mechanically stirrer. In literature there are thousands of articles that use this procedure. It's an easy technique and requires mild conditions. The disadvantage is the formation of aggregate (A manuscript in preparation describe the interactions between nanoparticles obtained by co-precipitation and thermal decomposition method, "Lorentz microscopy sheds light on the role of dipolar interactions in magnetic hyperthermia" M. Campanini, R. Ciprian, E. Bedogni, V. Chiesi, A. Mega, C. de Julián Fernàndez, F. Casoli, F. Rossi, E. Rotunno, V. Grillo, F. Bigi, G. Salviati, and F. Albertini).

According to Massart's procedure, magnetite nanoparticles were prepared and dried. Then, I tried to coat them with Au, to obtain core-shell nanoparticles where the shell could add a plasmonic effect and can easily functionalized with thiol-ending molecules.

Results and Discussions

I synthetized two samples: the first one was soluble in water phase and the second one in organic phase. The samples were studied by electron microscopy at IMEM-CNR.

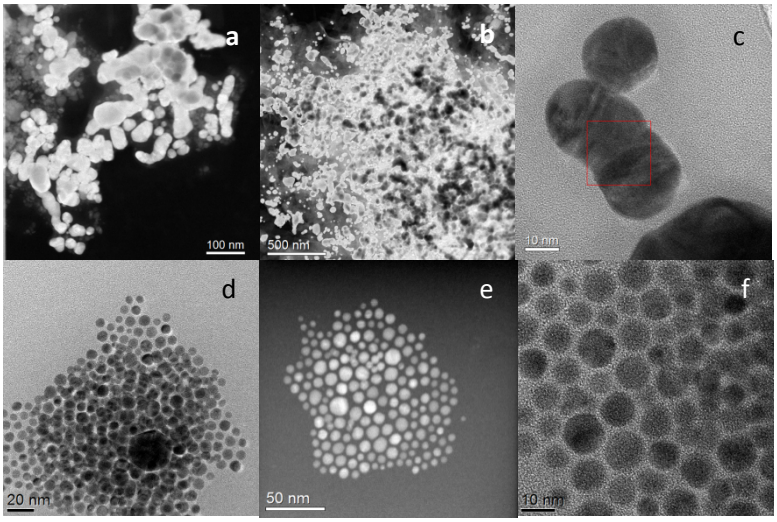

Figure 1. *TEM images of Au-Fe_3O_4 cluster water soluble (a, b, c) and Au-Fe_3O_4 organic soluble (d, e, f). TEM pictures show the broad size distribution in Au-Fe_3O_4 cluster organic soluble (images d, e, f). It is not easy understand if there are core-shell structures or if there are presence of both materials in a random distribution. Water soluble particles, as shown in the Figure 1a, 1b and 1c, are aggregate in big particles and cluster where it is easy see the presence of Fe_3O_4 and Au (like show in image HAADF: Z-contrast).*

This analysis (TEM images) shows the presence of stable nanoparticles (Figure 1, d, e, f pictures) with a large size distribution and a, b, c pictures show the presence of some aggregate and the absence of a core-shell structure. As reported in the literature, the method of co-precipitation leads to the formation of aggregates which even if "covered" gold damage formation of aggregates in the aqueous phase.

With regard to the organic phase that is watched and the formation of particles stabilized but with a large dimensional range.

Then I tried the magnetite synthesis using microwave method in order to use also a different surfactant.
As described by Reimhult in 2011[1] nanoparticles were synthetized using a microwave loop, starting from a precursor of iron (III), $Fe(ac)_3$, and benzyalcohol as reducing agent-solvent in a flask, a lot of energy for few minutes. After that a solution of nitro-DOPA in DMF was added as stabilizer.

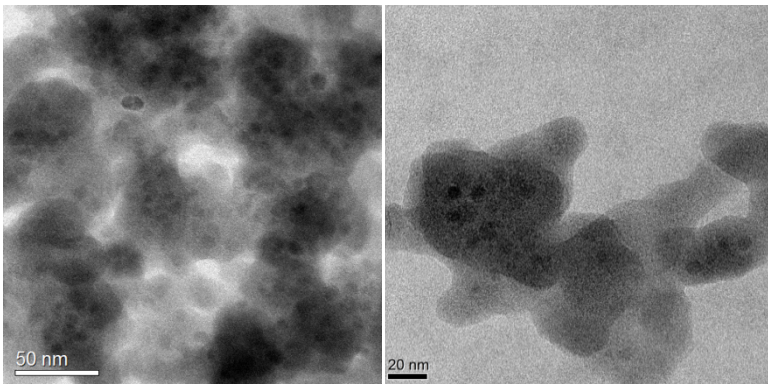

Figure 2. *TEM pictures of nanoparticles obtained by a microwave method*

I did not obtain good results; indeed, as shown in the pictures, nanoparticles are immersed in a large amount of organic materials. They have a narrow size distribution and the diameter of inorganic material is centered at 5 nm, is too small for our applications.
I also experimented the synthesis based on the thermal decomposition method. In literature there are many articles that describe this procedure for several applications. This methodology makes possible the use of different surfactants, opening the possibility to have different functional groups.
This type of synthesis starts from a precursor of iron (III) as $Fe(acac)_3$ in presence of a reducing agent, surfactants and high boiling point solvent. Some of a preliminary experiments are reported below.

I tried using phenyl ether as solvent, oleic acid and oleylamine as surfactants and tert-butylcathecol as reducing agent. The reaction was heated at 300°C for 30'.

I obtained magnetic nanoparticles in a large size distribution. TEM images (Figure 3).

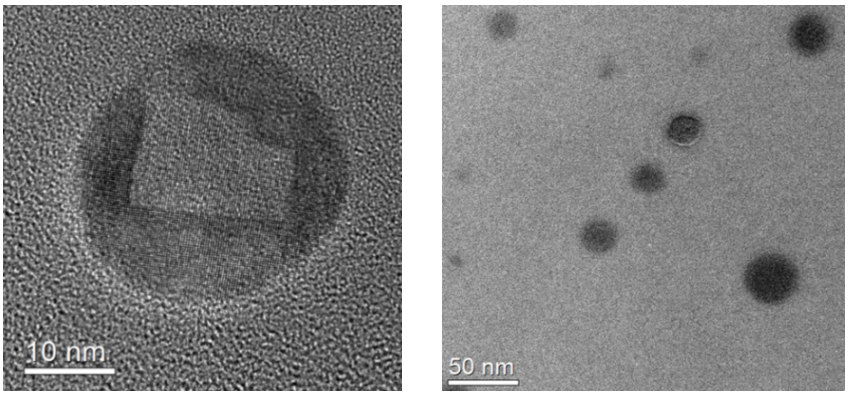

Figure 3. *TEM pictures of samples obtained by thermic decomposition*

The media diameter is 18 nm. There are many sizes and different shape. An usual shape was observed that looks like red blood cells.

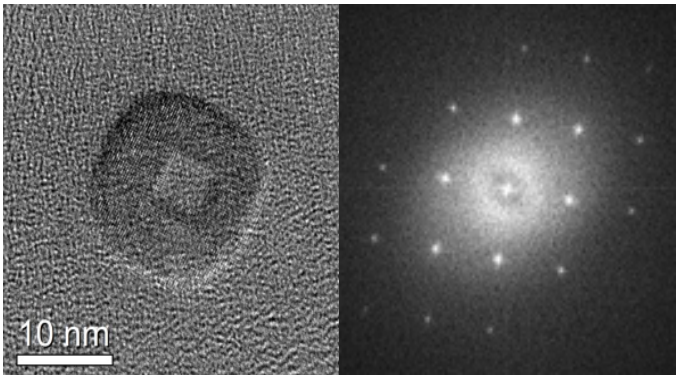

Figure 4.

These nanoparticles show the presence of monocrystalline structure like show in *Figure 4*, that correspond at Fe_3O_4 crystal structure.

This picture shows a single nanoparticles with a single crystal structure, like shown in a diffraction patter. The results that we obtained were different from the results that Sun and Zang proposed in 2002, the explanation could be the different set up and different reducing reagents (the articles propose the use of 1,2-hexadecanediol).

In another experiment, I used phenyl ether as solvent, oleylamine as surfactant and ters-butylcathecol as reducing agent. The reaction was heated at 300°C for 30'. The nanoparticles obtained were stable and with a narrow size distribution and a media diameter centered around 9 nm. The negative aspect of this good sample was the difficulty to obtain a functional group easily to use to conjugate nanoparticle with other system.

I decided to follow a procedure reported in the literature to obtain nanoparticles of different sizes and stabilized by an organic shell that

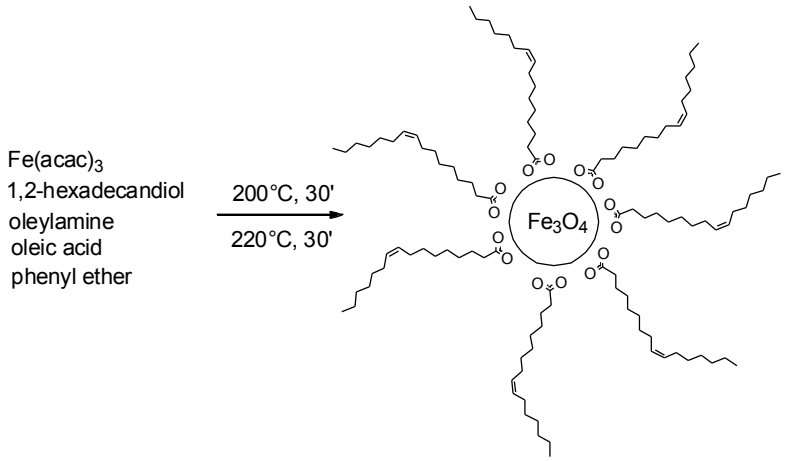

Figure 5. *Synthetic approach for thermal decomposition method*

could be modified successively. Good quality nanoparticles were obtained reacting $Fe(acac)_3$ in the presence of 1, 2-hexadecanediol as reducing agent, oleic acid and oleylamine as surfactants and phenyl ether as solvent. 220 °C were reached for 30 minutes after a preheating at 200° C.

Preheating was important in order to produce in situ an homogeneous precursor of iron to produce nanoparticles with a narrow size distribution.

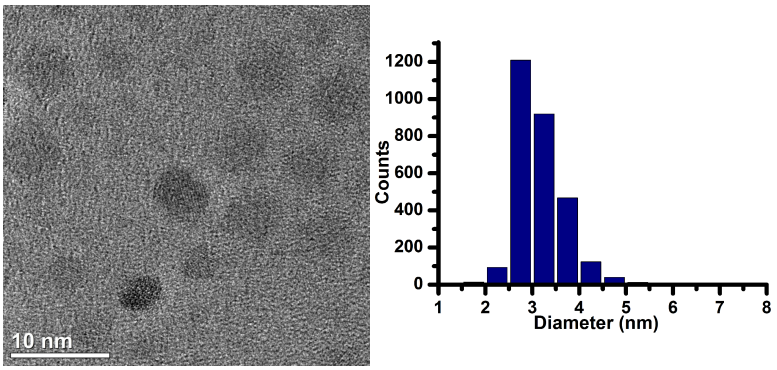

Figure 6. *TEM picture and dimension distribution of nanoparticles obtained by thermal decomposition (**c**)*

As it is show in the picture of Figure 6 the nanoparticles were small and with a narrow dimension distribution, with a diameter centered at 3-4 nm. These types of nanoparticles are stable also after long time (months). For the good size distribution, high stability for long time and for good crystal structure we decided to study also the magnetic properties.

At IMEM-CNR the magnetic properties of these nanoparticles were examined.

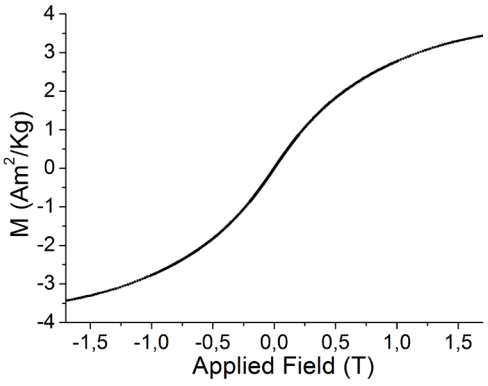

Figure7. Magnetic study of NP-4 nm. *It is in evidence that magnetization at highest field is 3.4± 0.3 /kg. This value is very low. Because of the small size, the particles are far from the saturation at room temperature.*

The value of saturation magnetization was 3.4 Am^2/Kg that was a low value but normal for magnetite nanoparticles with very small size.

In order to know the amount of magnetic material and organic part thermogravimetric analysis was performed. The total weight loss resulted to be 32%.

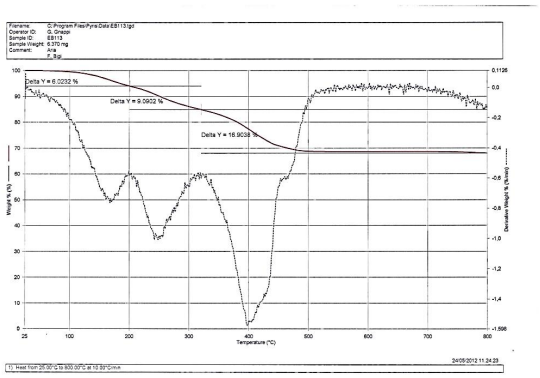

Figure 8. TGA analysis: *The operative condition are air flux, T_{start}= r.t., T_{max}= 800°C, rate=10°/min. the total* ***weight loss is 32%***

The idea developed to bind the magnetite nanoparticles to the SiC/SiO_2 nanowires, was the formation of a triazole ring between the two partners. This approach requires the introduction of complementary groups on the surface of the nanoparticles and of the nanowires, i.e. terminal alkyne on NPs and azide groups on nanowires.
The introduction of alkyne groups was accomplished by ligand exchange procedure. Nanoparticles obtained by a previous step were dissolved in hexane solution in presence of 10-undecynoic acid. The reaction was heated. Nanoparticles were washed several times and the presence of alkyne group was studied by FT-IR analysis that show the stretching of C≡C at υ~2100 cm^{-1} and the stretching C≡*C-H* at υ~3210 cm^{-1}.

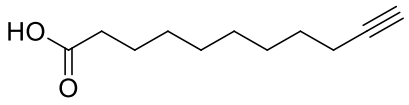

Figure 9. *Undecynoic acid*

Since the magnetic properties were unsatisfactory I increased the diameter of nanoparticles changing the thermal decomposition conditions. Dibenzyl ether was employed as solvent to reach highest temperature ~ 300 °C. After heating at 200 °C for 2 hours under nitrogen, the reaction was refluxed for 1 hour. These conditions give to particles more time to increase in dimension.

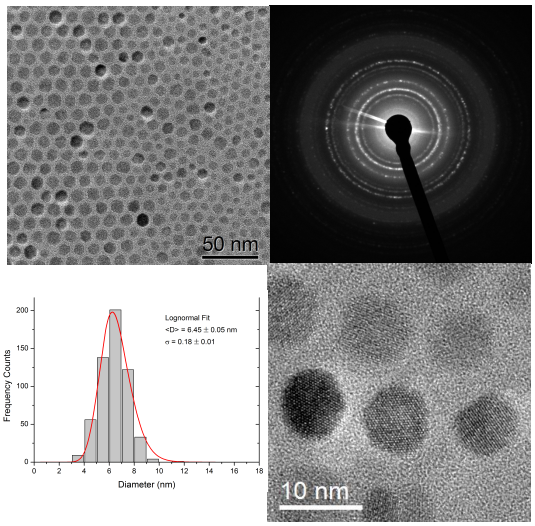

Figure 10. *TEM images, diffraction patter, size distribution are shown in this figure. The first pictures show good homogeneous distribution, and a detail is shown in the last one. Diffraction patter shows magnetite crystal structure and the narrow size distribution is shown with a d= 7 nm.*

As shown in TEM images (Figure 10) nanoparticles have a narrow size distribution with a media diameter centred at 7 nm, and as reported in diffraction pattern the crystal structure matches with magnetite crystal structure. The magnetic characterisation was performed.

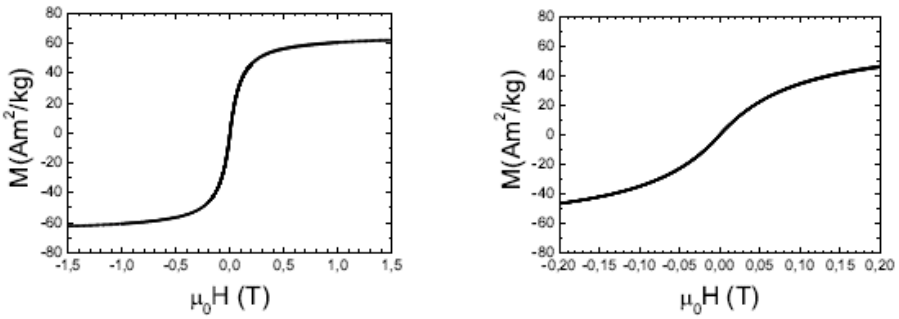

Figure 11. Hysteresis loop at room temperature of 8 nm MNPs obtained by thermal decomposition and: left: maximum field of 1.5 T, right: maximum field of 0.2 T.

As you can see in the *Figure 11*, the nanoparticles reach the saturation around 60 Am^2/kg and the zoom (right) shows the absence of hysteresis, evidencing that the nanoparticles have superparamagnetism properties and there is no-interaction between nanoparticles.

The nanoparticles synthetized in this way are stable and display a high magnetization value. Therefore it was also possible to study the hyperthermia properties.

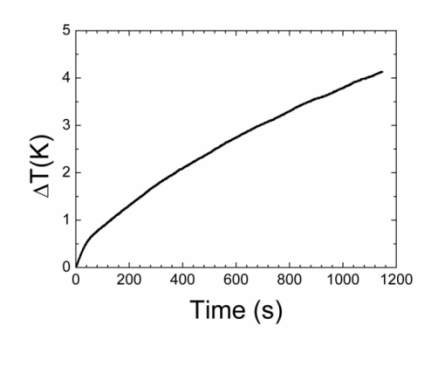

Figure 12.

As it is shown in Figure 12 nanoparticles, dispersed in hexane, increased the temperature of 4.2 K in 20 min if a frequency of 250 KHz and a magnetic field of 0.016 T were applied. This value showed the

possibility to use this type of nanoparticles for hyperthermia and urges us to search for increasing the particle dimensions.

Thanks to the collaboration with medical and veterinary groups, the biocompatibility of the synthesized nanoparticles was studied and the internalization was confirmed.
In literature there are many works dealing with the biocompatibility of magnetite nanoparticles. Indeed, the biocompatibility depends from the organic or inorganic shell around the nanoparticles and from their specific nature.[2]
The polarity of the organic shell can totally change also the mechanism of internalization. It also known that the shell should have both polar and apolar characteristics, since the nanoparticles have to pass through the cell wall (apolar) and have to stay inside the cytoplasm area (polar solution).

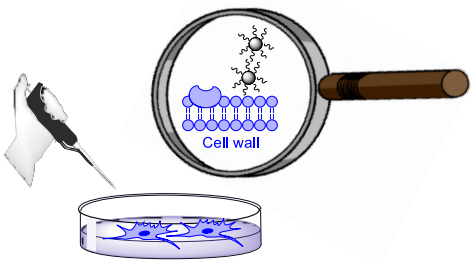

Figure 13.

The internalization study was accomplished using A549 culture cells. The nanoparticles sample was solubilized in DMSO (small amount) and after that diluted in water in order to decrease the concentration of DMSO (in high concentration this is toxic for cells).

The cells, after 24 hours (uptake time) were fixed in a resin using a protocol performed by Prof. Cacchioli and the resin-wafer was examined by TEM spectroscopy.

The nanoparticles were internalized inside the cells at intracytoplasmonic level, in cytoplasm area as shown in the following picture (Figure 14).

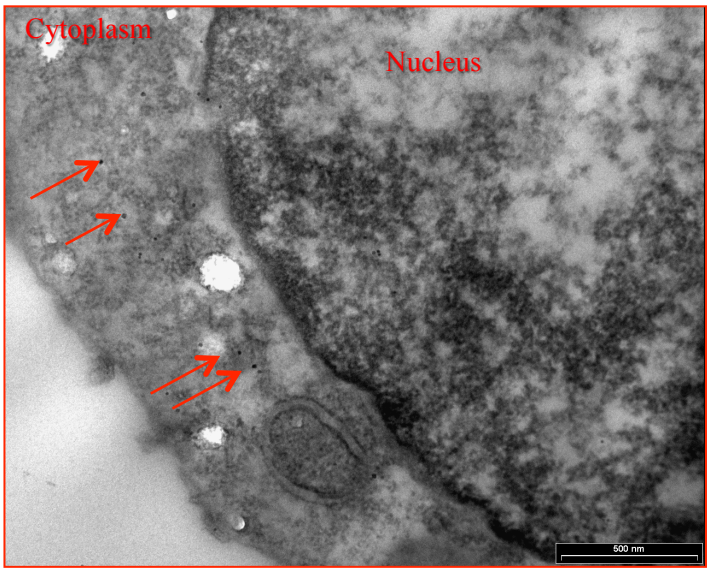

Figure 14. *TEM image (obtained at 80 MeV) show the presence of nanoparticles inside the cytoplasm area.*

Biocompatibility of nanoparticles was studied evaluating the number of cells in life and death cells at different concentrations.

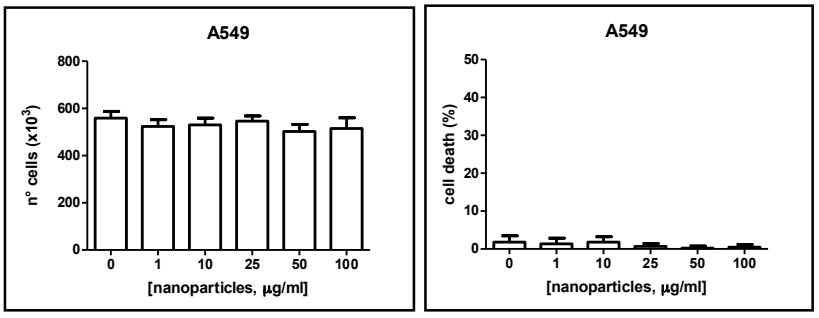

Figure 15. *Histograms show that there isn't inhibition of proliferation and absence of cell death also for high nanoparticles concentration.*

The histograms reported in Figure 15 show that no inhibited proliferation and cell death is found. Apoptosis evaluation was done by Trypan Blue Test (Figure 16) that evidenced the absence of apoptosis.

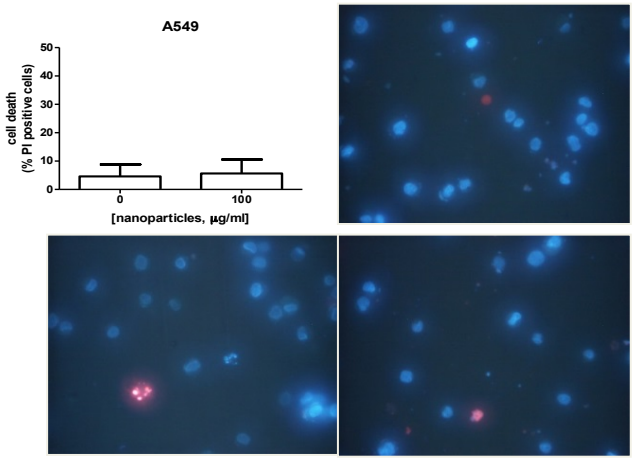

Figure 16 *Trypan test shows the absence of apoptosis (cell in life are in blue and dead cells are in red). Histogram shows the absence of apoptosis by cells count.*

This study bring to light that the prepared nanoparticles can be incorporated inside the cells (the study was performed only in A549, cancer cells) and are biocompatible. Therefore they can be anchored to biocompatible nanowires.

Very recently I obtained preliminary experiments promising results from nanoparticles with a **cubic shape** obtained by thermal decomposition. The synthesis started from the same reagents previously employed, i.e. $Fe(acac)_3$, 1, 2-hexadecanediol, oleic acid, oleylamine, and benzyl ethers. The temperature was increased at a heating rate of 7 °C/min up to 300 °C and maintained for 1 h. Some procedures are reported in the literature to obtain a cubic form, but they are not easy to reproduce, since the heating conditions are crucial. Small changes in the temperature values and also in the heating rate determine shape and dimension variation.[3] TEM images show the size of particles, that was

around 10 nm. The dimension distribution was good, as reported in the Figure 17.

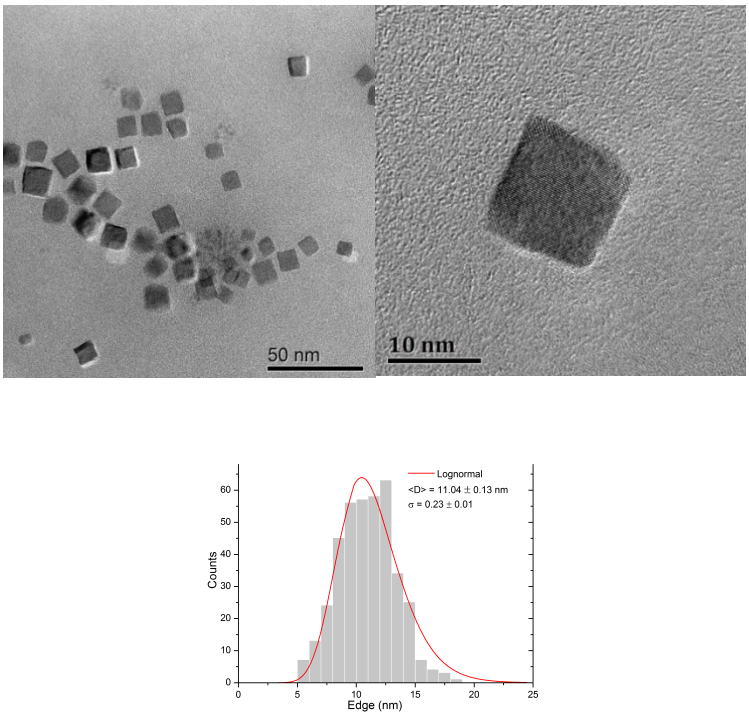

Figure 17.

The study of hyperthermia property was done. Using 9.3 mg of sample dispersed in hexane. TGA analysis was performed, showing a total amount of organic part was 30% of the total sample weight.

$$SLP = \frac{Cp(tol)\cdot d(tol)}{C_{\mathrm{NP}}(g/mL)} \cdot \frac{\Delta T}{\Delta t}$$

Equation 1

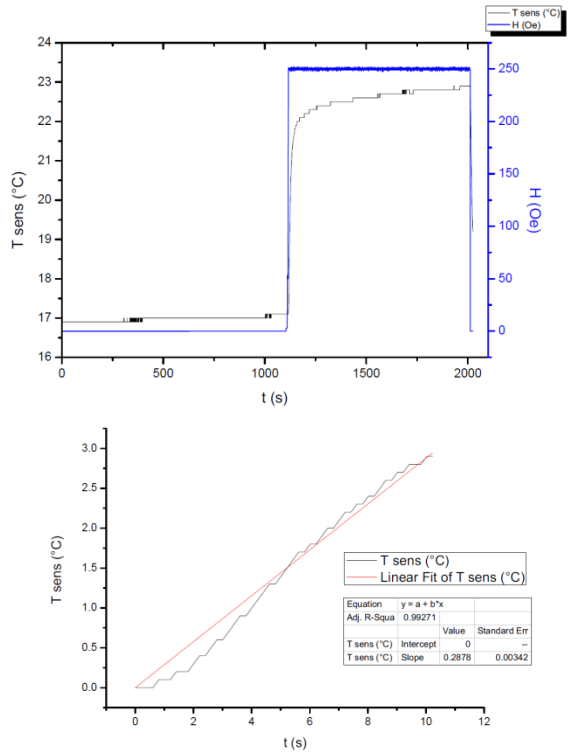

Figure 18.

Talking into amount the real magnetite weight, a value of SLP was 65.4 W/g calculated using the magnetic field of 250 Oe and the frequency of 429 KHz.

The high SLP value evidenced, the good hyperthermia properties.

Experimental section

Synthesis of Au-Fe_3O_4 cluster

In a 500 mL 3 neck round bottom flask 11 g of $FeCl_3*6H_2O$ (40 mmol) was dissolved in 120 mL of deionized water. After the dissolution 4 g of $FeCl_2*4H_2O$ (20 mmol) was added and the solution was heated at 85°C under argon atmosphere. The pH was adjusted to 10 with the addition of ammonia solution, and the nanoparticle were formed and stirred for 4 hours under argon atmosphere. After cooling the MNP were washed several times with distilled water in order to remove the excess of ammonia. The MNPs were dried under high vacuum for one hour and characterized.[4]

Then I decided to try different methods: the first it will produce nanoparticles organic soluble-dispersible and the second one water-dispersible.

A. $HAuCl_4$ (0.5 mmol) was dissolved in 30 ml of water, Tetraoctylammonium bromide (TOABr, 2 mmol) were dissolved in toluene. The reaction is on interface and all the Au was transferred in toluene. The nanoparticles are added in toluene after sonication in the same solvent and added to the solution containing Au. The finally suspension is mechanically stirred for few minutes then $NaBH_4$ (1 mmol) was added. After 5 min in the suspension was added dodecanthyole (1 mmol) and sonicated for one hour. After that, the reaction is mechanically stirred for 4 hours. The nanoparticles obtained were collected by centrifugation and washed several times.
B. In Fe_3O_4 -water suspension were added $HAuCl_4$ and $NaBH_4$ in sequence and mechanically stirred for few min. A solution of 3-thyolcarboxylic acid in water was added drop by drop and mechanically stirred overnight. The nanoparticles obtained were collected by centrifugation and washed several times.

c

Synthesis by microwave of Fe_3O_4 nanoparticles

Like described by Reimhult in 2011[5] nanoparticles were synthetized using a microwave method. $Fe(ac)_2$ (0.33 mmol) was dissolved in benzyalcohol (5 ml) and heated for 3 min at 180 °C in the microwave. The nanoparticles were washed with EtOH and re-dispersed in EtOH (10 ml). I changed the precursor with $Fe(acac)_3$ (0.33 mmol) was dissolved in benzyalcohol (5 ml) and heated for 3 min at 180 °C in the microwave. The nanoparticles were washed with EtOH and re-dispersed in EtOH (10 ml).

This 10 ml were added to a solution of nitro-DOPA (dopamine, 1 mol) in DMF. The suspension was stirred overnight at 50 °C. The nanoparticles weren't easily perceptible.

Synthesis of Fe_3O_4 nanoparticles by thermal decomposition[6] (A)

In a 250 mL 3 neck round bottom flask 355 mg of $Fe(acac)_3$ (1 mmol) was dissolved in 10 mL of phenyl ether with 850mg oleic acid (3 mmol), 802 mg of oleylamine (3 mmol), 1.2 g of 3,5-tersbutylcathecol and mechanically stirred under flue of N_2. The reaction is heated at 300°C for 30', and after that cooling down. The nanoparticles are precipitated in EtOH by centrifugation and re-dissolved in hexane (several times).

Synthesis of Fe_3O_4 nanoparticles by thermal decomposition[7] (B)

In a 100 mL 3-neck round bottom flask 530 mg of $Fe(acac)_3$ (1.5 mmol) was dissolved in 7.5 ml of oleylamine and mechanically stirred under N_2 flue. The reaction is heated at 110°C for 60', so 300°C for one hour. In order to avoid loss of temperature the flask is coated with aluminum foil. The heater is obtained with a sand bath. The

nanoparticles are precipitated in EtOH by centrifugation and re-dissolved in hexane (several times).

Synthesis of Fe_3O_4 nanoparticles by thermal decomposition[8] (C)

$Fe(acac)_3$ (2 mmol), 1, 2-hexadecanediol (10 mmol), oleic acid (6 mmol), oleylamine (6 mmol), and phenyl ether (20 mL) were mixed and magnetically stirred under a flow of nitrogen in a 3 neck round bottom flak. The mixture was heated to 200 °C for 2 h and then, under a blanket of nitrogen, heated to reflux (~220 °C) for 30'. The black-colored mixture was cooled a room temperature by removing the heat source. Under room conditions, ethanol (40 ml) was added to the mixture and black material was precipitated and separate via centrifugation (5000 rpm, 15 min).

Synthesis of Fe_3O_4 nanoparticles by thermal decomposition[9] (D)

$Fe(acac)_3$ (2 mmol), 1, 2-hexadecanediol (10 mmol), oleic acid (6 mmol), oleylamine (6 mmol), and benzyl ether (20 mL) were mixed and magnetically stirred under a flow of nitrogen. The mixture was heated to 200 °C for 2 h and then, under a blanket of nitrogen, heated to reflux (~300 °C) for 1 h. The black-colored mixture was cooled a room temperature by removing the heat source. Under room conditions, ethanol (40 ml) was added to the mixture and black material was precipitated and separate by centrifugation (5000 rpm, 15 min). The black product was dissolved in hexane and
disperse by sonication in 10 minutes. Ethanol was added (40 mL) to the mixture and black material was precipitated and separate via centrifugation (5000 rpm, 15 min).

Synthesis of Fe_3O_4 nanoparticles by thermal decomposition (E) cubic shape

$Fe(acac)_3$ (2 mmol), 1, 2-hexadecanediol (10 mmol), oleic acid (6 mmol), oleylamine (6 mmol), and benzyl ether (20 mL) were mixed and magnetically stirred under a flow of nitrogen. The mixture was heated to 200 °C for 2 h and then, under a blanket of nitrogen, the temperature was increased at a heating rate of 7°C/min up to 300 °C and maintained for 1 h. The black-coloured mixture was cooled a room temperature by removing the heat source. Under room conditions, ethanol (40 ml) was added to the mixture and black material was precipitated and separate by centrifugation (5000 rpm, 15 min). The black product was dissolved in hexane and
disperse by sonication in 10 minutes. Ethanol was added (40 mL) to the mixture and black material was precipitated and separate via centrifugation (5000 rpm, 15 min).

References

[1] E. Amstad, A. U. Gehring, H. Fisher, V.V. Nagaiyanallur, G. Hähner, M. Textor, and E. Reimhult *J. Phys. Chem. C*, 115, 683-691 (**2011**)

[2] M. P. Calatayud, B. Sanz, V.Raffa, C. Riggio, M. R. Ibarra, G. F. Goya, *Biomaterials*, (**2014**)

[3] M.V. Kovalenko**,** M. I. Bodnarchuk , R. T. Lechner , G. Hesser , F. Schäffler , and W. Heiss. *JACS*, 129, 6352-6353 (**2007**)

[4] Massart, R.: *IEEE Trans. Magn.* 17, 1247 (**1981**)

[5] E. Amstad, A. U. Gehring, H. Fisher, V.V. Nagaiyanallur, G. Hähner, M. Textor, and E. Reimhult *J. Phys. Chem. C*, 115, 683-691 (**2011**)

[6] Shouheng Sun, Hao Zang *JACS*, 124. 8204-8205 (**2002**)

[7] Z. Xu, C. Shen; Y. Hou, H. Gao, S. Sun, *Chem. Mater.,* 21, 1778-1790 (**2009**)

[8]Y. Hou, J. Yu,S. Gao, *Journal of Materials Chemistry* 13(8), 1983-1987(**2003**)

[9] T. Horiuchi, H. Miura ,K. Sumioka, and S. Uchida *JACS* 126, 1, (**2004**)

Synthesis of a nanosystem composed by Fe_3O_4 nanoparticles bound to SiC/SiO_x nanowires

Introduction

Among nanostructured magnetic materials, magnetite nanoparticles derivative have shown very promising properties for applications in nanomedicine[1], such as hyperthermia, drug delivery and biological separation.[2],[3] BioNiMed project, as explained in first chapter, has the aim to synthetize new nanosystems for biomedical applications, in particular for anticancer therapy.

The anchoring of Fe_3O_4 MNPs could improve the hyperthermic effect, since (100) SiC NWs are also interesting for their high thermal conductivity. This last property can in particular improve and optimize the heat distribution generated by MNPs along the NWs and in turn inside the cancer cells. SiC nanowires are known be biocompatible[4],, thus we supposed that also SiC/SiO_x nanowires are biocompatible. However, the biocompatibility has to be established by specific study. Even SiC/SiO_2 is a material studied since 2002,the first evidence of *in vitro* cytocompatibility of SiC/SiO_x $_c$ore-shell nanowires has been published last year[5]. As cellular model in view of future therapeutic applications, three tumor cell lines (adenocalcinomic alveolar basal epithelial cells, A549, monocyte cell line derived from an acute monocyte leukemia (THP-1), breast cancer cells (MCF-7) and normal human derm fibroblast cells (HuDe)) were selected. In particular the A549 and MCF-7 cells were chosen both for the high incidence of these tumors in nude mice model. Further, the THP-1 cells were used for their macrophage activity and finally the HuDe fibroblasts as *non*-cancer control cells. The cytocompatibility of the nanowires was proved by the analysis of cell proliferation, cell cycle progression and oxidative stress on the cells treated with NWs as compared to controls. Different internalization mechanisms were observed. The internalization occurs mainly for micropinocytosis and sporadically by direct penetration I all cell models considered, where as it occurred for phagocytosis only in monocyte leukemia cells. We designed to link the biocompatible magnetite nanoparticles to the biocompatible SiC/SiO_x nanowires by covalent bond by exploiting the Huisgen 1, 3-dipola cycloaddition reaction (click chemistry).

Both MNPs and NWs have to be properly functionalized to allow their mutual reactivity. To this purpose azide groups were introduced on the surface of the silica shell of the NWs and C-C triple bonds were introduced in the stabilizing layer of the MNPs.

We choose undodecynoic acid as the molecular anchor because it is able to exploit its polar head to bind tightly the surface of metal oxides (including iron oxide) via M-O bonds.[6,7,8,9]

In this study we presented for the first time a general approach to functionalize core shell SiC-SiO_x nanowire with magnetite nanoparticles.

Nanowires were grown on a Si (100) wafer using $Fe(NO_3)_3$ as catalyst in VPE reactor (previously Ni salt catalyst was used, but for avoid cytotoxicity of this metal, it was changed).[10].

As Attolini et al. publish in 2008[11] the growth of this material starting from Si wafer, following the procedure described below.

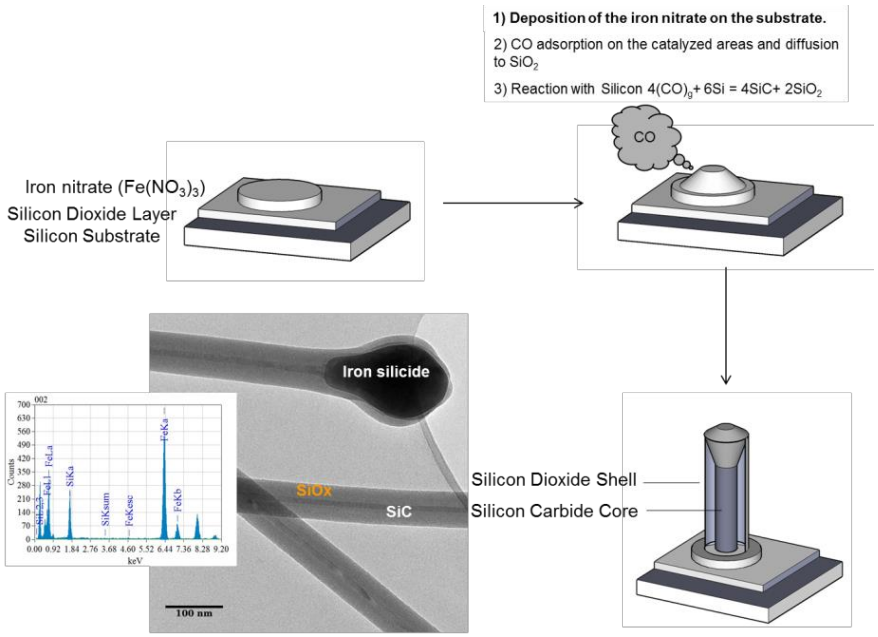

***Figure 1**: Scheme shows the process to synthetize nanowires*

Summarized in Figure 1 nanowires were grown by VPE synthesis starting from the catalyst deposition of a solution of iron nitrate as catalyst on a Si wafer. A steam of CO mixed with N_2 and Ar as carrier gas was introduced in the reactor and the growth of the nanowires occurs at temperatures between 1050-1100 °C. These nanowires were obtained with a core shell structure as shown in the previous TEM picture.

Click chemistry

Click chemistry is a term applied to chemical synthesis tailored to generate substances quickly and reliably by joining small or big units together. Click chemistry is not a single specific reaction, but describes a way of generating products in a very easy way. The term was coined by K. Barry Sharpless in 1998, it means to obtain a reaction very quickly and, as imaginable, easily as a click obtained by computer-mouse.[12] The most famous reaction known as click reaction is the called [3+2] cycloadditions known as the Huisgen 1,3-dipolar cycloaddition, in particular the Cu(I)-catalyzed version are often referred simply as *Click reactions*.

It is interesting to read the original words used by Sharpless defining a "*click reaction"* for the first time.

"Following natures lead, we endeavor to generate substances by joining small units together with heteroatom links. The goal is to develop an expanding set of powerful, selective, and modular block that work reliably in both small- and large-scale applications. We have termed the foundation of this approach click chemistry. and have defined a set of stringent criteria that a process must meet to the useful in this context. The reaction must be modular, wide in scope, give very high yields, generate only inoffensive byproducts that can be removed by non-chromatographic methods and be stereospecific. The required process characteristics include simple reaction conditions, readily available starting materials and reagents, the use of no solvent or a solvent that is benign or easily removed, and simple product isolation. Purification, if required, must be by non-chromatographic methods, such as crystallization or distillation, and the product must be stable under physiological conditions.
It is important to recognize that click reactions achieve their required characteristics by having a high thermodynamic driving force, usually greater than 20 kcal/mol. Such processes proceed rapidly to completion and also tend to be highly selective for a single product: we think of these reactions as being spring loaded for a single trajectory. Carbon-heteroatom bond forming reactions comprise the most common examples, including the following classes of chemical transformations:

- *Cycloadditions of unsatured species, especially 1,3-dypolar cycloaddition reactions, but also the Diels Alder family transformation*
- *Nucleophilic substitution chemistry, particular ring-opening reactions of strained heterocyclic electrophiles such as epoxides, axiridines, aziridinium ions, and episulfonium ions*
- *Carbonyl chemistry of the non-aldol type, such as formation of ureas, thioureas, aromatic heterocycles, oxime ethers, hydrazones, and amides*

- *Addition to carbon-carbon multiple bonds, epecially oxidatiev cases such as epoxidation, dihydroxylation, aziridination, and sulfenyl halide addition, but also Michael additions of Nu-H reactants*."

There are two types of azide-alkyne Huisgen cycloaddition:

1. Cu(I)-catalyzed reaction, that gives the stereo-selective formation of 1,4-substituted triazole (Figure 2). The selective formation of 1, 5-isomer can be catalyzed by Ru (Figure 3)
2. Thermal reaction that produces both the possible isomeric products.

In Figure 30 the mechanism of Cu-catalyzed reaction id shown[13].

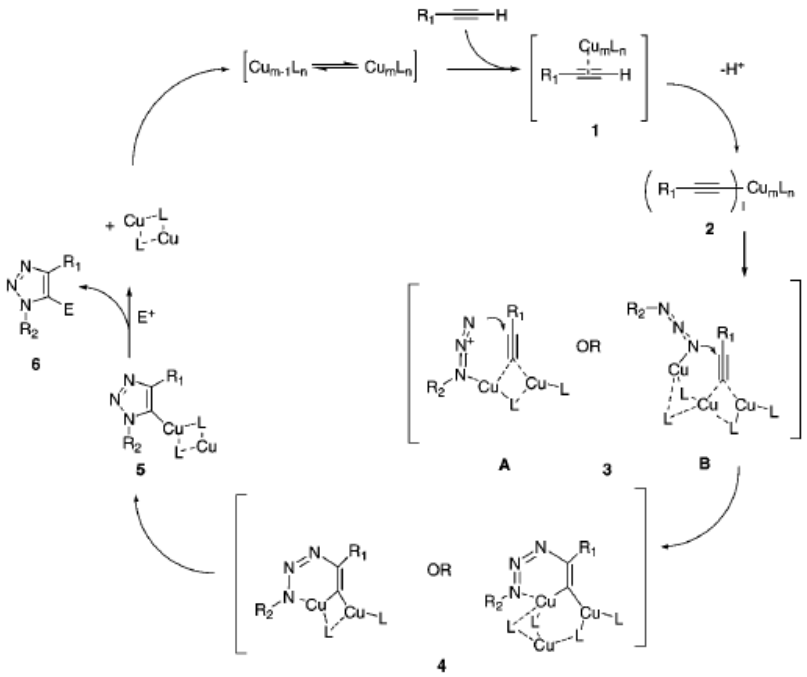

Figure 2. *Cu-assisted catalytic process in "click chemistry"*

This mechanism is specific for 1,4-triazole formation. There is also the possibility to obtain the other product (1,5-triazole) by using the Ru catalyst. The mechanism is shown in the following picture (Figure 3).

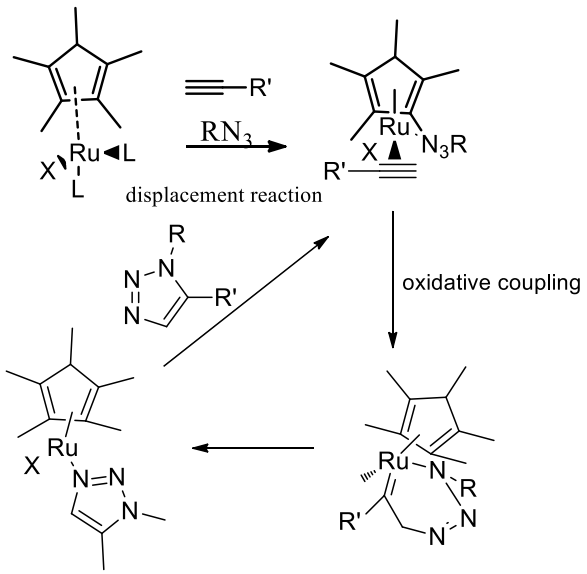

***Figure 3**. Ru-assisted catalytic process in "click chemistry"*

The scheme shows the reactivity of Ru-complex with azido group and alkyne group, which create a covalent bond in the second step called oxidative coupling. In that step the breakup of C-C triple bond and the formation of covalent bond between N and C happened.
Then occurs the reaction that forming the triazole-ring and after that the formation of the final product and the regeneration of original catalyst. The geometry of the product is 1,5-triazole. Figure 4 summarizes the different paths.

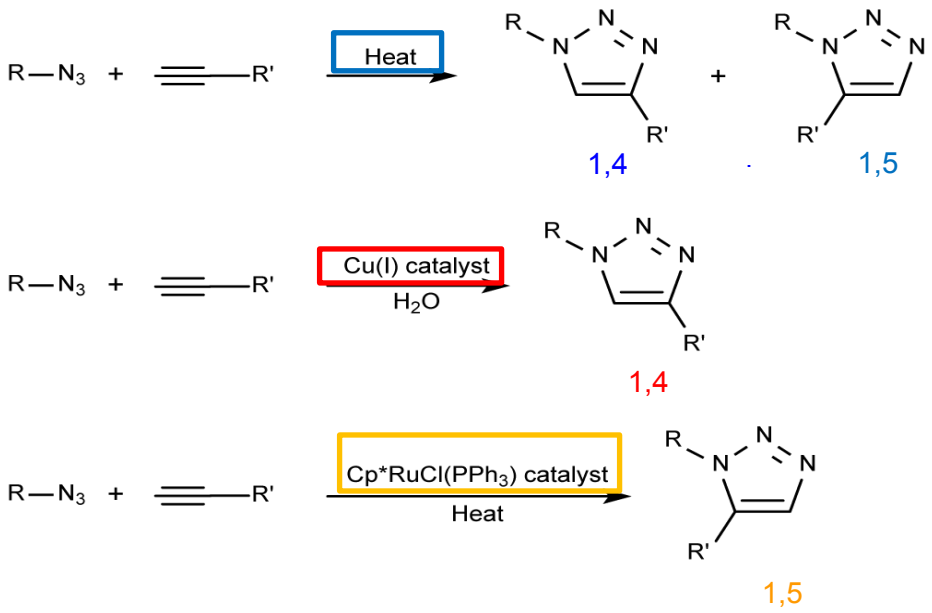

Figure 4. *Summary catalytic processes in "click chemistry"*

Results and Discussion

The SiC/SiO_2 nanowires were functionalized by a *click chemistry* reaction. Thermal conditions were avoided to exclude the possibility to change even in part the crystal structure of nanoparticles and to be sure to not alter the organic shell stabilizing the nanoparticles.

As depicted in the previous Figure the nanowires were functionalized

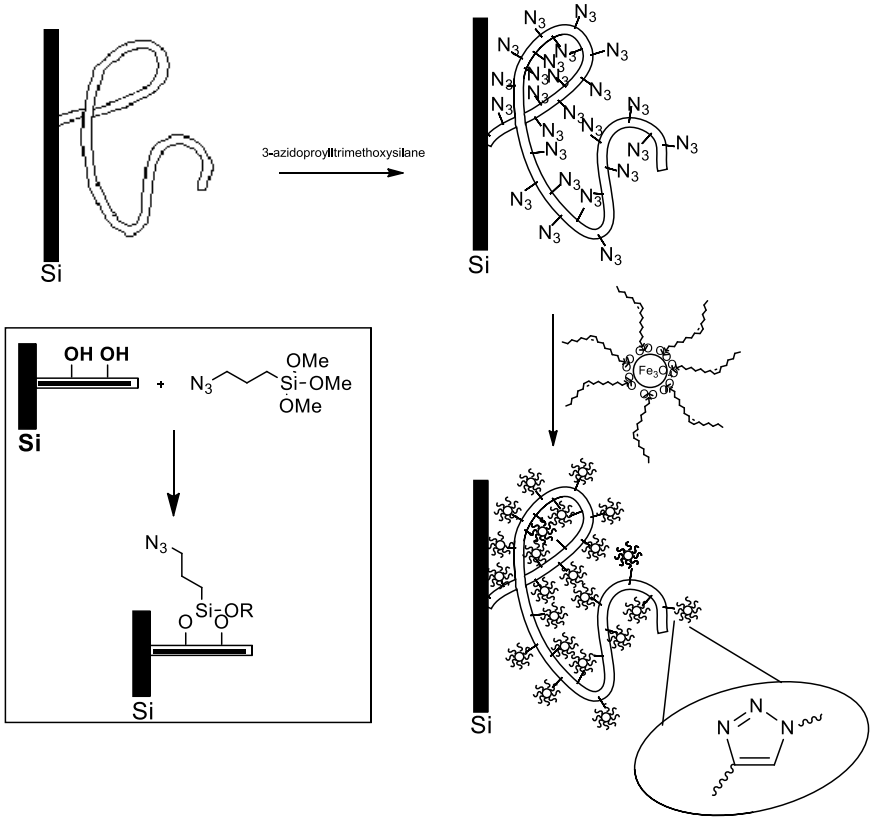

Figure 5. *Synthetic approach for the functionalization of the nanowires*

with 3-azidopropyltrimethoxysilane. This reagent is not commercially available, and was synthetized starting from the chloro precursor by a nucleofilic substitution (Scheme 1). The high reactivity of the alkoxy groups of this compound allows a very short "life" for this reagent that must be freshly prepared.

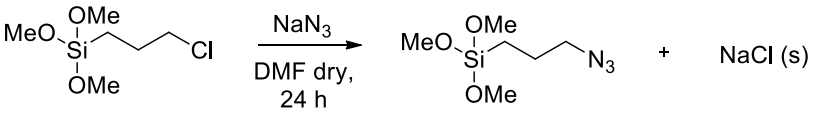

Scheme 1.

The nanowires were functionalized boiling at reflux in toluene in the presence of this reagent. The reaction occurred by hydrolysis of the methoxy groups and subsequent condensation with surface hydroxyl groups of the silica shell, giving Si-O-Si bond formation. The reaction was performed in toluene at reflux twice, thoroughly washing the plate with acetone in between.

Then, they were decorated with the Fe_3O_4 nanoparticles of 8 nm and having carbon-carbon bonds in the outer shell, described in the previous chapter, *via* click-reaction. To this end, the nanoparticles were dispersed in hexane and added to a vessel containing the nanowires as grown on Si wafer covered by a mixture of solvents (CH_2Cl_2, MeOH, $(CH_3)_2CO$, hexane in 1:1:1:1 ratio) in the presence of CuI catalyst.

The reaction was left overnight at room temperature without stirring. TEM studies demonstrated the successful functionalization.

The synthetic methodology was optimized by varying the concentration of the silane, the solvents, the catalyst amount optimized and the reaction time with the aiming to achieve a good degree of covering and uniform coating.

Some preliminary results are shown in the Figure 6. TEM pictures show the presence of some aggregate and not homogeneous distribution of nanoparticles on the surface of core-shell nanoparticles.

The presence of some aggregates should to be avoid because we observed[14] that aggregate of nanoparticles have a different magnetic behaviour than single nanoparticles (paper under submission). These undesured distribution are ascribable to the *non*-uniform distribution of silane on the NW surface.

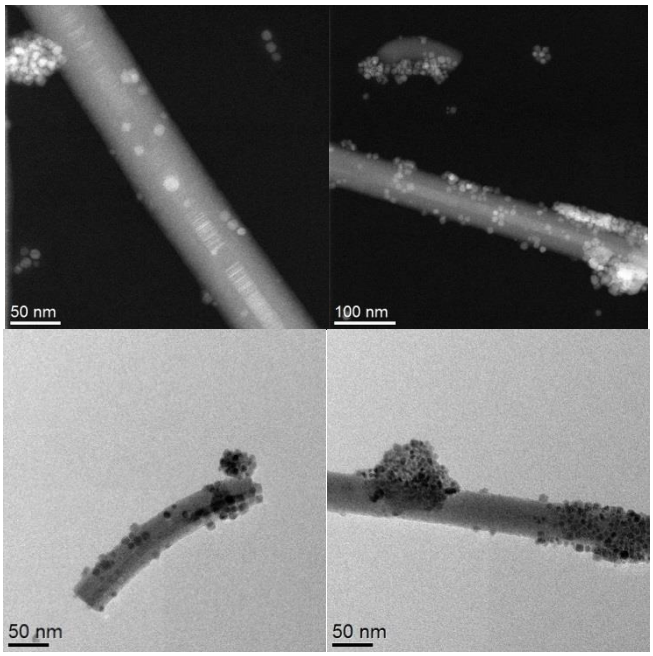

Figure 6. *TEM images of nanowires decorated with Fe_3O_4 nanoparticles. Obtained in optimization studies.*

Homogeneous samples were obtained after several attempts as you will find in the following Figure. Last in Figure 7: HR-TEM and STEM images show the success reached in binding MNPs to the NWs under optimized conditions.

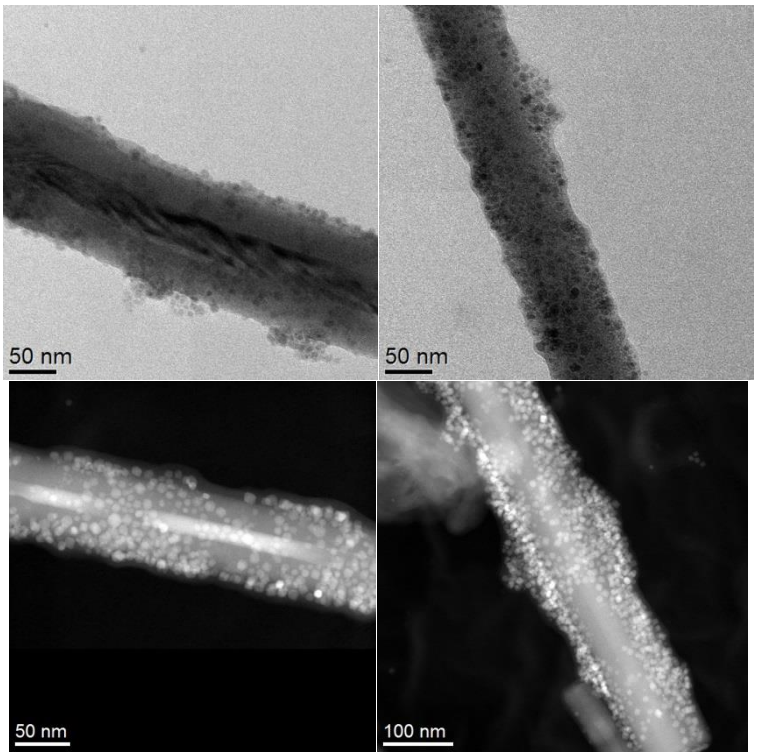

Figure 7. *TEM images: HR-TEM and STEM image show the homogeneous presence of nanowires decorated with nanoparticles by "click reaction". There are very small aggregate of nanoparticles caused by the presence of small amount of polymerized silane.*

In order to remove the nanowires from silicon wafer several procedure (scotch, curettage) were explored. The best results were obtained using a ultrasound-tip for 10 min (MISONIX, Ultrasonic liquid processors), maintained the fix distance tip-wafer (1 cm) operating with the power around 20% of the amplification (6-7 Watts) in an acetone solution.

The nanosystem was characterized by magnetic study.. The nanowires were dispersed in a small amount of acetone. As shown in Figure 8 magnetization has a value of 10^{-4} emu. This value is very small, and can be attributed to the not sufficient degree of loading and also to the prevalent contribution of nanowires to the weight of the nanosystem.

ICP analysis showed that the total amount of Fe in the sample is 2.4 % meaning that the total amount of Fe_3O_4 results 3.4% of total weight.

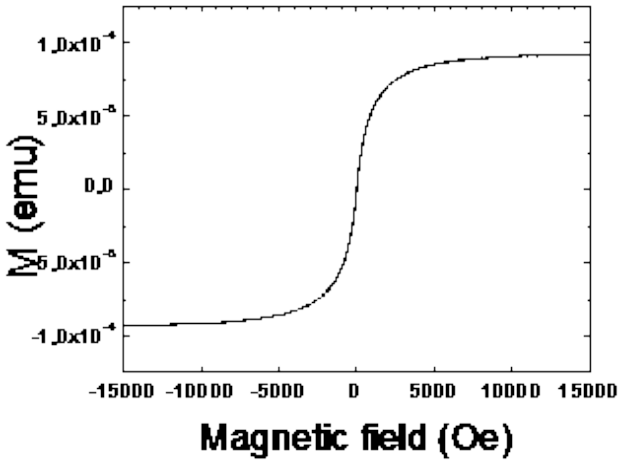

Figure 8. Magnetic Properties: show the saturation value around $1x10^{-4}$ (the value was obtained without normalization)

The graphic, with values normalized for magnetite content, is shown in

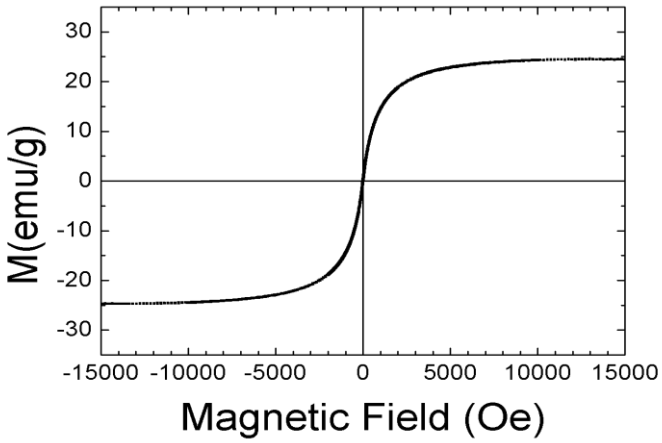

Figure 9 Magnetization vs Magnetic field applied. The value was normalized for the real amount of magnetic nanoparticles.

the Figure 9.

On the basis of this results, we have planned to increase the nanoparticles dimension to improve the magnetic properties.

Experimental Section

Activation of the surface hydroxyl group on Si(100) wafer with nanowires SiC-SiO_x

The wafer sample where were growth nanowires was immersed in 20 mL of HCl (37%) for two hours and heated to reflux for others two hours to active hydroxyl groups (Fig.34).

After it was cleaned in water for restore the neutral pH, so it was dried for few minutes at the air condition.

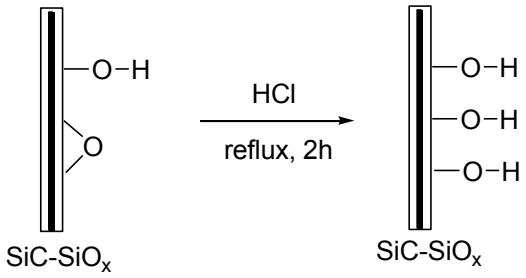

Figure 10: *Surface nanowires activation by acid solution.*

Synthesis of 3-azidopropyltrimethosilane[1516]

To a 25 mL round bottom flask, 3-chloropropyltrimethoxy-silane (1 mL, 5.33 mmol), sodium azide (0.7 g, 10.7 mmol), and N,N-dimethilformamide (7 mL) were added. The reaction mixture was stirred at 100°C for 24 h. After cooling down, the mixture was filtered on Millipore paper and the filtrate was concentrated under reduced pressure to yield yellow liquid that was distilled in oven bubble and obtain transparent liquid as product.

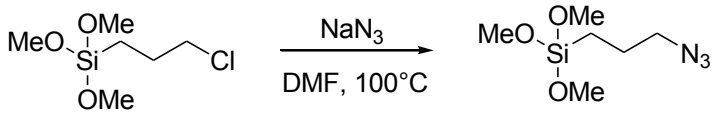

Figure 11: *Synthesis of 3-azidopropyl-trimethoxysilane*

^{1}H-NMR ($CDCl_3$) δ 3.59 ppm (9H, s, OC*H*$_3$), 3.30 ppm (2H, t, J=6.92 Hz, C*H*$_2$-N_3), 1.74 ppm (2H, quint, J=7.76 Hz, CH_2-C*H*$_2$-CH_2-N_3), 0.74 ppm (2H, t, J= 8.08 Hz, Si-C*H*$_2$-).

Yield= 90%.

Functionalization nanowires with of 3-azidopropyltrimethosilane[17]

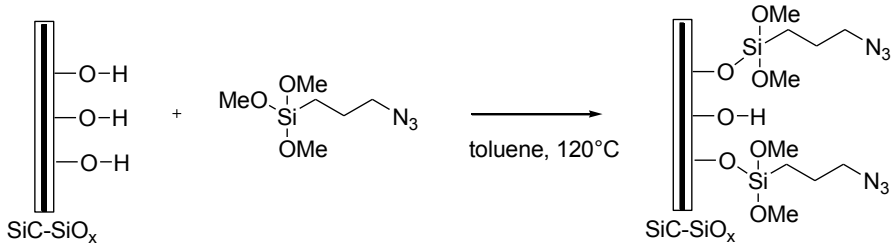

Figure 12: *Functionalization of nanowires with silane*

To a 100 mL round bottom flask, nanowires sample, 3-azidopropyltrimethoxisilane (1 ppm, in toluene) was added; it was stirred at 120 °C overnight. After cooling down, the wafer was washed with dry toluene for several times, so it was cleaned and sonicate for 15 minutes in dry toluene. The Si-wafer was dried for few minutes at the air condition.

Synthesis of a new link between the nanoparticles and nanowires by click chemistry

The functionalised sample was placed in a solution of hexane (7 mL), dichloromethane (7 mL), acetone (7 mL), methanol (7 mL) with CuI (2 mg, 0.01 mmol) as catalyst, MNP (10 mg), mechanically stirred overnight. The wafer was cleaned by many washing with different *solvents, and then dried*.

The wafer with nanowires was leave inside a glass becker with the nanowires on the top surface, and 40 ml of acetone and after the centrifugation the suspension was moved into micro-desposeable for centrifugation and after that centrufigated for 5' at 13000 rpm. The extra acetone was removed and the nanowires were concentrated in less disposable until the total remotion of acetone.

References

[1] *C*. Streffer, P. Valupel and G. M. Hahn, *Biological Basis Of oncologic Thermotherapy*, Springer, Berlin, (**1990**)

[2] I. Ojima, G.D. Vite and K. H. Altmann *Anticancer Agents: Frontiers in Cancer Chemotherapy*, ed., American Chemical Society, Washington DC, (**2001**)

[3] H. Gu, K. Xu, Z. Yang, C. K. Chang and B. Xu *Chem*. *Commun*., *4270-4272(***2005**)

[4] S. Saddow, Silicon Carbide Biotechnology: A Biocompatible Semiconductor for Advanced Biomedical Devices and Applications, Elsevier MA, USA, / *ISBN-10: 0123859069 / ISBN-13: 978-0123859068 / Edition: 1(***2011***)*

[5] A. Cacchioli, F. Ravanetti, R. Alinovi, S. Pinelli, F. Rossi, M. Negri, E. Bedogni, M. Campanini, M. Galetti, M. Goldoni, P. Lagonegro, R. Alfieri, F. Bigi,and G. Salviati doi.org/10.1021/nl501255m (**2014**)

[6] M. Klokkenburg, B. H. Erné, A. Wiedenmann, A. V. Petukhov, and A. P. Philipse, *Phys*. *Rev*. E 75, 051408, (**2007**); K Yang, H Peng, Y Wen, N Li. *Applied Surface Science* 256 (10), 3093-3097, (**2010),** M.Klokkenburg, J. Hilhort, B. H. Ernè *Vibrational Spectroscopy* 43 243; (**2007**)

[7]G. Attolini, F. Rossi, M. Bosi, B.E. Watts, G. Salviati Journal of non-crystalline solids 354 5227-5229 (**2008**)

[8] [9] G. Kwak, M. Lee, K. Senthil, and K. Yong; *Langmuir*, 26 (14), 12273-12277 (**2010**)

[9] W. Chang; *2008 NNIN REU Research Accomplishment* (**2008**)

[10] S. Saddow, Silicon Carbide Biotechnology: A Biocompatible Semiconductor for Advanced Biomedical Devices and Applications, Elsevier MA, USA, / *ISBN-10: 0123859069 / ISBN-13: 978-0123859068 / Edition: 1(***2011***)*

[11] G. Attolini, F. Rossi, M. Bosi, B.E Watts., G. Salviati, J. *Non-Cryst*. *Solids*, 354, 5227 (**2008**)

[12] H. C. Kolb, M. G. Finn and K. B. Sharpless *Angewandte Chemie International Edition* **40** (11): 2004–2021(**2001**)

[13] *Chemical Reviews*, Vol. 108, No. 8 2957 (**2008**)

[14] "Lorentz microscopy shed light on the role of dipolar interactions in magnetic hyperthermia" M. Campanini, R. Ciprian, E. Bedogni et al.

[15] P. Paoprasert, J. W.Spalenka, D. L.Peterson, R. E. Ruther, R. J. Hamers, P. G. Evans and P. Gopalan *J.Mater.Chem.,* 20, 2651-2658*(**2010**)*

[16]S. Sun, H. Zeng, D. B. Robinson, S. Raoux, P. M. Rice, S. X. Wang, and G. Li *J. Am. Hem. Soc*. 126, 1, (**2004**)

[17] F. Cattaruzza, D. Fiorani, A. Flamini, P. Imperatori, G. Scavia, L. Suber, A. M. Testa *Chem. Mater*., 17, 3311-3316 (**2005**).

Synthesis and characterization of various porphyrins

Introduction

Porphyrins constitute a large class of fluorescent pigments, of synthetic or natural origin, characterized by an intense red or purple color. They are formed by a macrocyclic containing 22 π electrons, 18 of which are delocalized in the aromatic ring, according to the Huckel rule [4n + 2] for the aromaticity (n = 4). The porphyrin ring is formed by four pyrrole rings linked by four methine bridge carbons. The synthesis of porphyrins has gained special attention in recent years because of their relevant applications in biomedical sciences[1]

The IUPAC nomenclature provides for the numbering of all the carbons of the ring, including the nitrogen atoms, so that the two saturated nitrogens receive the numbers 21 and 23. The positions 1, 4, 6, 9, 11, 14, 16 and 19 are indicated as α-pyrrole, the positions 2, 3, 7, 8, 12, 13, 17 and 18 are called β-pyrrole and the positions 5, 10, 15 and 20 meso.

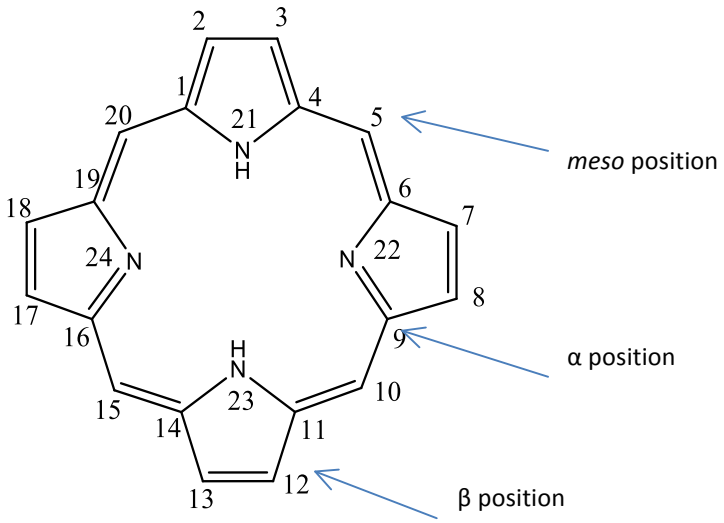

Figure 1.

The atoms of alkyl chain substituents are indicated with the number of carbon porphyrin which are linked to, with an apex that represents the number of links away. NMR analysis, crystallographic and theoretical studies have shown that the forms thermodynamically more favored for symmetrically substituted porphyrins are the two degenerate tautomer *trans* NH. The migration of protons between the two seems to proceed through a mechanism in stages, through the less favored *cis* tautomer.

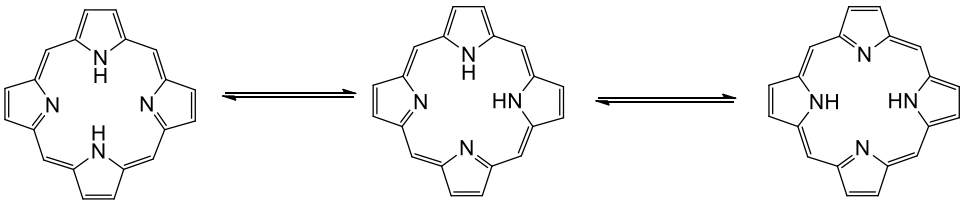

Figure 2

Porphyrins are used for many applications: for example, as catalysts in oxidation reaction[2], or in electron transport chains or as a photosensitizer for photodynamic therapy in cancer treatment.[3]

Each application requires different substituents on the porphyrins, in order to improve different characteristics. Naturally occurring porphyrins are synthetized by living systems. Among the best known natural porphyrin-based molecules, there are vitamin B_{12}, chlorophyll and Heme[4]. Heme, the most important porphyrin for human life, is an iron-protoporphyrin complex functionalized in β position, as depicted in *Figure 3*. Protoporphyrin IX, with highly reactive vinyl groups, is the fundamental skeleton of Heme B, and it is present in living systems, since hemoglobin and myoglobin are examples of oxygen transport proteins containing Heme B. (*Figure 3*).

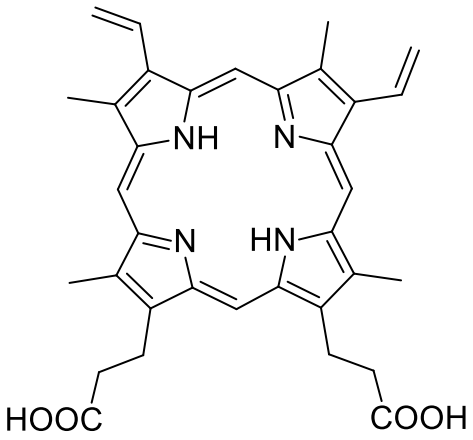

Figure 3. Protoporphyrin IX.

Carboxy-substituted porphyrins are attractive synthetic targets since they are present in many different natural porphyrins. Moreover, the presence of carboxy groups allows the further functionalization of porphyrins and allows to anchor them on different inorganic surface to obtain hybrid-nanosystems.

The aim of my PhD work was to functionalize the surface of core-shell SiC-SiO_2 nanowires with a monolayer of porphyrins by covalent bonds. The coverage of this type of nanowires with a fluorinated porphyrin was performed by Dr. Iannotta's group in Trento (CNR Institute) using a high energetic technique called SUMBD (SUpersonic Molecular Beam Deposition). A tetra-phenylporphyrin with perfluorinated phenyl rings was employed because the presence of halogen was reported to improve the porphyrin activity in singlet oxygen generation. Moreover a sufficient thermal stability and volatility of the sample is required in this technique. An energy transfer from the SiC-SiO_2 nanowires to the attached porphyrin was observed, causing fluorescence emission of the porphyrin when the sample was irradiated by X-Rays. [5]

We designed a new approach for the functionalization of the nanowires, consisting in the formation of a monolayer of the organic compounds linked by covalent bonds. Exploiting this method, a large variety of porphyrins can be used and it is also possible to link additional

nanostructures such as magnetic nanoparticles. Tetraphenyl porphyrins containing different number of perfluorinated and carboxylated phenyl rings were prepared and then derivatized to introduce functional groups able to covalently bind the nanowires.

Results and Discussions

The porphyrins reported in Figure 4, containing different number of perfluorinated and carboxylated phenyl rings, were prepared following different synthetic approaches.

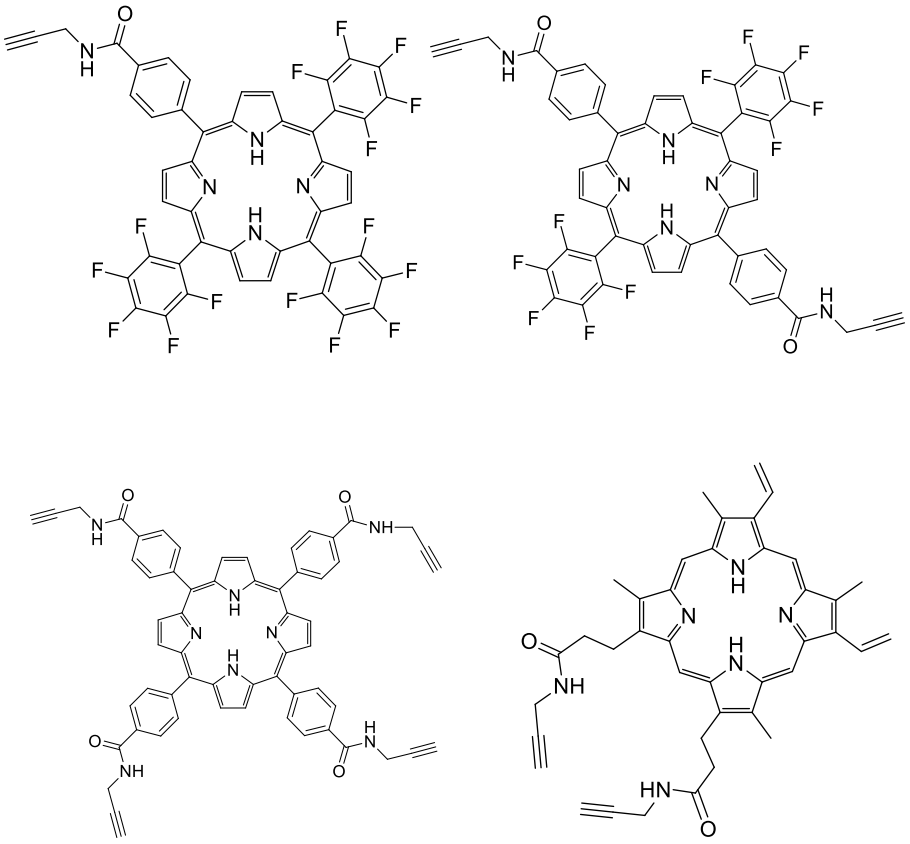

Figure 4.

The most common methods to synthetize porphyrins *meso* and or β-substituted are:

- The tetramerizationof pyrroles with aldehydes,

- Condensation [2+2],
- Condensation [3+1],
- The cyclization of tetra-pyrroles.

In all the cases the addition of oxidant to obtain the aromatic porphyrin ring is required.

The Linsdey method[6], involving pyrrole and aldheydes, is suitable for the synthesis of porphyrins with four identical groups in the *meso* positions , and it can be also used for porphyrins having different substituents, This method consists in mixing aldehyde and pyrrole in a specific ratio, at room temperature in presence of BF_3*OEt_2, followed by addition of oxidant reagent. If different aldehydes are present, a mixture of various isomeric products is obtained, thus a burdensome chromatography work is required for separation. A more rational synthesis involves dipyrromethanes units formed by two pyrrole rings joined by a methine bridge. In this case, the synthesis of porphyrins is performed via [2 + 2] condensation in the same conditions of the Lindsey's method of. By dipyrromethans you can get other intermediates, participating in the condensation [3 + 1] with a fourth unit or intermediate tetrapyrrolic that are also useful in the synthesis of asymmetric porphyrins through intramolecular cyclization.

The general syntheticsteps to obtain the porphyrins **depicted in Figure 4,** are the following:

- synthesis of macrocycle, there are different methodologies
- oxidation of macrocycle with 2,3-Dichloro-5,6-dicyano-1,4-benzoquinone (DDQ) to obtain the porphyrin ring (as reported in the following picture).

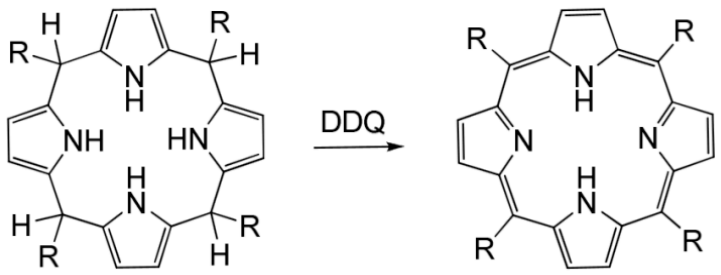

Figure 5. *Oxidation of porphyrinogen cycle to porphyrin ring.*

- conversion of the free carboxy groups present in the phenyl ring into amide group containing a carbon-carbon triple bond. To this end, the carboxy groups were activated by the typical condensing agents employed in peptide synthesis.

In particular, the acid carboxy group of porphyrin was reacted with N-(3- dimethylaminopropyl)-N'-ethylcarbodimide (EDC) producing active intermediate (PT), that further reacted with1-hydroxybenzotriazole (HOBt) forming the intermediate PV. This compound can react directly with an alkyl amine or can form a further intermediate salt with 4-dimethylaminopyridine (DMAP) before reacting with the alkylamine. (*Scheme 1*)

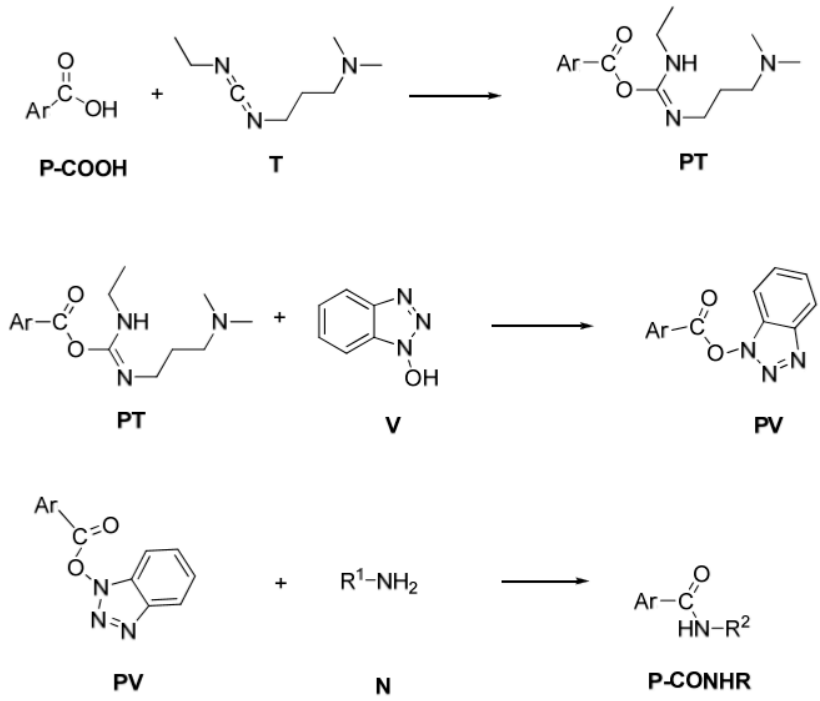

P-COOH= acid porphyrin, T= 1-ethyl-3-(3dimethylaninepropyl)carbodimmide (EDC), PT=intermediate1; V=hydroxybenzotriazole (HOBt), PV=intermediate2, N= amine, P-CONHR=amide porphyrin

Scheme 1. *Mechanism of activation of acid carboxy group to give amide group.*

We decided to functionalize the porphyrin through an amide bond rather than an ester group in order to minimize the possibility of hydrolysis in aqueous medium, that will cause porphyrin loss from the hybrid nanosystem.

Compound **9** was prepared following the synthetic scheme reported below.

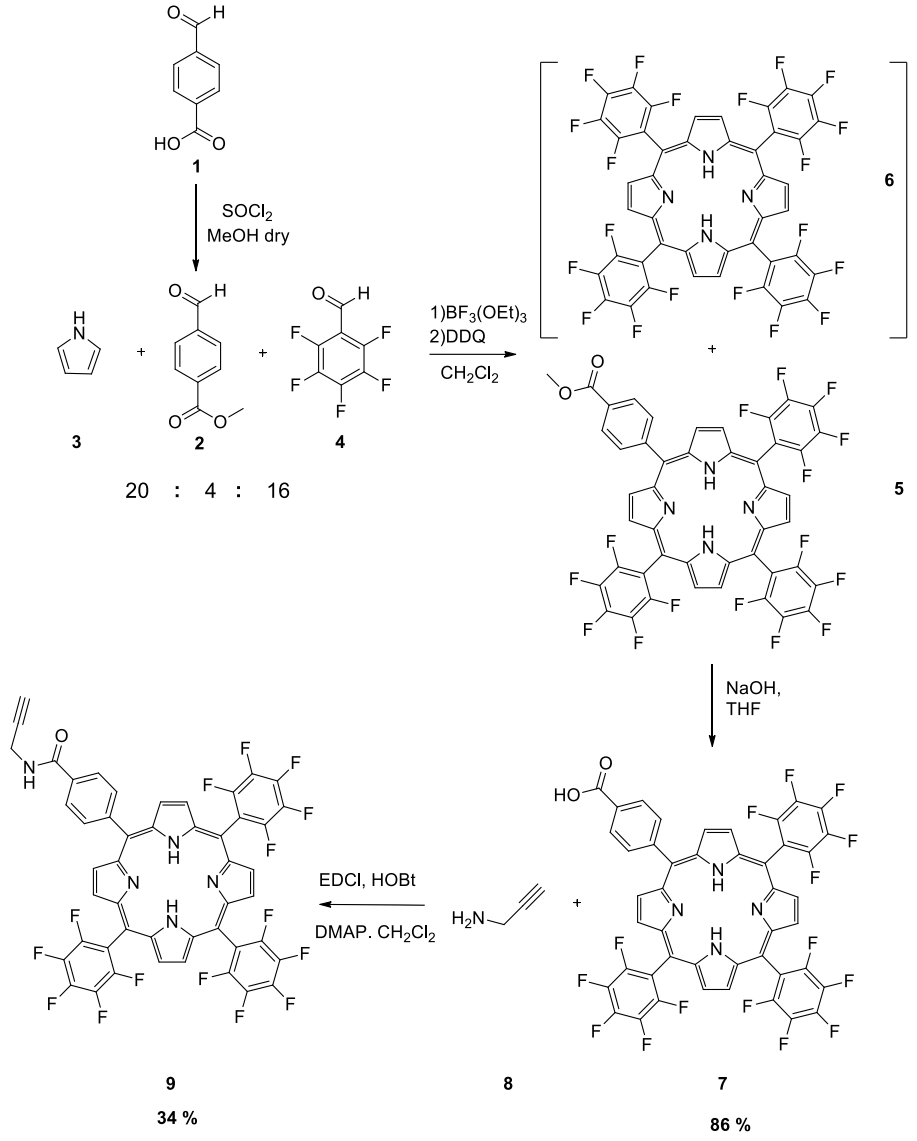

Scheme 2. *Reactive scheme for the synthesis of compound* ***9***

Following a method reported in the literature [9], the synthesis of the porphyrin **5** occurred via one pot procedure starting from pyrrole and the two different aldehydes, the pentafluorinated benzaldehyde **4** and 4-methoxycarbonylbenzaldehyde **2**.

Obviously, this reaction was not selective and the desired porphyrin was isolated by column chromatographic separation from the *meso*-porphyrin having four perfluorinated phenyl rings and from other porphyrins as well as from other kind of by-products, such as *non*-cyclic oligomers and derivatives of oxidizing agents. It is well known that the syntheses of porphyrin macrocycles often give low yields due to the presence of various by-products.

The porphyrin **5**, isolated in 9% yield, was treated with NaOH to hydrolyze the ester group (86% yield). The acid carboxylic group was converted into amide group using condensing agents for its activation. After reaction with propargyl amine, the desired compound **9**, a porphyrin bearing a terminal alkyne-terminal group useful for conjugation to the nanowires, was obtained in 34% yield.

Compound **9,** unreported in the literature, was fully characterized by ^{1}H-NMR, ^{13}C-NMR, UV-Vis and fluorescence spectroscopies and MALDI-TOF mass spectrometry. In *Figure 6* the UV-Vis and fluorescence spectra are shown.

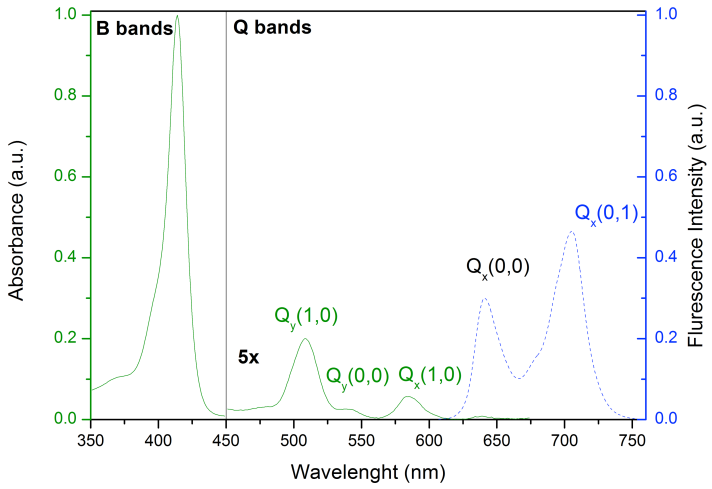

Figure 6. *UV-Vis and Fluorescence spectra of porphyrin* ***9.***

One of the most distinctive features of porphyrins is their UV-Vis absorption spectrum, determined by the aromatic π electronic system. These compounds show intense absorption bands in the visible between 400 and 450 nm with some variability due to the presence of substituents in the meso positions and β-pyrrole. These bands, called B or **Soret**, represent transitions attributable to the second excited state, $S_0 \rightarrow S_2$. At higher wavelengths, about 500-700 nm, much less intense bands denominated **Q** are observed, as identification of electronic transitions $S_0 \rightarrow S_1$ "semi-permitted" by the selection rules. These bands are in turn divided into two further signals due to vibronic transitions 0-0 and 0-1. The number and the relative intensity of the bands Q (classified increasing order of λ as IV, III, II and I) are diagnostic to determine the symmetry of substitution of the porphyrin and the state of metalation. In the case of metalated *meso* porphyrin the Q bands are only two, due to the symmetry change.

Figure 7 reports the ^{1}H-NMR spectrum and the signal attribution. In particular, diagnostic signals are the singlet at -2.8 ppm (violet), due to pyrrole NH inside the aromatic macrocycle, and the triplet at ca. 6.7 ppm (green), due to amide NH.

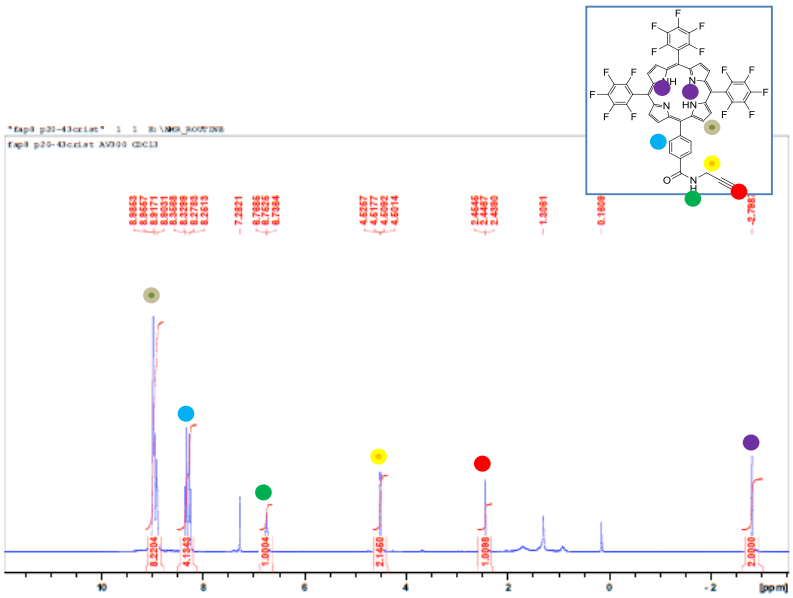

Figure 7. *^{1}H-NMR of porphyrin* ***9***

In the aromatic area there are protons due to pyrrole (light gray) and to *para*-substituted phenyl ring (light blue). The yellow and red signals are attributed, respectively, to CH_2 and terminal CH of the propargylic chain.

To synthesize compound **13**, the [2+2] condensation procedure was followed, as depicted in *Scheme 3*.

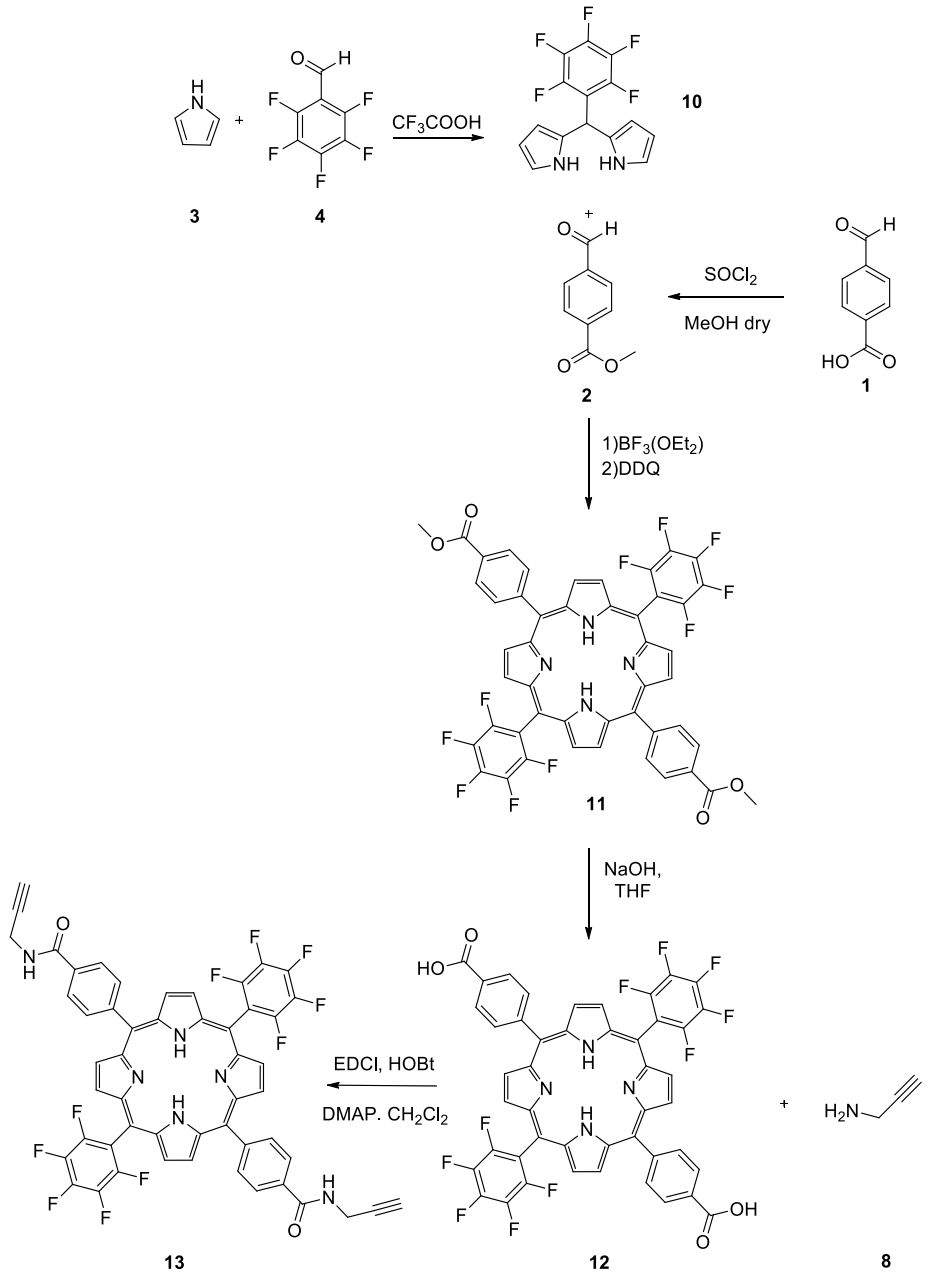

Scheme 3.

The synthesis of porphyrin **13,** having two perfluorinated aromatic rings and two carboxylated aromatic rings, was performed in two steps, according to a condensation [2 + 2]. First dipyrromethane (**10**) was

prepared by reacting the pyrrole **3** and the pentafluorobenzaldehyde **4** under acid catalysis using CF_3COOH. It was then reacted with methyl 4-formylbenzoato (**2**) in the presence of $BF_3(OEt_2)$ to form the cycle, which is oxidized "one pot" with 2,3-dichloro-5,6-dicyano-1,4-benzoquinone (DDQ) to give porphyrin **11.** The hydrolysis of the two ester groups under basic conditions afforded the porphyrin **12** with the two acid groups , compound not reported in the literature. We were able to separate the product, formed in high yield, from unreacted substrate just washing the aqueous phase with CH_2Cl_2, where the ester derivative is soluble while the carboxylic acid is not. Dichloromethane extracted quantitatively the porphyrin **13** from the aqueous phase, as easily observed by the change of the color of the two phases. The last step was the transformation of the functional group into amide, activating the carboxy group by the condensing agents as previously described, and reacting it with the propargyl amine **8**. Compound **13** was obtained in 60 % yield after purification by preparative thin layer chromatography.

Compound **13**, unknown in literature, was fully characterized by ^{1}H-NMR, ^{13}C-NMR, UV-Vis and fluorescence spectroscopies, MALDI-TOF mass spectrometry.

The ^{1}H NMR spectrum and the UV-Vis and fluorescence spectra are reported in *Figure 8* and *9* respectively, and are quite similar to those described for porphyrin **9**.

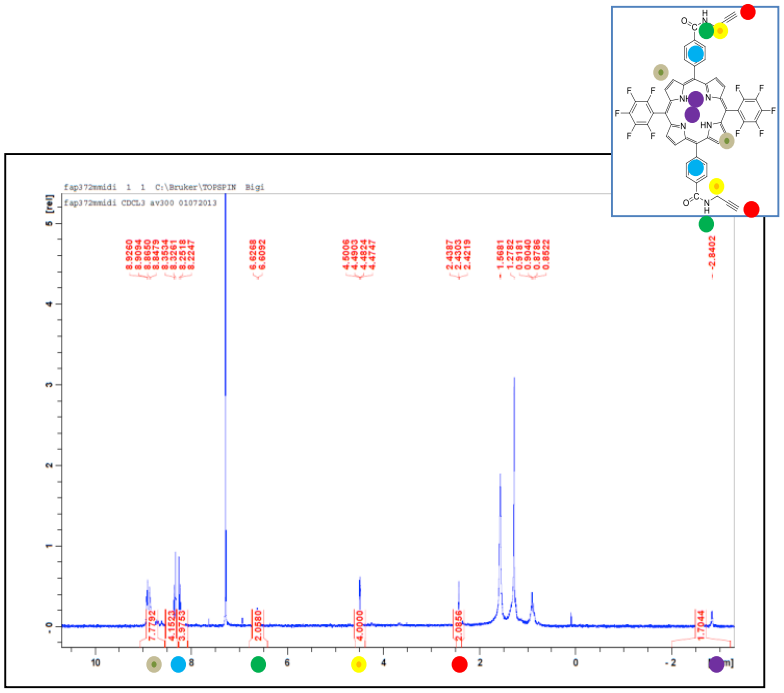

Figure 8. *^{1}H-NMR shows protons of porphyrin* ***13***

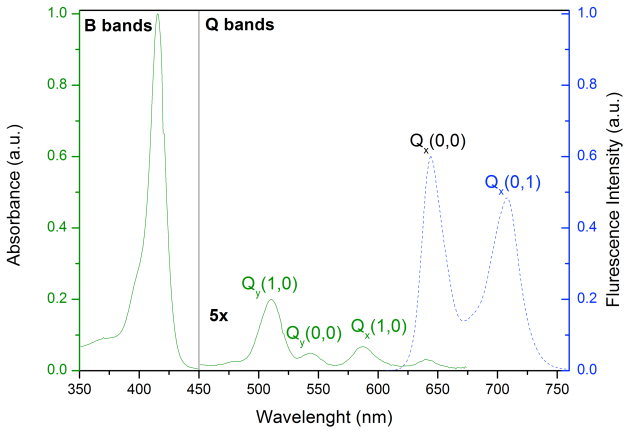

Figure 9. *UV-Vis and fluorescence spectra of compound* ***13***

The synthesis of porphyrin **15**[7] was accomplished starting from the *meso* tetra(4-carboxyphenyl)porphyrin (H_2TCPP) **14**, a commercially available compound that can be easily prepared by reaction of pyrroles and 4-carboxybenzaldehyde in the presence of propionic acid.

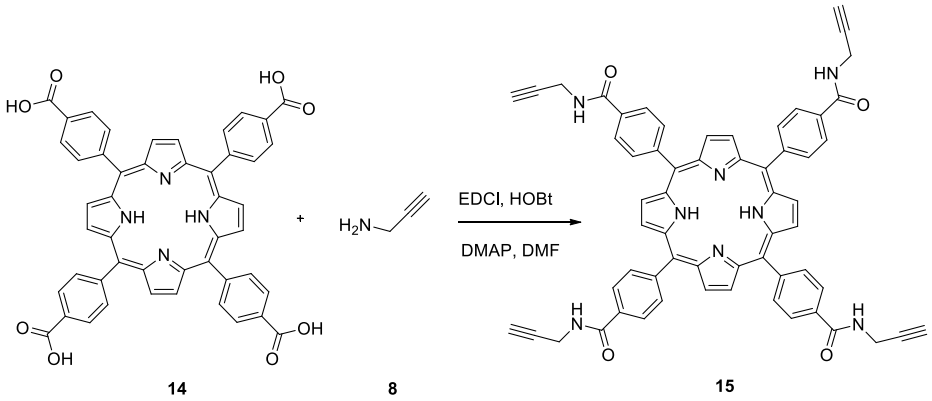

Scheme 4. *Scheme of synthesis of porphyrin* ***15***

In this case the derivative product contains four C≡C ending groups, that should allow an easier functionalization of the nanowires. As usually occurs for porphyrin separation, the purification of **15** by flash chromatography was not satisfactory, giving only a 65 % yield even if the reaction conversion was complete. Therefore, we studied the optimization of the isolation and purification procedure.

After DMF rimoval, the crude was dissolved in ethyl acetate and washed with water. After acetate evaporation, the ^{1}H-NMR analysis of the crude product showed traces of the coupling agents (in particular DMAP and HOBt). Examining the solubility of the porphyrin and the condensing agents in various solvent (*Figure 10*), we found out a procedure that allowed to skip the chromatographic separation.

Solvent	DMAP	HOBt	Porphyrin*
CH_2Cl_2	S	NS	PS
$CHCl_3$	S	PS	PS
ACOEt	PS	S	PS
hexane	NS	NS	NS
MeOH	S	S	PS
AcOEt: MeOH 1:9	S	S	PS
EtOH	S	S	PS
Et_2O	NS	NS	NS
THF	PS	S	S
1-propanol	PS	PS	PS
MeOH: H_2O 9:1	S	S	PS
MeOH: H_2O 1:1	S	S	NS
MeOH: H_2O 1:9	S	S	NS
H_2O	S	PS	NS

Legend: $S = soluble$, $PS = partially\ soluble$, $NS = not\ soluble$

***Figure 10**. Study of solubility.*

The low solubility of the porphyrin ruled out the possibility to purify it by crystallization from a single solvent. Thus, it was decided to dissolve the crude in THF and then to use water as precipitating agent. Indeed, dropping increasing amount of water (100 mL in 5 mL of THF) the precipitation of the pure porphyrin **15** was obtained in 90% yield. The compound was characterized by ^{1}H and ^{13}C-NMR, UV-vis and fluorescence spectroscopies. ^{1}H-NMR spectrum of the isolated porphyrin shows the typical signals at $\delta = -2.92$ ppm, due to the pyrrolic N-H, and one due to the amidic N-H at $\delta = 9.33$ ppm (*Figure 11*), evidencing that the amidation reaction occurred completely.

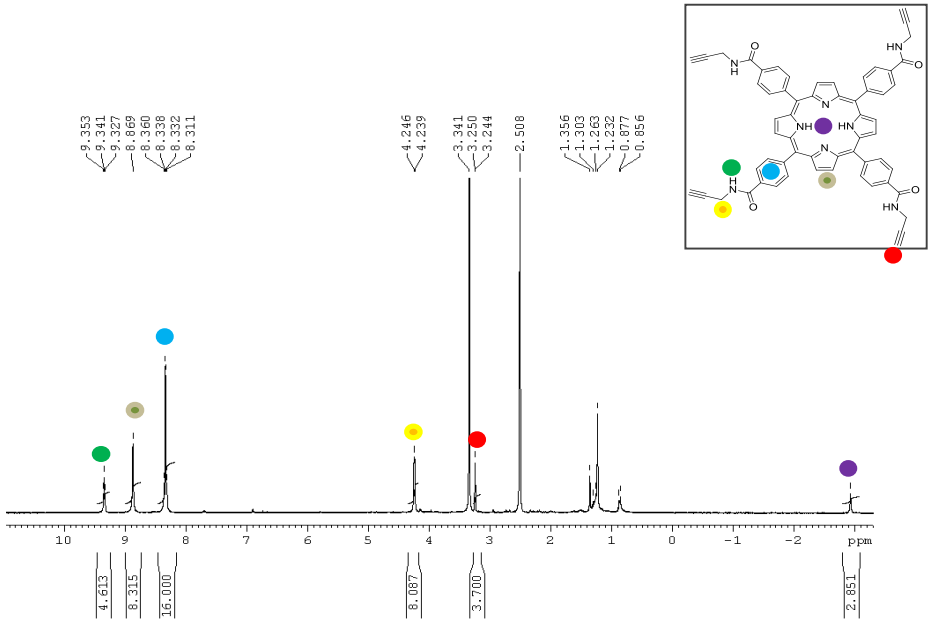

Figure 11. *^{1}H-NMR of compound **15** (300 MHz, DMSO-d6))*

Figure 12 shows the typical absorption profile of a porphyrin compound: the so-called B band (or Soret band) in at 419 nm and the Q bands at 515, 553, 589 and 645 nm. The absorption bands arise from transitions between HOMOs and two LUMOs: the transition from the ground state to the second excited state corresponding to the Soret band while the transition from the ground state to the first one corresponds to the Q bands. The Q bands are a set of four absorption arising from HOMOs to $\pi*$ transitions. Of these, the first set of two lines is x-component of Q while the second set is its y-component. Both of these Q_x and Q_y components are composed of two types of vibrational excitations too, the lower energy one being Q (0,0) and the higher one Q (0,1). Thus the four lines in set are Q_x(0,0), Q_x (0,1), Q_y (0,0) and Q_y (0,1) in the increasing order of energy. In the fluorescence spectrum two bands are shown, at 522 nm and 557 nm, due to the Q_x (0,0) and Q_x (0,1) transitions.

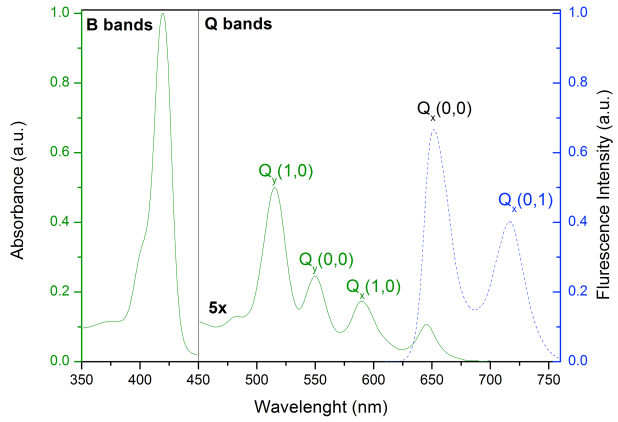

Figure 12**. UV-Vis Spectra of compound **15

The synthesis of porphyrin **17** was performed starting from commercially available protoporphyrin IX (PpIX) **(16),** through a coupling reaction as reported in the previous synthesis.

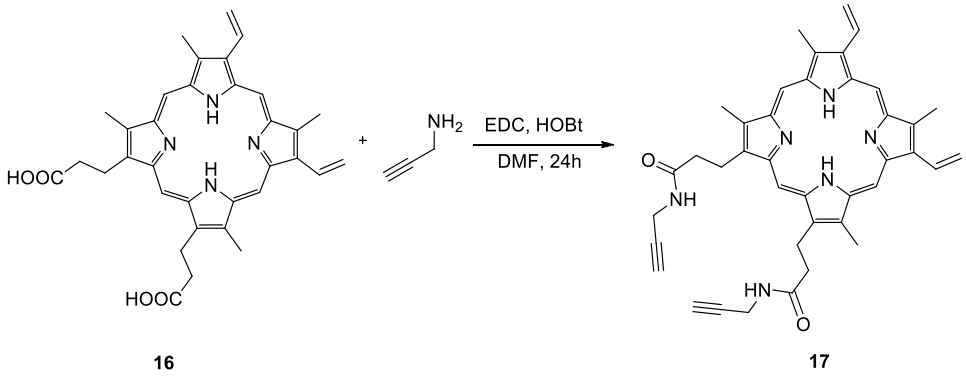

16 **17**

***Scheme 5.** Synthesis of porphyrin **16,** starting from PpIX (16) this compound is photosensitizer II generation in PDT.*

The synthesis reported in the literature[8] resulted to be *non* reproducible mainly regarding the isolation and purification steps, and in addition

the compound characterization was not well described. Therefore, we developed a new procedure.

The formation of the amide bonds was carried out using the coupling agents following the procedure reported above. The reaction was protected from light sources, as the vinyl groups of PpIX easily give a photooxidation process. The obtained product has a very low solubility in most common organic solvents; this fact, combined with its instability, made difficult the process of purification.

The search for a low-boiling solvent able to extract compound **17** from water showed that chloroform could be employed successfully. However, it was not able to dissolve the product completely making troublesome the anhydrification procedure. In addition, the purification resulted very difficult since the chromatographic separation on gel (by column or thin-layer) met very serious problems due to product degradation. To overcome this drawback, the purification by crystallization or precipitation was examined. Good results were obtained dissolving the crude in chloroform and adding hexane, a solvent in which it is insoluble. The precipitation of porphyrin **17** occurred in pure form. Other pairs of solvents which gave good results were CH_2Cl_2 / hexane and CH_2Cl_2 / MeOH. This procedure allowed to isolate **17** in 78% yield. The product was then stored at 4 °C, in the dark and under N_2.

The problems related to the PpIX and his derivative is that they present a high photoreactivity with oxygen, which results in the oxidation of the vinyl groups by simple exposure to ultraviolet/ visible in the presence of air, when the molecule is in solution. Studies reported in the literature showed that the photo-oxidation of PpIX dimethyl ester can proceed through two mechanisms. The photo-induced degradation products of the PpIX are reported in the following figure.

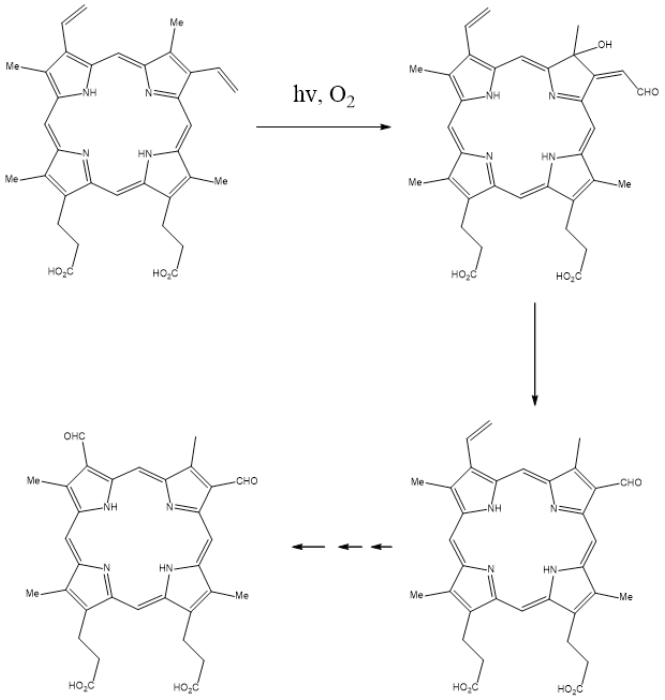

Scheme 6. *Degradation of Pp IX*

The UV-Visible spectrum of porphyrin **17** in chloroform is reported in Fig. *13*, and shows the typical absorbment bands, the Soret band (or B band) and the four Q bands. *Figure 14* shows the fluorescence spectrum of **17**.

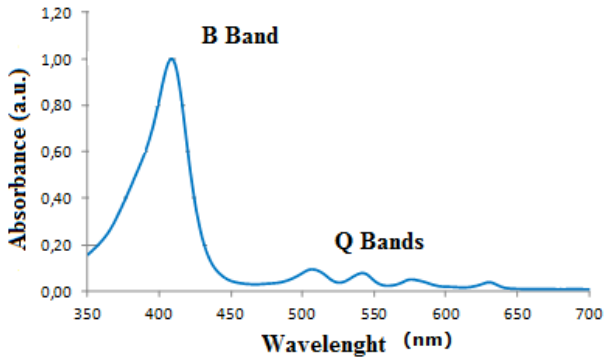

Figure 13. *UV-Vis spectrum of Porphyrin 17.*

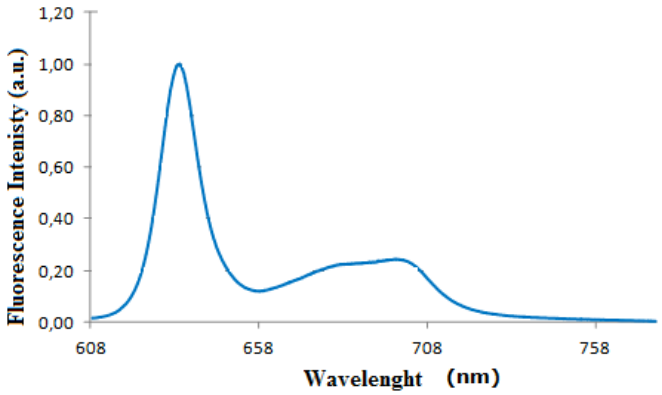

Figure 14 *Fluorescence spectrum of porphyrin 17.*

Experimental section

Synthesis of compound **2**[9]

In a three-necked flask of 100 ml was introduced the acid-4-formylbenzoic (1.5 g, 10 mmol) and 30 ml of anhydrous methanol under nitrogen flow. The solution was immersed in a bath of ice and water in order to cool it down to 0 °C and kept under stirring by magnetic stir bar. Upon reaching the temperature, $SOCl_2$ (6 ml, 84 mmol) was dropped in . The reaction was allowed to go under stirring at room temperature overnight. The solution was filtered and evaporated by rotary evaporator, giving an oil as residue. The oil was added drop wise to 100 ml of distilled water. During the addition it was observed the formation of a yellow suspension which was subsequently filtered on a Buchner funnel and collected in a volumetric flask. The remaining aqueous phase was extracted twice with ethyl acetate using a separatory funnel. The collected organic phase was dried with anhydrous Na_2SO_4, filtered and evaporated, giving a solid that was added to the previuos one. The purification was done by recrystallization: the yellow oil was dissolved in hot hexane and crystallized giving a white solid, that was filtered and dried under vacuum. 1.19 g (73 % yield) of compound 2 were obtained.

^{1}H-NMR (300 MHz) $CDCl_3$ δ: 3.98 ppm (3H, s, CH_3), 7.98 ppm (2H, d, H-arom , J=8.7 Hz), 8.22 ppm (2H, d, H-arom, J=8.4 Hz), 10.12 ppm (1H, s, C*H*O).
MS (EI, 70 eV): M^+ 164 (52), 133 (100), 105 (36), 77 (45), 51 (39)

Synthesis of compound **5**[10]

In 1 L flask with one neck were introduced the three reagents and dissolved in CH_2Cl_2, the solution was then degassed by N_2 flow for 30' and kept under stirring by magnetic stir bar. The reaction system was protected from light by covering the flask and the condenser with

aluminum foil. It was added to the catalyst BF_3: diethyl ether (1: 1). Using a water bath the reaction was brought to 37 ° C and kept under magnetic stirring for 40 hours. To follow the oxidant was added the tetrachloro-1,4-benzoquinone and the reaction was allowed to go under stirring for a further 3 hours always at 37 °C. The crude reaction was pulled dry with a rotavapor and was then purified by column chromatography (yield = 9%).

^{1}H-NMR (300 MHz) $CDCl_3$ δ: -2.82 ppm (2H, s, NH), 4.15 ppm (3H, s, CH_3), 8.33 ppm (2H, d, H-arom, J= 8.1 Hz), 8.50 ppm (2H, d, H-arom, J= 8.1 Hz), 8.83-8.95 ppm (8H, m, βH pyrroles).
Product **6** was obtained like at secondary product with a yield of 10%.
^{1}H-NMR (300 MHz) $CDCl_3$ δ: -2.89 ppm (2H, s, H-Pyrrole, NH), 8.94 ppm (8H, s, H-arom).

Synthesis of compound **7**[11]

In a 100 ml flask was introduced that the porphyrin was dissolved in THF, the solution was added of 2 M NaOH under magnetic stirring. The reaction was brought to 70 °C using an oil bath and was allowed to reflux for 10 hours; the reaction system was protected from light by covering the flask with aluminum foil. The reaction was maintained for a further 2 hours under stirring magnetic at 80 °C.

The solvent was evaporated by rotatory evaporator; the residue was dissolved in 300 ml of CH_2Cl_2 and acidified with a solution of HCl at 37% by weight until the mixture became a dark green color. With separating funnel, the organic phase was collected moment it was observed a color change of the solution from green to purple. The organic phase was dried with anhydrous Na_2SO_4, filtered and evaporated to dryness in a rotavapor. The obtained solid was dried by use of a pump (yield = 86%).

^{1}H-NMR (300 MHz) $CDCl_3$ δ:-2.87 ppm (2H, s, N*H*), 8.41 ppm (2H, d, H-arom, J= 7.8 Hz), 8.63 ppm (2H, d, H-arom, J= 8.1 Hz), 8.89-8.98

ppm (8H, m, βH-pyrrole).

Synthesis of compound **9**

In a three-necked flask of 100 ml was introduced reagent and dissolved in CH_2Cl_2. To the solution were added condensing agents maintaining the system under nitrogen flow and under stirring by magnetic stir bar. After thirty minutes was also added to the DMAP and propargylamine, the reaction was allowed to go under stirring for a whole night. The crude reaction was carried out a TLC control (eluent hexane: CH_2Cl_2 =7: 3) to verify the successful disappearance of the acid-porphyrin. The reaction solvent was pulled dry with a rotavapor and extraction was performed in CH_2Cl_2 and H_2O *via* separatory funnel. The organic phase was dried with anhydrous Na_2SO_4, filtered and evaporated to dryness in a rotavapor. On the product was carried out a new TLC to check the actual purity of the compound obtained and it was decided to proceed with a chromatographic column to separate it better, as the eluent was used with 100% CH_2Cl_2. After extraction by column chromatography were combined, the test pieces which had the same spots in different balls, the eluent was evaporated by rotatory evaporator and pulled dry by the use of a pump. To further purify the product it was effectuated a recrystallization in MeOH (yield = 34%).

^{1}H-NMR (300 MHz) $CDCl_3$ δ: -2.80 ppm (2H, s, N*H*), 2.45 ppm (1H, t, -C≡C*H*, J_2= 2.4 Hz), 4.51 ppm (2H, dd, -CH_2N, J_1=5.1 Hz, J_2= 2.4 Hz), 6.75 ppm (1H, t, -N*H*CO, J_1= 5.1 Hz), 8.26 ppm (2H, d, H-arom, J= 8.1 Hz), 8.34 ppm (2H, d, H-arom, J= 8.1 Hz), 8.89-8.99 ppm (8H, m, β).
^{13}C-NMR (400 MHz, CDCl3) δ: 30.15 ppm; 72.20 ppm; 79.54 ppm; 125.78 ppm; 134.76 ppm; 134.76 ppm.

^{19}F-NMR (400 MHz, CDCl3) δ: -161.49 (6F, m, ArF), -151.54 (3F, m, ArF), -136.60 (4F, dd, J=7.6 Hz, 25.2 Hz, ArF), -136.45 (2F, dd, J=7.6 Hz, 24.8 Hz, ArF).

MALDI-TOF MS

Matrix: alpha-cyano-4-hydroxycinnamic acid

m/z calculated: 965,679 *m/z* experimental: 965,367

Spectroscopy UV-Vis
Solvent: CH_2Cl_2
Sample concentration: 2,068 x 10-6 M
λ = 414 nm ε = 306552 M-1·cm-1
λ= 509 nm ε = 5817 M-1·cm-1
λ= 414 nm ε = 18442 M-1·cm-1
Spectroscopy IR
υ 3999 cm-1 stretching N-H amide
υ 2124 cm-1 stretching C≡C
υ 1649 cm-1 stretching C=0
Dark purple powder

Synthesis of compound **10**[12]

In a 100 ml flask were introduced 0.5 ml (4.05 mmol) of pentafluorobenzaldehyde (4), 12.58 ml (180 mmol) of pyrrole (3) and nitrogen flush was done for 20 minutes, before adding 0.031 ml of CF_3COOH under magnetic stirring, and left to react at room temperature for 30 minutes. After this time the mixture of reaction is diluted with about 100 ml of CH_2Cl_2, and then treated with 100 ml of NaOH 0.1 M. It the organic phase is separated from the aqueous phase by separating funnel and is washed 3 times with H_2O. The organic phase was dehydrated with anhydrous Na_2SO4; the CH_2Cl_2 was removed for means of rotary evaporator. You get dark brown oil; this was due to the pyrrole. The unreacted pyrrole is was removed under high vacuum by heating at 60 °C. Analysis is performed on the GC-MS for control the degree of removal of the pyrrole. It was decided to proceed with the transition without subsequent purification of the compound. The compound obtained with a yield of 80% (1.01 g).

GC-MS: m/z = 312 (M+), 291 (11.4), 246 (45.7), 145 (72.4), 67 (45.7)

Synthesis of compound **11**[13]

In a 500 ml flask were placed 1.096 g (3.51 mmol) of 10, 0.577 g (3.51 mmol) of 2 in 353 ml of $CHCl_3$, was made flush nitrogen for 20 minutes, stirring magnetically then are added 0.143 ml of BF3 (OEt_2). After 24 hours, were added 0.597 g (2.63 mmol) of DDQ and the reaction was under stirring for 24 hours. It been eliminated the solvent and the residue was dissolved in 200 ml of toluene. They were added 0.597 g (2.63 mmol) of DDQ and were heated to reflux for 2.5 hours, then the solvent was removed in a rotary evaporator and was carried out chromatographic column with silica to purify the product, using as eluent CH_2Cl_2. The desired porphyrin was isolated in a yield of 10 % (319 mg).

Dark purple powder
Rf = 0,7 (CH_2Cl_2)
^{1}H-NMR (300 MHz, CDCl3) δ: -2.83 (2H, s, N*H*), 4.15 (6H, s, CO_2CH_3), 8.33 (4H, d, J=8.2 Hz, ArH), 8.50 (4H, d, J=8.1 Hz, ArH), 8.90 (8H, m, βH).

Synthesis of compound **12**[14]

In a 100 ml flask were placed 0.093 g (0.112 mmol) of compound **11**, 9 ml of THF and 20 ml of NaOH 2 M. Under magnetic stirring was reacted at room temperature for 24 hours. The organic solvent was removed under reduced pressure, after that CH_2Cl_2 added and put all in a separating funnel. Here was then added 3 M HCl solution until the porphyrin wasn't colored green (initially burgundy). It is extracted with CH_2Cl_2 the unreacted porphyrin, while with ethyl acetate was possible to extract the porphyrin having sought the two free carboxyl groups. They are then carried out several washes with H_2O until the mixture returns to burgundy. Dried over Na_2SO_4 and the solvent was removed at the rotary evaporator. The product was isolated in a yield of 50% (49 mg), less than expected. This is probably due to loss of product during the various extractions.
Dark purple powder
Rf = 0,1 (CH_2Cl_2)
^{1}H-NMR (300 MHz, DMSO-d$_6$) δ: -3.05 (2H, s, N*H*), 8.42 (8H, s, βH), 8.96 (4H, s, ArH), 9.28 (4H, s, ArH), 13.32 (2H, s, O*H*).

Synthesis of compound **13**

In a 50 ml flask were put 0.026 g (0.03 mmol) of porphyrin 11, 0.017 g (0.09 mmol) of EDC, 0.013 g (0.09 mmol) of HOBt and 6 ml of dry THF. The whole was placed under magnetic stirring for 30 min and in nitrogen flow. After the half hour it was added 0.007 g (0.06 mmol) of DMAP and 0.004 ml (0.06 mmol) of **8**. The flask fitted with a valve to $CaCl_2$ is allowed to react under stirring for 24 hours. The crude reaction product was dissolved in CH_2Cl_2, washed with H_2O, dried over

Na_2SO_4, and then the solvent was removed by rotary evaporator and vacuum pump. The product was purified by preparative plate using as eluent a mixture of hexane:ethyl acetate 1:1. The desired product, compound not known in the literature, was isolated with a yield of 60 % (17 mg).

P.M. ($C_{52}H_{26}F_{10}N_6O_2$) = 956,80
Light purple powder Rf = 0,67 (Hexane:ethyl acetate 1:1)
^{1}H-NMR (300 MHz, CDCl3) δ: -2.84 (2H, s, N*H*), 2.43 (2H, t, J=2.5Hz, C≡C*H*), 4.49 (4H, dd, J=5.5 Hz, 3 Hz, CH_2), 6.65 (2H, t, J=5.5 Hz, N*H*), 8.23 (4H, d, J=8.1 Hz, ArH), 8.33 (4H, d, J= 8.2 Hz, ArH), 8.86 (4H, d, J= 5.1 Hz, βH), 8.91 (4H, d, J= 5 Hz).
^{19}F-NMR (400 MHz, CDCl3) δ: -161.73 (4F, t, J=16 Hz, ArF), -151.95 (2F, t, J=20.8 Hz, ArF), -136.81 (4F, d, J=24.96 Hz, ArF).
^{13}C-NMR (300 MHz, CDCl3) δ: δ 29.71, 77.011, 125.67, 134.74 ppm.
MALDI-TOF MS
Matrix: alpha-cyano-4-hydroxycinnamic acid
m/z calculated: 956,800 *m/z* experimental: 957,218.

Synthesis of porphyrin **15**[15]**.**

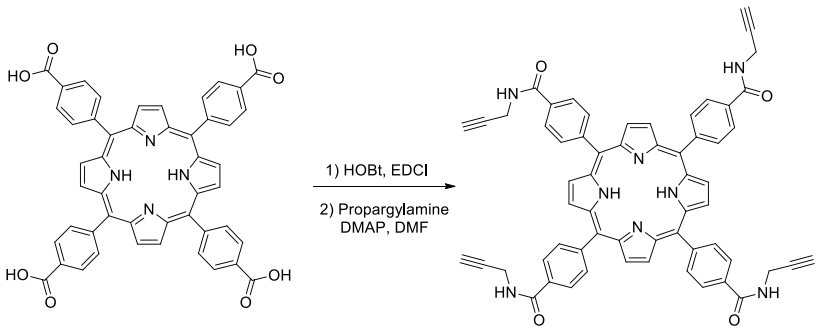

According to a literature procedure[15], EDCI (146 mg, 0.76 mmol) and HOBt (103 mg, 0.76 mmol) were added to a solution of H_2TCPP (100 mg, 0.126 mmol) in 4 ml of anhydrous DMF. After stirring for 30 min, propargylamine (36 µl, 0.56 mmol) and DMAP (68 mg, 0.56 mg) dissolved in 1 ml of anhydrous DMF were added. The reaction mixture was stirred at room temperature for 24 hours. Then the solvent was

evaporated under vacuum giving a purple semisolid. AcOEt (50 ml) and water (50 ml) were added, and the organic phase was washed with water (50 ml x 3) and dried over anhydrous Na_2SO_4. The solvent was evaporated and the column chromatography of the solid, using CH_2Cl_2/MeOH (90:10) as eluent, afforded the product as a purple solid (71 mg, 60%).

^{1}H-NMR (300 MHz, DMSO-d$_6$) δ: 9.39 (4H, t, *J*=5.4Hz, N*H*), 8.86 (8H, s, βH), 8.34 (16H, m, ArH), 4.24 (8H, m, CH_2), 3.23 (4H, *t*, J=2.3Hz C≡C*H*), -2.92 (2H, s, N*H*).

^{13}C-NMR (300 MHz, DMSO-d$_6$) δ: 166.4, 144.6, 134.7, 133.9, 126.4, 119.9, 81.9, 73.5, 29.

MALDI-TOF: MS *m/z* calculated: 939.043, *m/z* found: 939.329

Synthesis of porphyrin **17**

In a Schlenk tube equipped with magnetic stirrer protoporphyrin IX (95 mg, 0.169 mmol), HOBt (76 mg, 0.565 mmol) and anhydrous DMF (10 ml) were introduced under nitrogen flow at a temperature of 0 °C . The reactive system was shielded from light. Keeping the system at 0 °C , the mixture was stirred for 30 min, then EDC·HCl (98 mg, 0.51 mmol) was added. After 30 min propargylamine (35µl, 0.55 mmol) was added. The reaction was left under stirring for 1 h at 0 °C and overnight at room temperature. The DMF was removed by evaporation under reduced pressure, heating at 60 °C; the viscous residue was take up in chloroform (90 ml), resulting in a turbid solution which was poured into a separatory funnel and washed with 3 × 90 ml of saturated solution of $NaHCO_3$, 1 × 90 ml water and 1 × 90 ml of brine successively. The organic phase was recovered, the solvent removed by evaporation at reduced pressure. The crude product obtained was dispersed in a minimum amount of chloroform and precipitated with hexane . The solid was recovered in the form of red crystals by filtration under vacuum with Buchner funnel (84.2 mg ; 78% yield).

^{1}H-NMR (300 MHz DMSO-d$_6$) δ: 10.28 (1H, s, C*H-meso*), 10.21 (3H, s, C*H-meso*), 8.48 (2H, dd, J_{cis} = 12.1 Hz, J_{trans} = 15.0 Hz, C*H*α-*vinilico*), 8.43 (2H, t, N*H-amide*), 6.44 (2H, d, J = 17.7 Hz, C*Hcis*-β-*vinilico*), 6.22 (2H, d, J = 11.8 Hz, H-*trans-β-vinilco*), 4.33 (4H, t, NHCOCH$_2$C*H$_2$*), 3.85 (4H, d, J = 2.8 Hz, C*H$_2$ propargyl*), 3.85 (6H, d, J = 4.6 Hz, C*H$_3$*), 3.72 (6H, d, J = 4.6 Hz, C*H$_3$*), 3.08 (4H, t, J = 6.2 Hz, NHCOC*H$_2$*CH$_2$), 2.96 (2H, s, C*Hpropargyl*).

^{13}C-NMR (300 MHz DMSO-d$_6$) δ:172 (C17), 131 (C2), 121 (C1), 97.9, 97.7, 97. 5 (C5+C9), 81.5, 73.4, 38.6 (C15), 22.3 (C18), 20.13 (C16), 13.1 (C7), 11.8 (C12).

MALDI TOF MS *m/z* calculated: 636.3, *m/z* experimental 636.3

FT-IR (attenuated total reflectance, ATR) ν = 3281, 3066, 2909, 2855, 1637, 1539, 1445, 1225, 1104, 1068, 985.2, 909.0, 834.7, 780.0, 726.6, 705.8, 678.2, 558.1, 528.5 cm^{-1}.

References

[1] J. S. Linsdey *Catalysis by Metal Complexes* 17, , 49-86 (**1994**). Montanari, F. and Casella, L. Eds., Academic Publishers, The Netherlands, (**1994**). Milgron, L.R. The Colours of Life, Oxford University Press, New York, (**1997**)

[2] D. Dolphin, T. G. Traylor, L. Y. Xi *Acc. Chem. Res.*, 30, 251 (**1997**).

[3] R. Bonnett. *Chem. Soc. Rev.*, 19 (**1995**); O. Gaud, R. Granet, M. Kaouadji, P. Krausz, J. C. Blais, G. Bolbach. *Canadian Journal of Chemistry*, 74(4): 481-499, (**1996**), K. Driaf, R. Granet, P. Krausz, M. Kaouadji, F. Thomasson, A. J. Chulia, B. Verneuil, M. Spiro, J. C. Blais, G. Bolbach, *Can. J. Chem. 74*, 1550 (**1996**).

[4] V. Král1, J. Králová, R. Kaplánek, T. Bříza, P. Martásek, *Physiol. Res. 55* (Suppl. 2): S3-S26, (**2006**)

[5] L. Aversa, R. Verucchi, M.V. Nardi, M. Bosi, G. Attolini, F. Rossi, B. Watts, L. Nasi, G. Salviati, S. Iannotta (2009) "**SiC functionalization by porphyrin supersonic molecular beams"**in 26th European Conference on Surface Science (ECOSS 26), Parma, (2009)

[6] Lindsey, J. S.; Hsu, H. C.; Schreiman, I. C. *Tetrahedron Lett.* , 27 , 4969 (**1986**). Lindsey, J. S.; Schreiman, I. C.; Hsu, H. C.; Kearney, P. C.; Marguerettaz, A. M. *J. Org. Chem.* , 52 , 827 (*1987*). Lindsey, J. S.; MacCrum, K. A.; Tyhonas, J. S.; Chuang, Y.-Y. J. *Org. Chem.* , 59 , 57 (**1994)**

[7] T. Gianferrara, A. Bergamo, *J. Med. Chem.*, 53:12, 4678-4690 (**2010**).

[8] S. Mukherjee, K. Sengupta, M. R. Das, S. S. Jana, A. Dey*J. Biol. Inorg. Chem.*, **2012**, *17*, 1009-1023

[9] H. Tang, Z. Zhang, C. Cong, K. Zhang, *Russian J. Org. Chem.*, 45(4), 559 (**2009).**

[10] K. Iida, M. Nango, k. Okada, *Bull. Chem. Soc. Jpn.*, 68 (7), 1959-1968 (**1995**)

[11] X. Li, M. Tanasova, C. Vasileiou, *J. Am. Chem. Soc.*, 130 (41) 1885-1893 (**2008**)

[12] G. F. Moore, S.J. Konezny, *J. Phys. Chem. C*, 116, 4892-4902 (**2012**)

[13] B. A. Wacaser, K. A .Dick *Adv*. *Mater*. 21 153 (**2009)**

[14] a) A.L. Gryshuk, Y Chen, *J*. *Med*. *Chem*. 49 (**2006**)

b) A. Villanueva, E.N. Durantini, *Anti-Cancer drug des*. 16 279-290 (**2001**)

c) S.p. Songca, J. Pharm. Pharmacol. 53, 1469-1476 (**2001**)

[15] T. Gianferrara, A. Bergamo, *J*. *Med*. *Chem*., 53:12, 4678-4690 (**2010**).

Synthesis of a novel nanosystem composed by SiC/SiO_x nanowires conjugated with porphyrins

Introduction

In this chapter the preparation of a novel hybrid nanosystem is presented, based on cytocompatible inorganic SiC/SiO_x core/shell nanowires conjugated with an inorganic photosensitizer, a tetra(4-carboxyphenyl)porphyrin derivative. This idea was first proposed in 2011 by Dott. Salviati in the BioNiMed Project, aiming at preparing a new tool active in anticancer therapy of deep tumors, since the photosensitizer is activated by the emission of the inorganic component under highly energetic X-Ray irradiation.

In a paper published in 2006[1] and in further works[2], Chen and Zhang proposed a new type of photodynamic therapy, the **Self Lighted Photodynamic Therapy** (**SLPDT**). They described that scintillating nanoparticles can potentially be used to activate a photosensitizer for photodynamic therapy as a promising deep cancer treatment modality.

This approach is a variation of the Photodynamic therapy (PDT), that is defined by US-National Cancer Institute the treatment tumor a just under the skin or on the lining of internal organs or cavities through the generation of an active form of oxygen (singlet oxygen) that destroys nearby cancer cells.

In SLPDT the light is generated by scintillating nanoparticles functionalized with photosensitizers when they are irradiated by X-Ray. The photosensitizers in the tumor adsorbs the light and produce the toxic species, singlet oxygen.[3]

As X-Ray can penetrate through tissues, deep tumors can be reached and treated. Here I present a novel hybrid nanosystem based on biocompatible SiC/SiOx nanowires (NWs) functionalized via 'click' reaction or amide bond formation with tetra(N-propynyl-4-aminocarbonylphenyl)porphyrin (H_2TPACPP). The generation of singlet oxygen species by this nanosystem was experimentally verified carrying out experiments in water solution under 6 MV X-ray irradiation.

The possible application of this nanosystem in Self Lighted Photodynamic Therapy was also demonstrated by *in-vitro* tests on lung cancer cells cultured with the functionalized NWs using a linear accelerator for Radiation Therapy.

The result described in the present chapter have been recently published in a great paper: "Porphyrin conjugated SiC/SiO_x nanowires for X-Ray –excited photodynamic therapy" (Scientific Report, Nature Group 5, 7606, **2015**)

Results and Discussions

A. Preliminar studies for porphyrin conjugation to NWs

The SiC/SiO_x nanowires (NWs) functionalized with porphyrins was planned to occur via thermal "click" reaction, following a procedure summarized in the following Scheme.

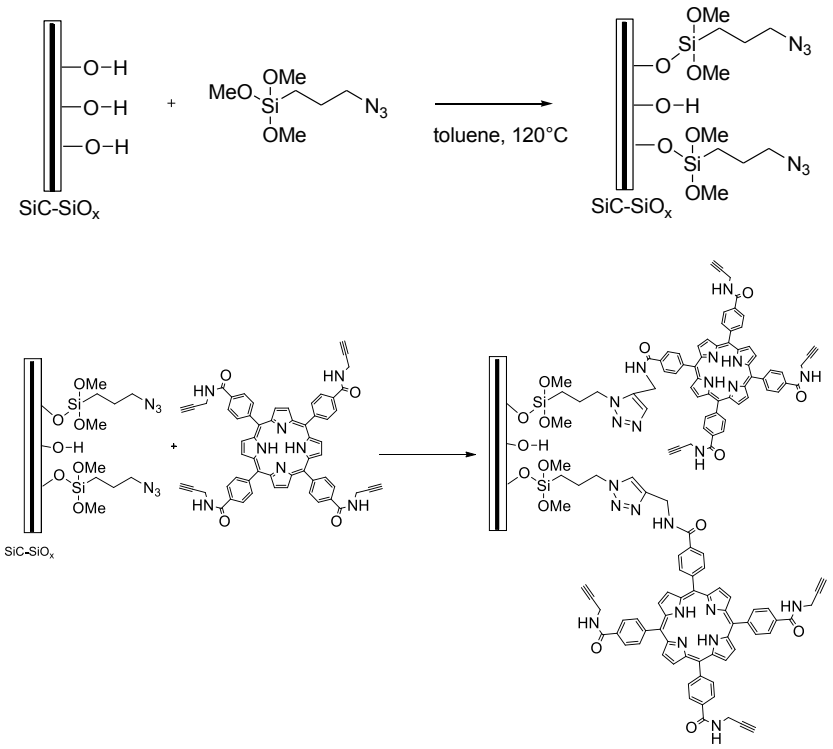

In order to find out the better conditions to perform the thermal Huisgen 1,3-dipolar cycloaddition giving the linker by triazole ring formation, a kinetic study was performed by ^1H NMR spectroscopy at different temperatures.

Taking into account that the trimethoxy- and triethoxy-silanesilanes are very sensitive to humidity, giving hydrolysis and autocondensation, the (3-azidopropyl)trisopropoxysilane was synthesized starting from trichloro(3-chloropropyl)silane (Scheme 1).

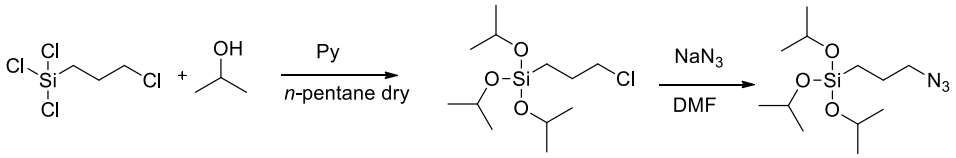

Scheme 1.

The alkoxysilane stability to hydrolysis was estimated by recording ^{1}H NMR spectra at 0, 1, 6, 24 hours, heating the sample in DMSO-d_6 at 100 °C inside an NMR tube. It was observed a considerable degradation induced by heating, particularly increased in the presence of porphyrin.

Therefore, a more stable octylazide was prepared as model reagent (*Scheme 2*).

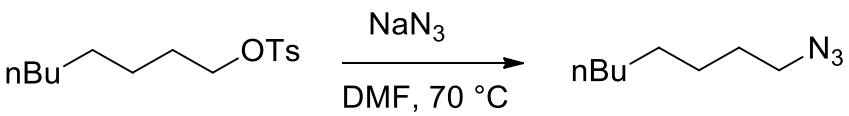

Scheme 2.

The reaction of the octlazide and the H_2TPACPP porphyrin in homogeneous solution was studied by ^{1}H NMR spectroscopy as model reaction of the conjugation of nanowires with the porphyrin.
In order to assign the ^{1}H NMR signals correctly, the following compound was first synthesized in the presence of Cu-catalyst.

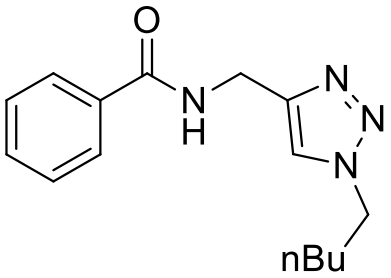

Figure 1.

The spectrum showed two characteristic signals at δ 9.0 ppm (1H, t, J = 5.6 Hz) and 7.96 ppm (1H, s) due to amide NH and triazole CH respectively.

The thermal Huisgen cycloaddition of the octylazide and porphyrin was carried out in DMSO-d_6 at various temperature (100, 120, 130, 140, 160 °C) and was checked during the time. The best reaction temperature was 130 °C, giving almost complete conversion after 24 h, without any reagent degradation.

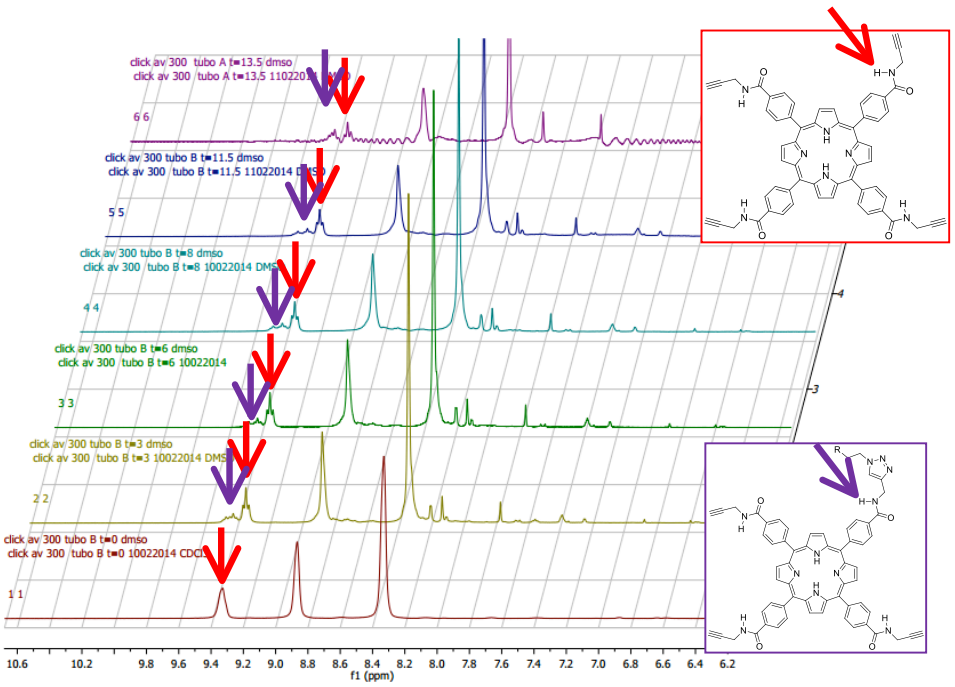

Figure 2.

In *Figure 2* the low field part of the spectra recorded at different time are reported. Indeed, in this region we can observe diagnostic signals: triplets due to NH of reagent and products, and triazole CH singlets of the products. At time=0 three signals of the reagent porphyrin are present at 9.33, 8.87and 8.33 ppm, due to NH, pyrrole β-H and H aromatic protons.

During the reaction progress two overlapping triplets at lower field appeared, ascribable to the two *regio*isomers, *i.e.* 1,4- and 1,5 substituted triazole, expected for thermic click reaction. Also two singlets (in the region 7.6-8.2 ppm), attributed to CH triazole, increased during the time. As shown in the figure, the conversion was about 50% after 13.5 h.

Further, to verify that that the triazole linker does not influence the spectroscopic properties of the porphyrin, the derivative reported in Scheme 3 (having the same linker of the final product anchored to the NWs) was synthesized.

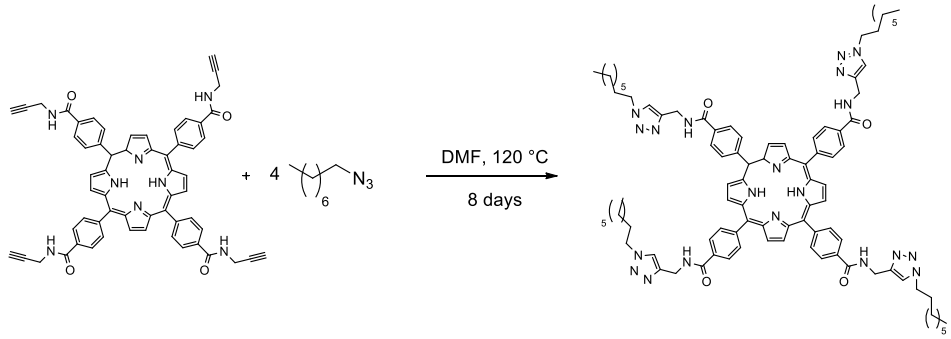

Scheme 3.

As expected, Figure 3 shows that the linker does not influence the spectroscopic properties of the porphyrin.

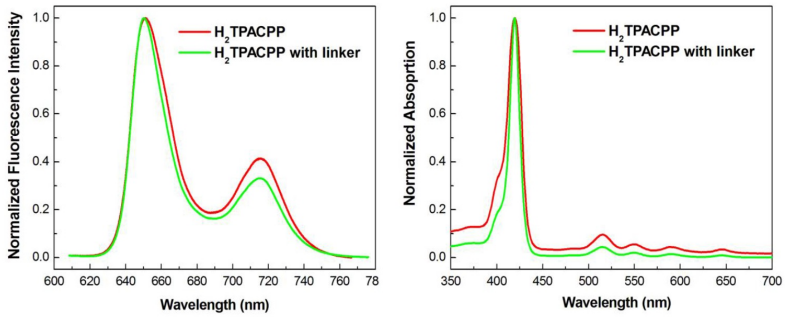

Figure 3. Fluorescence (left panel) and Absorption (right panel) spectra of the starting molecule (H_2TPACPP) and its derivative, in dichloromethane solution

B. Synthesis and characterization of the hybrid nanosystem

Core-shell SiC/SiOx (with1.8 < x < 2) nanowires were grown on Silicon substrates with a CVD (chemical vapour deposition) technique, using a Vapor-Liquid-Solid process catalyzed by Iron salt at IMEM-CNR by Attolini's Group, as described in the first chapter.

This nanosystem presents an optical emission spectrum which matches well the absorption bands of many organic photosensitizers and can be easily functionalized with inorganic crystals as well as with organic molecules. Among the different photosensitizers, the class of porphyrins has a well-established application in photodynamic therapy, with initial approvals by the U.S. Food and Drug Administration. In this work we designed to link porphyrins to the SiC/SiO_x NWs by formation of covalent bonds *via* 1,3-dipolar cycloaddition of terminal alkynes to azides (usually called *click reaction*). Therefore, azide functional groups were introduced on the NWs surface and carbon-carbon triple bonds in the phenyl rings of the porphyrin.

All the reactions involving the nanowires were carried out leaving them anchored on the Si supporting plate. The silica shell surface of the nanowires was activated with a solution of HCl at reflux for 2 hours to increase the number of the free hydroxy groups. The sample was washed with water to neutrality, then with acetone, and finally dried. Then, the azide groups were introduced on the nanowires by reaction of the hydroxyl groups with an alkoxysilane compound, the (3-azidopropyl)trimethoxysilane, not commercially available.

The alkoxysilane was prepared by nucleophilic substitution reaction from the corresponding chloride, commercially available (Scheme 4), carrying out the reaction in DMF. After removal of NaCl by filtration, the product was distilled furnishing a colorless oil in 90% yield.

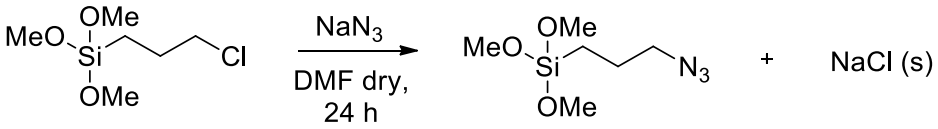

Scheme 4.

The functionalization reaction occurred by hydrolysis of the methoxy groups and subsequent condensation with surface hydroxyl groups, giving Si-O-Si bond formation. The reaction was performed in toluene at 100 °C twice, thoroughly washing the plate with acetone in between.
Then, the tetrakis(N-propynyl-4-amino carbonylphenyl)-porphyrin (H_2TPACPP) was anchored to them via Hüisgen cycloaddition. This reaction can be carried out thermally or catalytically. The copper catalyzed version follows a regioselective path, while the thermal one leads to the formation of two regioisomers, the 1,4-adduct and 1,5-adduct. Since regionselectivity is not important for binding the porphyrin, it was opted to use thermal conditions to avoid the risk of copper inclusion in the cavity of the porphyrin.
The reaction was performed at 130 °C in DMSO, affording the nanowires conjugated with porphyrin. At the end of the reaction, the plate was washed with DMSO and acetone, in order to dissolve efficiently unreacted reagents and anything that was not covalently bound to the nanowires, and then left to air dry.
In Scheme 5 the two steps of the conjugation of porphyrin to SiC/SiO_x NWs are summarized.

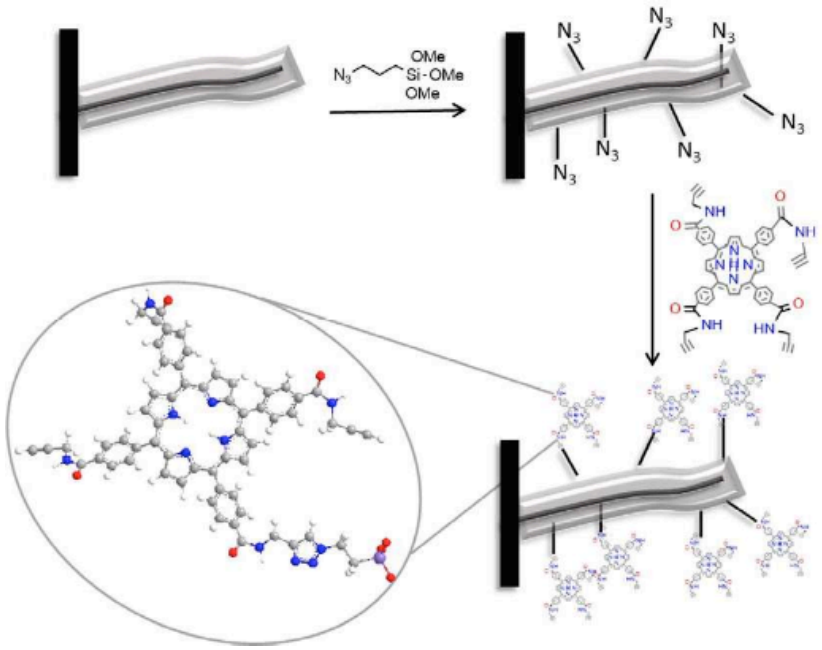

Scheme 5. *Design of the SiC/SiO$_x$/H$_2$TPACPP system*

The hybrid nanosystem was characterized by fluorescence spectroscopy.

Figure 4 shows the characterization of the hybrid nanosystem and of its constituents. In particular, the fluorescence properties of the free porphyrin (Fig.4 a) and of the hybrid nanosystem (Fig. 4c) are well evidenced. Figure 2c-top shows the pictures of the hybrid nanosystem on large area (2.5 x 1.5 cm^2) silicon substrates, in ambient light (left) and in fluorescence conditions (excitation at 360 nm, right). In Figure 4c-bottom the comparison between the optical emissions from bare and conjugated NWs is reported.

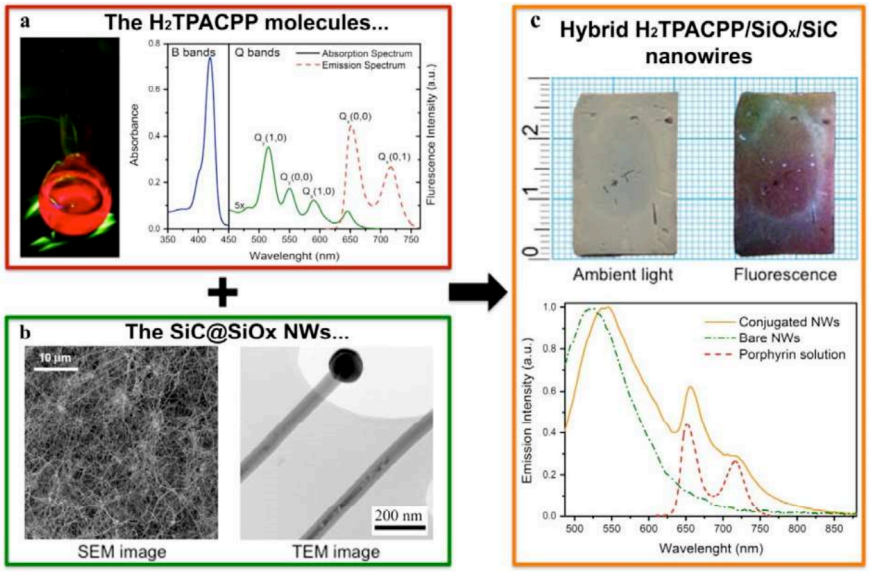

Figure 4. *Spectroscopic characterization of the NW-H_2TPACPP system. (a) Picture: vial containing the H_2TPACPP porphyrin in dichloromethane solution, illuminated by a mercury-vapor lamp. Plot: Absorption (solid line) and Fluorescence (dashed line) spectra of the H_2TPACPP solution. (b) Left: SEM image of the as-grown NW network on Si substrate. Right: TEM image of two neighbor NWs over a holy-carbon support film. (c) Pictures: NW-H_2TPACPP sample illuminated by ambient light (left) or mercury-vapor lamp (right). Plot: fluorescence spectra acquired at room temperature over as-grown NWs (dashed-dotted line) and NW-H_2TPACPP (solid line). The porphyrin emission (dashed line, from panel (a)) is also shown for sake of clarity.*

The emission from bare NWs consists of a single large peak centered at λ = 523 nm**,** in excellent agreement with the near band-edge emission (NBE) of 3C-SiC. The spectrum of the hybrid system contains both the signals, one due to inorganic component and one to organic one. The SiC NBE transition in the hybrid nanosystem is red shifted to 545 nm, as reported by other authors.[4].

As optical excitation is performed at 473 nm, *i.e.* inside the absorption of NWs but out of the main absorption band of porphyrin, the observed fluorescence, which has indeed a contribution from porphyrin, has to be ascribed to some form of electronic coupling between the NWs and the porphyrin, most likely of the form of Foster resonant energy transfer

between inorganic donor and organic acceptor. Cathodoluminescence (CL) analysis confirmed than an energy transfer occurs between the NWs and the bound porphyrin.
Figure 5 shows the comparison of the luminescence properties of the SiC/SiOx core/shell nanowires before and after the functionalization with H_2TPACPP.

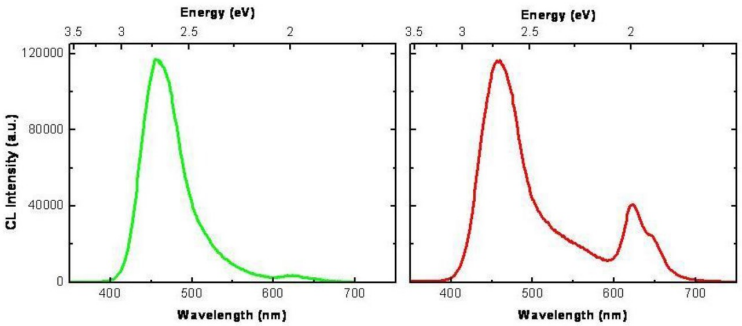

Figure 5. *Room temperature CL spectra of the as-grown SiC/SiOx core/shell NWs (left panel), and of the NWs functionalized with H_2TPACPP (right panel).*

It is worth noting that, after the functionalization, a new band composed by a main peak at 620 nm and a shoulder at 652 nm appears. The 620 nm emission is normally attributed to the non-bridging oxygen center (Si-O)[5] and then in our case the intensity increase is probably related to the residual SiOR group, used as functionalization anchor. The 652 nm emission is due to the porphyrin luminescence, in particular the Qx(0,0) emission as reported in Figure 4.

C. Activity of the hybrid nanosystem for singlet oxygen production and in vitro studies.

The same energy transfer mechanism is the basis of the proposed application, exploiting the singlet oxygen generation to induce oxidative stress in cancer cells.
H_2TPACPP-functionalised NWs were removed (detached) from the support using a ultrasound microtip in acetone (Misonix Sonicator

S4000, 5 W) and were recovered from the solvent by ultracentrifugation (14000 Hz)
The efficiency of the hybrid NW-H_2TPACPP system as a source of a singlet oxygen ($^1O_2$) was tested by exposing the nanowires in water solution to 6 MeV X-Ray in a clinical Linac Varian setup for radiation therapy (as show in Figure 6) of Parma Hospital [Dr. Benecchi].

A dish containing the sample solution is put on the couch and irradiated from the bottom, then it is transferred to a spectrophotometer to acquire the fluorescence spectrum of the SOSG marker, as reported in Figure 6.

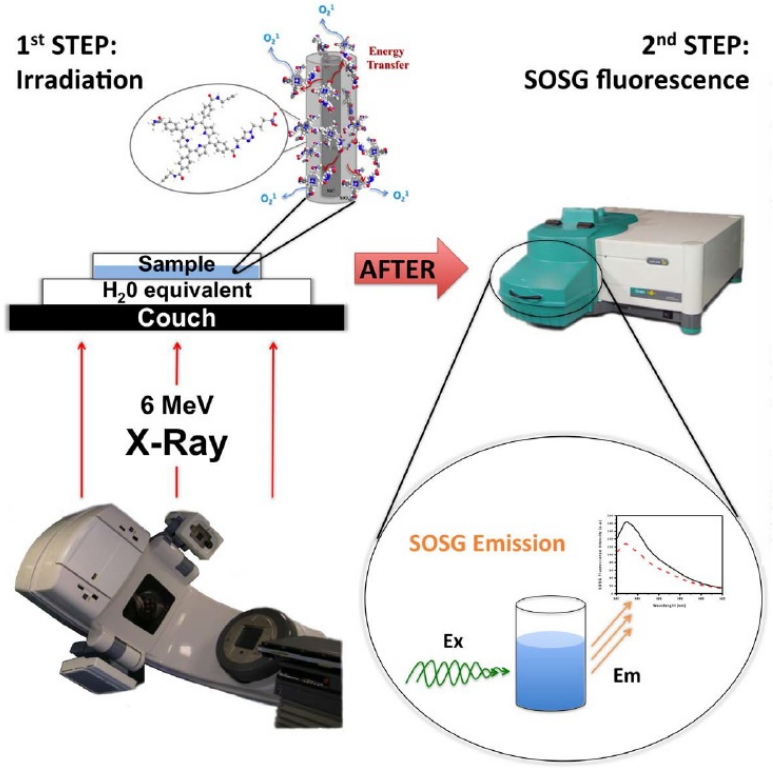

Figure 6. *The scheme represents the procedure that was used to analyse the sample.*

The amount of toxic oxygen that was produced by this nanosystem was revealed by using the SOSG (Singlet Oxygen Sensor Green[6]) kit. This kit shows a green fluorescence activated by interaction with $^1O_2$, showing high selectivity for this species.

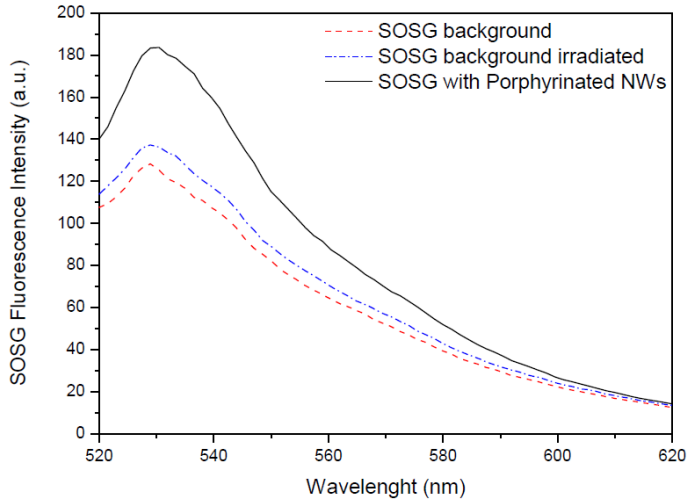

Figure 7. *Fluorescence spectrum from the SOSG kit.*

The enhancement of the green fluorescence in the SOSG after treatment with the conjugated nanowires exposed to radiation demonstrates its effective activation, related to the production of $^1O_2$ by the NW-H_2TPACPP system even in extremely low dose irradiation conditions (0.4 Gy). On the contrary, no SOSG activation was observed in treatments with bare NWs, nor with mere porphyrin solution, confirming that the $^1O_2$ production requires the conjugated NW-porphyrin system and occurs through the self- lighted photodynamic process.

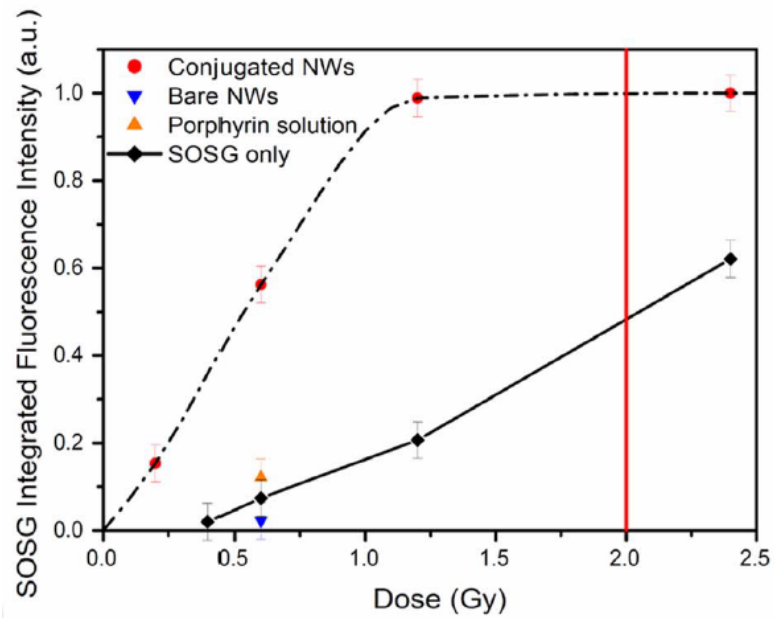

Figure 8. *Integrated fluorescence intensity in function of radiation dose.*

The plot of Fig. 8 reports the measured integrated fluorescence intensity, proportional to $^1O2$ generated, as a function of the radiation dose. The experimental points are obtained from SOSG kit in water, with H_2TPACPP-functionalised NWs (red circles) or without NWs (black diamonds). The orange up-triangle at 0.6 Gy is the experimental point obtained from SOSG kit in a water solution of mere porphyrin, while the blue
down-triangle is obtained from SOSG kit in a water suspension of NWs as grown. The usual dose for clinical treatment (2 Gy) is indicated by the red vertical line.

The $^1O_2$ concentration, as deduced from the integrated intensity of SOSG fluorescence, increases steeply as a function of the dose released up to 1 Gy.

The response of the nanosystem suspension (NW-H_2TPACPP in water, red circles) is well above the control solution (SOSG kit alone in water, black diamonds) and almost 5 times higher than the mere porphyrin response at the same dose (free porphyrin diluted in water, orange up-

triangle) as well as the NWs as grown (suspension in water, blue down-triangle).
The saturation in SOSG fluorescence signal reached around 1 Gy can be reasonably attributed to the finite capacity of SOGS molecules to detect $^1O_2$ immediately after it has been produced. This is limited on one side by the short lifetime of this species in water (it is estimated around 4μs[7]) and by the limited diffusion of this species between the nanosystem surface and the bulk solution.

To study the effect of the nanosystem on cells for possible self-lighted photodynamic therapy, *in vitro* experiments were performed [Prof. Mutti's, Prof. Cacchioli's and Dr. Benecchi's groups]. In particular, the A549 adenocarcinoma human alveolar basal epithelial cells were used. Our previous studies[7] demonstrated that A549 cells incubated with nanowires are able to actively internalize them, in 24 hours. The investigation was done by TEM and SEM analyses. In Figure 9 the internalization of nanowires and interactions with cells are shown.

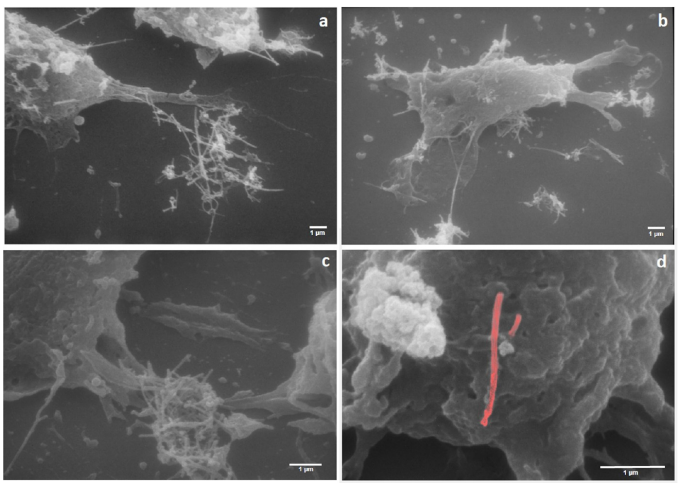

Figure 9. Scanning electron micrographs of A549 cells treated with NWs 50 μg/mL for 24 h.

For this study, A549 cells were incubated with H_2TPACPP-conjugated NWs and irradiated after 24 hours with 6 MV X-Rays at the dose of 2Gy, chosen accordingly to the standard conditions of clinical radiation therapy (only one session). After that, the clonogenic survival assay was performed. Cells were cultured for 12 days and the proliferation was checked.

The histograms in Figure 10 normalized to the control cells, report the surviving fraction of cells treated only with the NW-H_2TPACPP (50 mg/ml), only with radiation (2 Gy) or in combination of NW-H_2TPACPP and radiation.

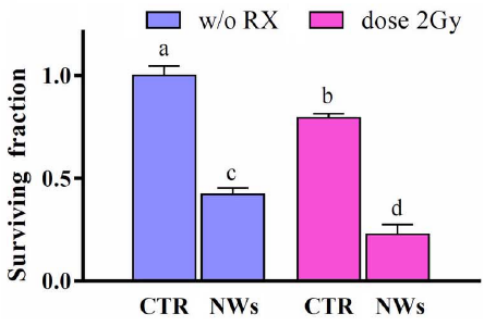

Figure 10. *Clonogenic survival assay*

The interesting result was that the nanosystem caused a decrease of cell proliferation, either under or without irradiation. The most striking result is that the cell plating efficiency after the radiation treatment is significantly lower for cultures incubated with the NWs than for control cells with the NWs than for control cells. Further, the best result is that this effect came from a lower power that it was used during the irradiation.

This study demonstrates that NWs-H_2TPACPP nanosystem has an additive antiproliferative effect compared to irradiation alone at the selected dose. In addition, the irradiation time used is significantly

shorter than the standard clinical treatment times. Indeed, the treatment time is usually 40 seconds or 90 seconds, and it is usually necessary to repeat the treatment several times.

Prompted by the good results obtained, it was planned to evaluate the effect of the nature and length of the linker used to conjugate the nanowires with the porphyrin H_2TCPP on the properties of the hybrid nanosystem. It was decided to react the porphyrin carboxy groups directly with amino groups conveniently introduced on the nanowires surface to obtain the formation of a shorter linker, that could favor the energy transfer process.

The amino groups were introduced on the nanowires by reacting the hydroxyl groups of the silica shell with (3-aminopropyl)triethoxysilane (APTES), following the same procedure previously described for functionalization with alkylazides. The reaction was carried out in toluene at 100 ° C and was repeated two times, thoroughly washing the plate with toluene and then with acetone in between. The H_2TCPP acidic carboxy groups were previously activated with condensing agents (EDC, HOBt and DMAP) to permit the reaction with the amino groups affording the amide bond formation between the two partners. (Scheme 6)

After this step, the carboxyl groups of the porphyrin, still in the form of active ester, were reacted with an excess of propargyl amine to obtain a hybrid nanosystem which differs from the previous one only for the linker.

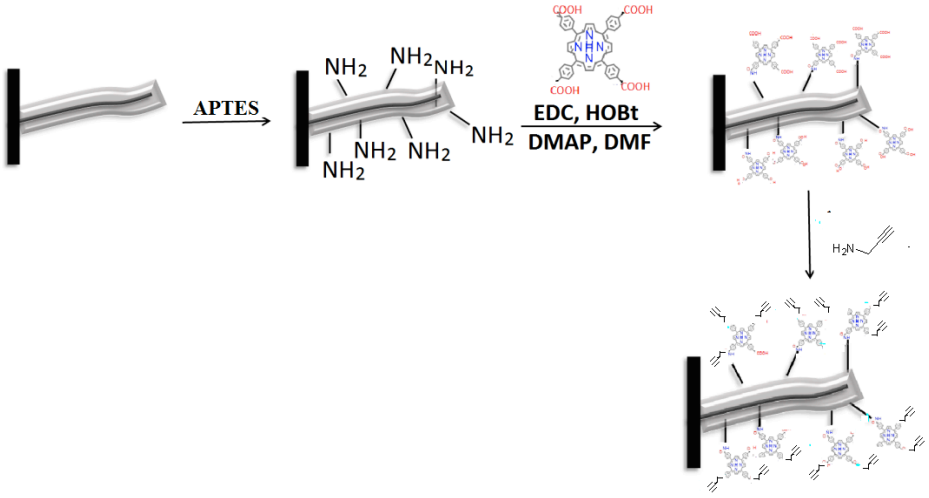

Scheme 6.

The formation of the conjugated system nanowire-porphyrin was confirmed by fluorescence spectroscopy on solid and by diffuse reflectance UV-vis. The fluorescence spectrum reported in Fig. 11, was obtained using a laser at 473 nm as excitation source.

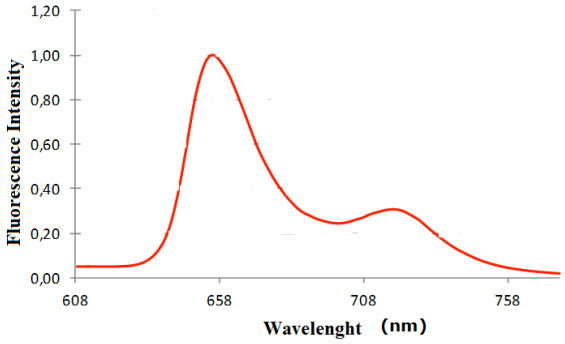

Figure 11. *Fluorescence spectrum of NW-H_2TCPP.*

The maximum intensity of fluorescence recorded on these nanowires was really higher than that recorded for the nanowires functionalized

with ‘click’ chemistry, suggesting that this procedure increased the porphyrin loading. This result can be attributed to the higher degree of shell functionalization with APTES, due to the known higher reactivity of APTES. Indeed, attention must be paid to avoid the formation of gel due to auto-condensation process. Furthermore, the formation of the amide bond can be more efficient than the cycloaddition reaction. This method has the additional advantage that the conjugation reaction occurs under milder conditions, *i.e.* at room temperature.

The diffuse reflectance UV-vis spectrum (Figure 12) showed the typical absorption bands of H_2TCPP porphyrin, *i.e.* the Soret band (421 nm)and also the four Q bands (518, 553, 594 and 651 nm), evidencing the integrity structural preservation of the photosensitizer after conjugation.

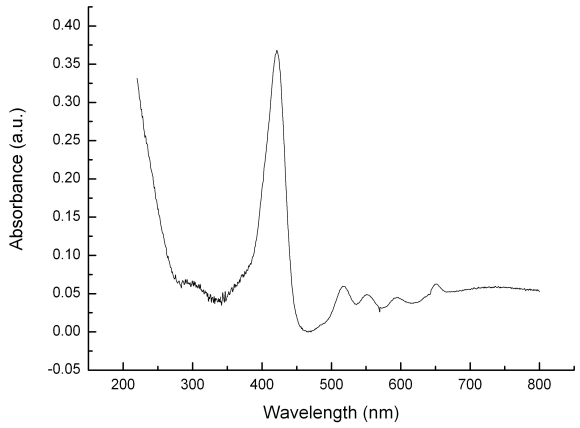

***Figure 12**. Diffuse reflectance UV-visible spectrum of NWs conjugated with porphyrin by amide bonds.*

Last, this procedure of conjugation offers the possibility to react the activated carboxy groups with various kinds of amines, different from propargylamine. Therefore, we have planned to use a hydrophilic amine (such es PEG-NH_2) to increase the dispersibility of the hybrid nonosystem in water.

Experimental Part

Synthesis of 3-chloropropyl-trisopropossysilane

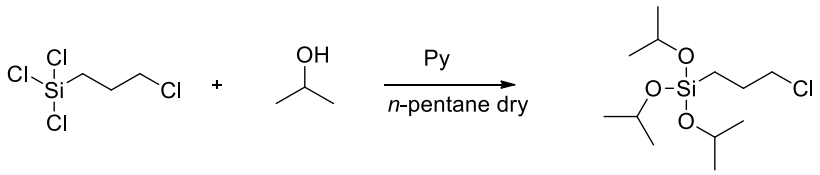

In a two-neck flask of 250 ml equipped with a magnetic stir bar, drip-funnel and bubble condenser connected to the line vacuum/nitrogen, are introduced isopropyl alcohol, pyridine and 100 ml of n-pentane; the temperature is raised to 0 °C and was added by slow dripping a solution of trichloro(3-chloropropyl)silane in 15 ml of dry n-pentane. When the addition of the reagent, the mixture is left under stirring for one hour at room temperature, then filtered on tapered glass fiber and pulled dry rotary evaporator. The desired product is obtained by distillation at reduced pressure in the furnace tube with bubbles in the form of colorless liquid in 40% yield. It was characterized by ^{1}H NMR.

^{1}H-NMR (300 MHz, $CDCl_3$) δ: 4.23 ppm (3H, m, J = 6.0 Hz, $CH(CH_3)_2$), 3.55 ppm (2H, t, J = 6 Hz, $SiCH_2CH_2CH_2Cl$), 1.90 ppm (2H, m, J = 4.8 Hz, $SiCH_2CH_2CH_2$), 1.21 ppm (18H, d, J = 6.1Hz, $CH(CH_3)_2$), 0.71 ppm (2H, t, J = 6 Hz, $SiCH_2CH_2CH_2$).

Synthesis of 3-azidopropyl-trisopropossysilane

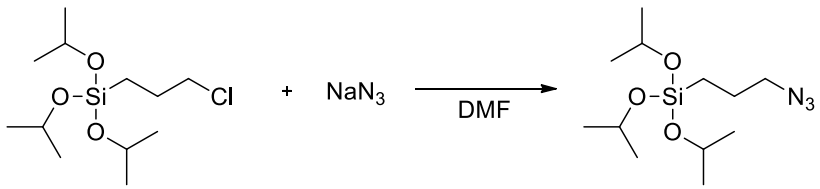

In a 25 ml flask were introduced (3-chloropropyl) triisopropossisilane, sodium azide and dry DMF. The mixture was left under magnetic stirring at 60 ° C over night. The solvent was removed by evaporation under reduced pressure at 60 °C. The residue was dispersed in 5 ml of diethyl ether, filtered through a tapered glass fiber and pulled dry rotary evaporator. The product was obtained as of colorless liquid (187.6 mg; yield: 63%) and was characterized by ^{1}H NMR.

^{1}H-NMR (300 MHz, $CDCl_3$) δ: 4.23 (3H, m, J = 3 Hz, C*H*$(CH_3)_2$), 3.28 (2H, t, J = 6 Hz, $SiCH_2CH_2CH_2N_3$), 1.71 (2H, m, J = 3 Hz, $SiCH_2CH_2CH_2$), 1.21 (18H, d, J = 6.0 Hz, $CH(CH_3)_2$), 0.64 (2H, t, J = 6 Hz, $SiCH_2CH_2CH_2$).

Synthesis of 1-octylazide

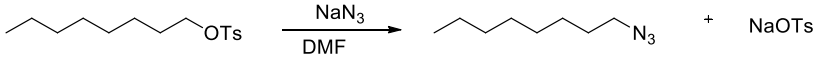

In a Schlenk tube are introduced 1-TsO-octane (543 µl, 2.04 mmol), sodium azide (373 mg, 5.75 mmol) and 14 ml of DMF dry. At the end of the reaction, the mixture was transferred into a separatory funnel and diluted with 140 ml of methylene chloride; the organic phase was washed with 5 × 140 ml of distilled water, destroying the emulsions that were formed with saturated saline solution, then was dried with Na_2SO_4, filtered and concentrated by evaporation under reduced pressure. The residual solvent was removed by evaporation and a colorless viscous liquid was obtained (183.6 mg; yield 57%). The density of the compound was d = 0.94 g / ml.

^{1}H-NMR (300 MHz, $CDCl_3$) δ: 3.28 (2H, t, J = 6 Hz, N_3- C*H*$_2$), 1.62 (2H, m, J = 6 Hz, N_3- CH_2 C*H*$_2$), 1.30 (10H, m; C*H*$_2$ C*H*$_2$ C*H*$_2$ C*H*$_2$ C*H*$_2$ CH_3), 0.91 (3H, t, J = 6 Hz, C*H*$_3$).

Synthesis of 3-azidopropy-trimethoxisilane

The synthesis is described in the Experimental part Chapter 3.

Functionalization of nanowires with 3-azidopropyl trimethoxysilane

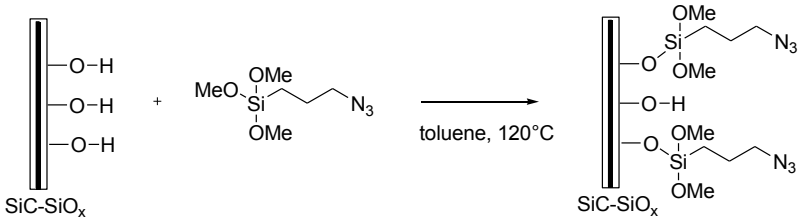

The silica shell surface of nanowires was preactivated at reflux in a solution of HCl for 2 hours. After washing with water until reached neutral pH, the sample was washed with acetone in order to be easily dried in air. Then, it was placed in a 50 ml round bottom flask and covered with toluene (7 ml) and 2 μL of a 5 mM solution of azide-derivative in toluene were added. The reaction was heated at reflux under stirring overnight. After cooling, the nanowires were thoroughly washed with dry toluene, with acetone and dried in air.

Nanowires conjugation with H_2TPACPP porphyrin

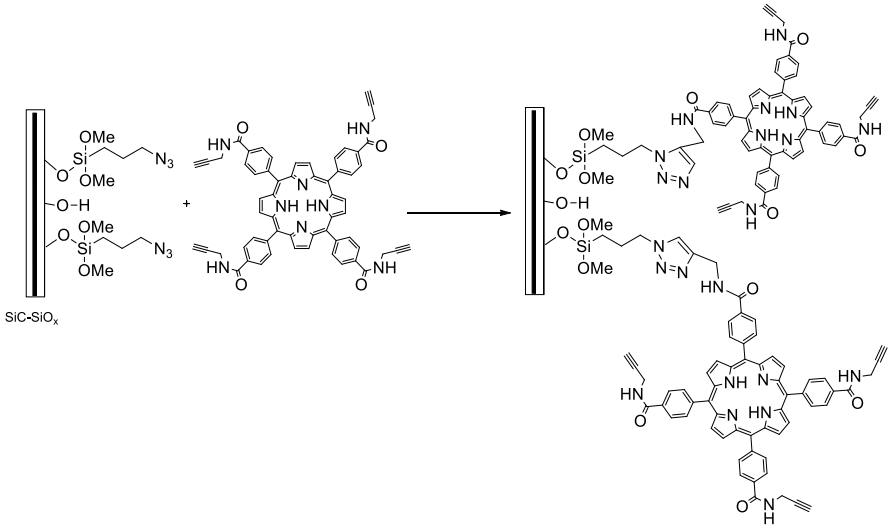

The wafer covered by the nanowires bearing azide groups was placed in a 50 ml round bottom flask containing the H_2TPACPP porphyrin (16 mg), and was covered with DMSO (around 7-10 ml). The reaction was carried out at 130°C for 24 hours to obtain the triazole ring formation. The samples were washed with DMSO, acetone, and air dried.

Last, the nanowires were removed (cut off) from the support using an ultrasound micro tip in acetone (Misonix Sonicator S4000, 5W) and were recovered from the solvent by ultracentrifugation (14000 Hz).

The detached nanowires were examined by fluorescence spectroscopy, that confirmed the presence of the porphyrins on the surface of nanowires.

Functionalization of nanowires with 3-aminopropyl triethoxysilane

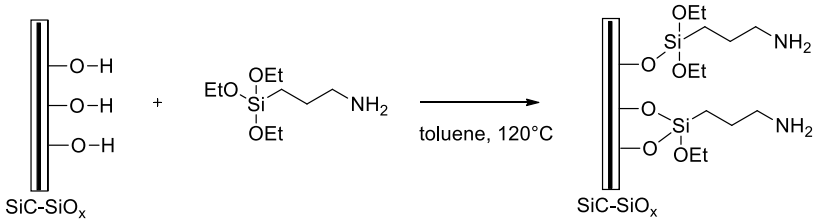

The silica shell surface of nanowires was preactivated at reflux in a solution of HCl for 2 hours. After washing with water until reached neutral pH, the sample was washed with acetone in order to be easily dried in air. Then, it was placed in a 50 ml round bottom flask and covered with toluene (7 ml) and 2 µL of a 5 mM solution of 3-aminoprophyltriethoxysilane in toluene were added. The reaction was heated at reflux 100 °C under stirring overnight. After cooling, the nanowires were thoroughly washed with dry toluene, with acetone and dried in air.

Functionalization of nanowires with porphyrin (H_2TCPP)

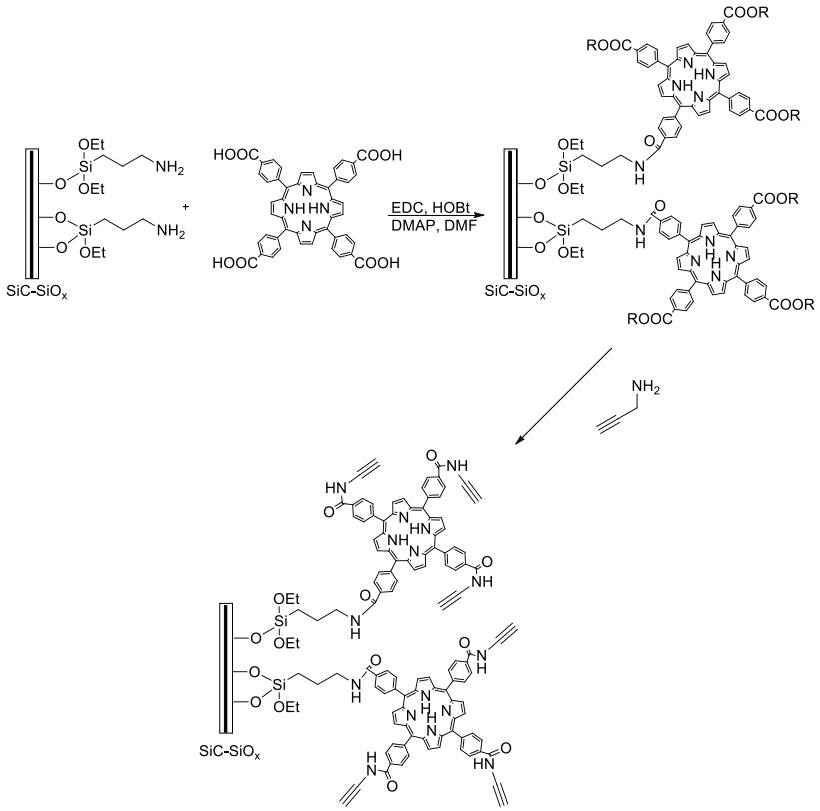

In a 50 ml round bottom flask, EDCI (14 mg, 0.076 mmol) and HOBt (10 mg, 0.076 mmol) were added to a solution of H_2TCPP (10 mg, 0.013 mmol) in 4 ml of anhydrous DMF. After stirring for 30 min, the wafer covered by the nanowires was placed in the flask and DMAP (7 mg, 0.06 mg) with 3 ml of anhydrous DMF were added. The reaction mixture was stirred at room temperature for 24 hours. Under nitrogen flux. the solution was completely removed from the flask and a solution of propargylamine in 7 ml of DMF dry was added to cover the wafer. The reaction was left at room temperature overnight under stirring. Then, the wafer was washed several times with DMF, acetone and dried in air.

References

[1] W. Chen, J. Zhang, *J. Nanosci. Nanotech.* 6:4 1159-1166 (**2006**)

[2] Y. Liu, W. Chen, S. Wang, A.G. Joly, *Appl. Phys. Lett.* 92, 043901 **2008**

[3] M.C. De Rosa, R.J. Crutchley. Chem. Rev. 233-234, 351-371 (**2002**).

[4] A. Wei, X. W. Sun, J. X. Wang, Y. Lei, X. P. Cai, C. M. Li, Z. L. Dong, W. Huang, *Appl. Phys. Lett.* 89, 123902 (**2006**).

[5] Fabbri, F. Carbon-doped SiOx nanowires with a large yield of white emission. *Nanotechnology* **25,** 185704 (**2014**).

[6] The SOSGR kit is produced by Molecular Probes (Product information, revised 30 January 2004) and has been acquired by Life Technologies;
http://tools.lifetechnologies.com/content/sfs/manuals/mp36002.pdf

[7] *Chem. Phys. Lett*. 163, 421-424 (**1989**)

Synthesis of Fe_3O_4 –mSiO_2 nanoparticles

Introduction

Magnetic nanoparticles with core-shell structure have received particular attention in biomedical field because this structure can increase the stability, decrease the cytotoxicity, improve the dispersity and, depending on the shell composition, it is possible to bind various kind of molecule.

The shell provides the ability to add specific properties, for example drugs can be loaded for drug delivery, molecular targeting can be useful to create interaction with biological substance, or again can increase the stability of the nanoparticles in solution (different pH, extreme condition…) and permit to introduce functional groups.[1]

The shell can be a polymeric material or a different metal. For example, coating magnetic particles with a layer of Au is high desirable because of its known reactivity with sulfur group, which makes easy to of bind organic molecules or different materials. An inorganic polymeric material often employed as coating is silica, which increases the biocompatibility and is easily modified with silanes.[2]

As summarized in a following picture (Figure 1), there are many applications for core-shell particles, depending on the different functionalization of the surface. It has also been observed that core-shell nanoparticles are more suitable and show better performance in biomedical applications than the simple nanoparticles.

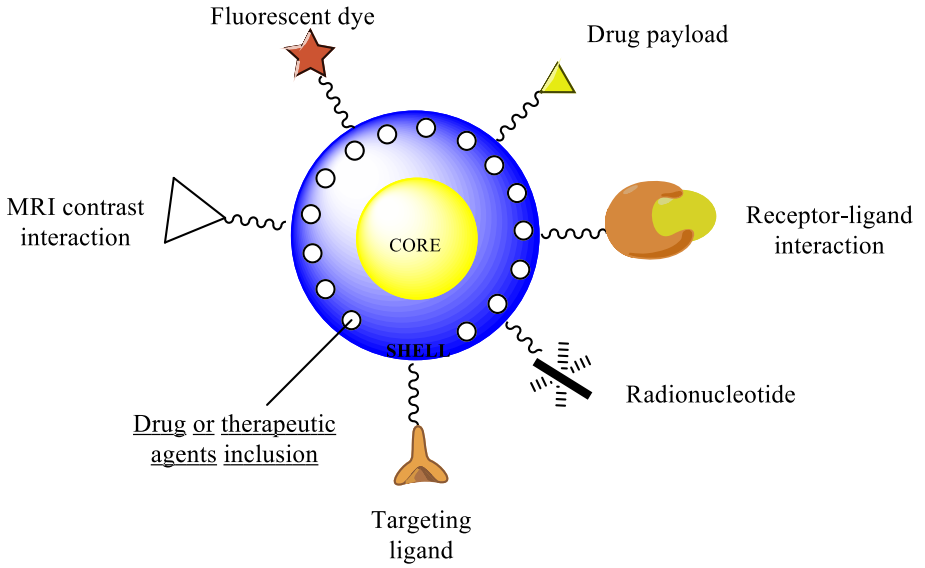

Figure 1. *Scheme of multifunctional nanoparticle for molecular imaging, drug delivery and therapy.*

Numerous problems that are usually associated with single particles are not present in a core-shell structure. Many different materials can be used to form the shell, like PEG with different ending functional groups, various types of silanes, polymers and surfactants.

In general electrostatic repulsion or steric repulsion can be used to disperse nanoparticles and keep them in a stable colloidal state, where is possible work, but the stabilization with stable interactions become necessary if the aim is to work in a biological environment, with changes in pH and temperature. Surfactants and polymers can be chemically anchored or physically adsorbed on magnetic particles to form a single or double layer. This effect can create a repulsive forces to balance the magnetic and the Van der Walls attractive forces acting on the nanoparticles. Polymers could contain functional groups such as carboxylic acid, amino or thiol groups etc., that can bind different complementary molecules. In order to obtain these core-shell nanoparticles there are different approaches, as micro-emulsion synthesis, polymerization, thermal passivation (with metal)…

Until now I described the preparation of a shell around the nanoparticles to increase the stability and to make possible their functionalization. Another properties that can be added is the shell porosity. Indeed, the creation of pores with different volume able to encapsulate drugs, add the property of drug delivery, that can occur slowly or under specific stimulations.

In this context, I developed the synthesis of nanoparticles formed by a Fe_3O_4 core and mesoporous-SiO_2 shell. The aim was to prepare magnetic nanoparticles larger than those previously obtained to increase the hyperthermia property and the hydrophilicity. It is known that the silica shell gives a good dispersibility in aqueous phase, is stable and easy to functionalize. The presence of *meso*pores ensure the capability to absorb and delivery specific drugs (d^{max}= 5 nm), and the core gives to the material hyperthermia properties and the possibility to act as contrast agent in MRI.

Results and Discussions

On the basis of my previous studies, I planned to increase the diameter of magnetic nanoparticles in order to increase the hyperthermia properties, and sequentially to cover them with mesoporous silica layer.

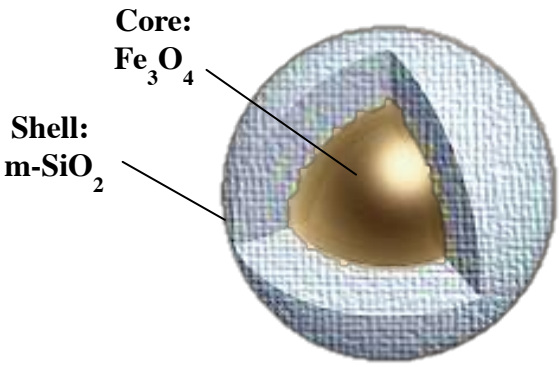

Figure 2. *Core-shell structure of nanoparticles. The core is composed by Fe_3O_4 , shell is mesoporous SiO_2.*

After the synthesis I decide to try the deliver a drug, I did the study of absorption and release of Indomethacin (antibacterial agent) as s molecule model.

Thanks to my background with porphyrins I decide to conjugate them on the surface of nanoparticles for imaging *in vitro* (biological studies are in progress), and I did the same with VivoTag®680-NHS that is one of the most famous compound for imaging *in vivo* (studies are in progress).

The synthesis of nanoparticles started from Fe-oleate complex preparation. The synthesis of this precursor was performed using $FeCl_3 \cdot 6H_2O$ in presence of sodium-oleate in a mixture of solvents. The reaction was left under heating and stirring several hours in order to obtain the complex. The complex was washed and dried.

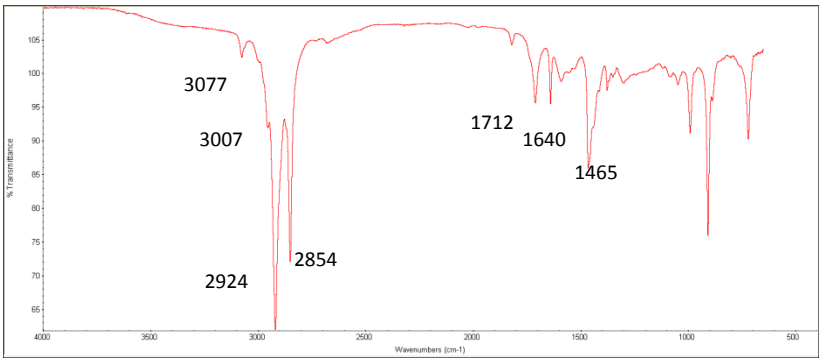

Figure 3. *FT-IR spectra of Fe-oleate complex; υ: 3077 cm^{-1}(C-H stretch), 3007 cm^{-1} (C=C-H stretch), 2924 cm^{-1}(asymmetric CH_2 stretch), 2854 cm^{-1}(symmetric CH_2 stretch), 1712 cm^{-1}(C=O stretch), 1640 cm^{-1} (C=C stretch), 1465 cm^{-1} (COO^- stretch and CH_2 scissoring bands).*

There are many works in literature stating the importance of the purity of Fe-oleate complex to produce nanoparticles with a narrow size distribution.[34]

The Fe-oleate complex was heated to 320°C in presence of oleic acid in 1-octadene, as reported in *Scheme 1*. I succeeded in preparing monodisperse iron oxide (magnetite) nanocrystals with a particle size of 15 nm.

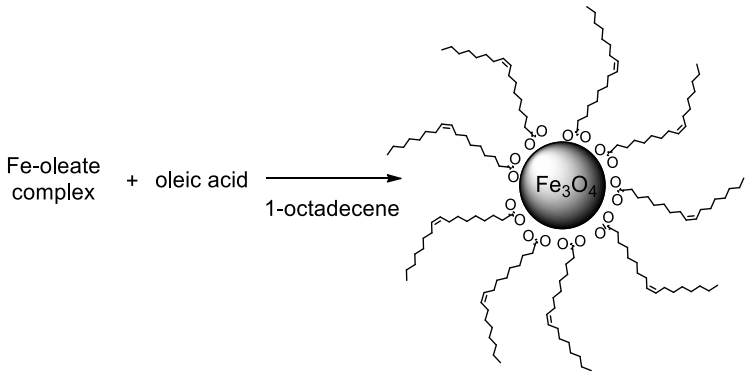

Scheme 1*: Synthesis of nanoparticles starting from Fe-oleate complex*

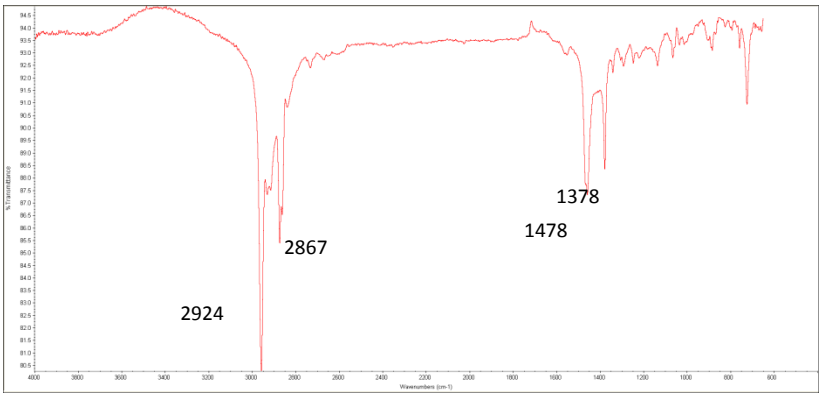

Figure 4. *FT-IR spectra of Fe_3O_4 nanoparticles; ν: 2924 cm^{-1}(asymmetric CH_2 stretch), 2867 cm^{-1}(symmetric CH_2 stretch), 1478 cm^{-1}adn 1378 cm^{-1} (COO^- symmetric and asymmetric stretch*

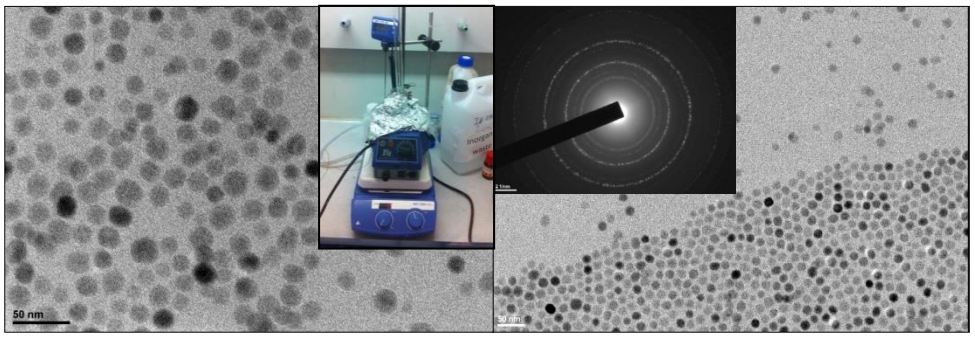

Figure 5. *From left: TEM picture that shows the homogeneous distribution and the narrow size distribution, inset the set up used to obtain the nanoparticles. On right TEM image and inset the diffraction pattern.*

As it is shown in *Figures 4* and *5*, nanoparticles were characterized by TEM, diffraction pattern, and FT-IR spectroscopy. TEM images show the narrow size distribution and the crystallinity of the particles. The size distribution was calculated giving a value of 15±2 nm (diameter).

The hyperthermia property was studied disperding the nanoparticles in hexane (*Figure 6*). The preliminary value of SAR is 1.39 W/g.

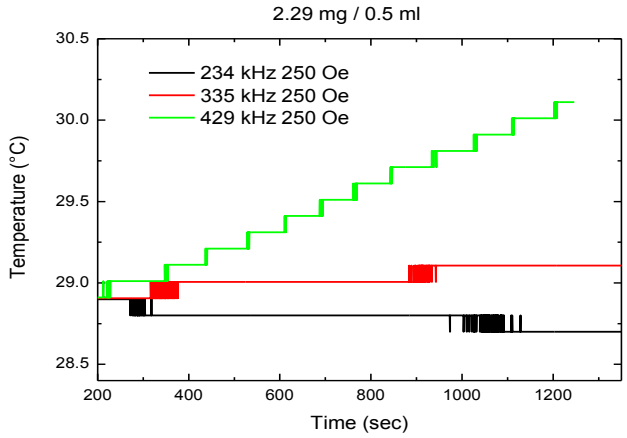

Figure 6. *Preliminary results in green produce SAR :1.39 W/g*

Thermo-gravimetric analysis showed a weight loss of 77 %, evidencing the presence of a large organic shell. ICP analysis was performed to know the exact amount of Fe in order to evaluate the amount of inorganic part (Fe_3O_4). Fe_3O_4 weight amount is 3.4 %.

After the characterization of these nanoparticles the synthesis of the silica shell was performed by using a dispersion of nanoparticles in $CHCl_3$ and a water solution of cetyltrimethylammonium bromide (CTAB, *Figure 7*), as describe in *Scheme 2*.

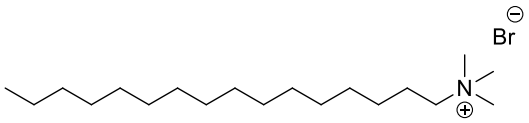

Figure 7. CTAB structure (cetyl trimethylammonium bromide)

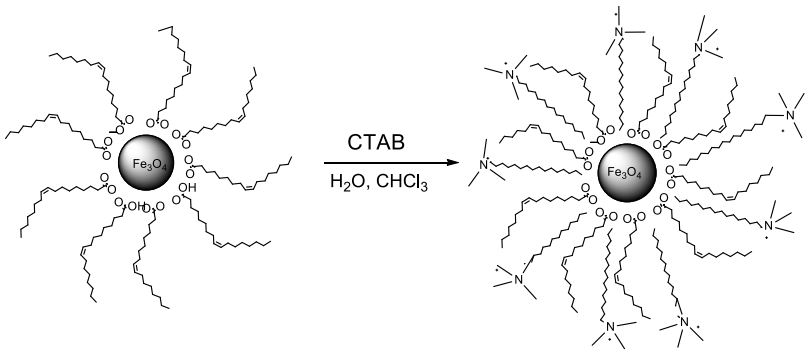

Scheme 2.

After the reaction time (30') the $CHCl_3$ was removed and the nanoparticles were stable in water phase for long time.
In order to synthetize the shell of silica oxide the nanoparticles were diluted in water and a basic solution was added, sequentially tetraethyl orthosilicate (TEOS) in little amount was added, then ethyl acetate (*Scheme 3*).

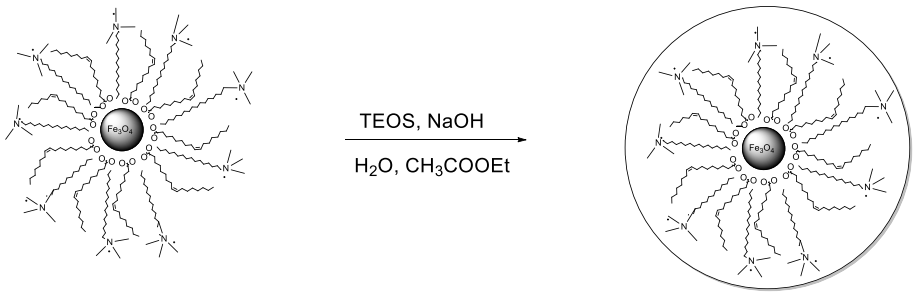

Scheme 3.

To transform the SiO_2 in m-SiO_2 was necessary to extract CTAB from mesopore channels by washing with a NH_4NO_3 solution (*Scheme 4*).

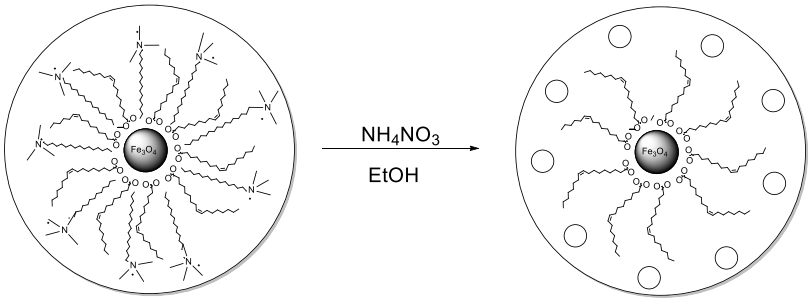

Scheme 4.

CTAB has to be removed to leave free the pores and also because it is toxic for cells. To better understand the extraction of this salt I report here the FT-IR spectra obtained before and after extraction, and the pure CTAB spectrum (*Figure 9*). In *Figure 10* in spectra before the extraction are clear the picks from CTAB (2870 cm^{-1}, 2848 cm^{-1}, and

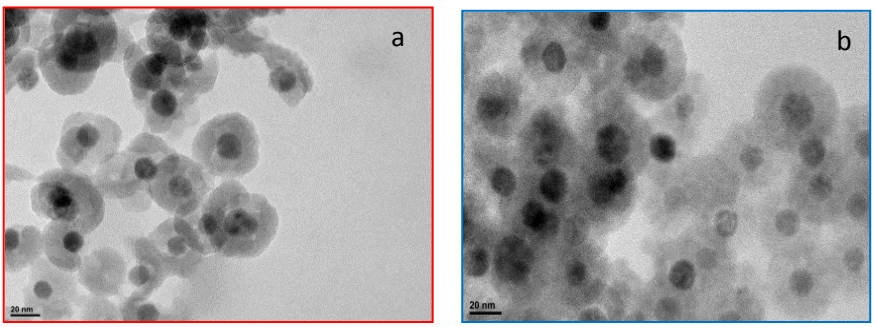

***Figure 8** .TEM pictures show the morphology before (a) and after extraction of CTAB (b)*

around 1470-1480 cm^{-1}), but after the extraction (twice extractions) there are just the signal from Si-O stretching. *Figure 8* reports the TEM images of the NPs before and after extraction. In the image on the right it is possible to observe the mesoporous structure of the silica shell after the removal of the surfactant.

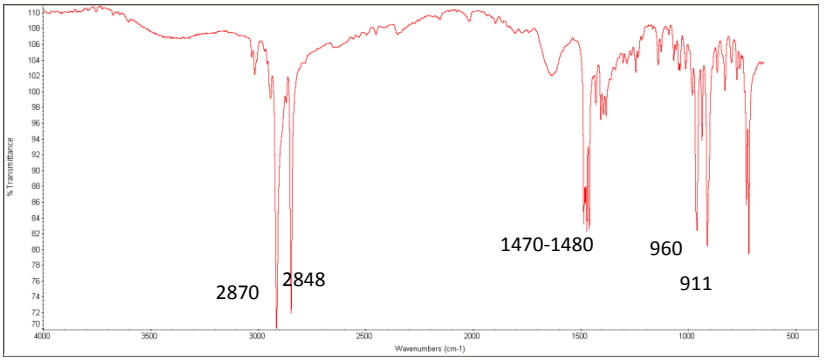

Figure 9:*CTAB FT-IR spectra ν: 2870 cm^{-1}(asymmetric CH_2 stretch), 2848 cm^{-1}(symmetric CH_2 stretch), 1470-1480 cm^{-1} (CH_2 scissoring), 960 cm^{-1} and 911 cm^{-1} (CH_2 rock)*

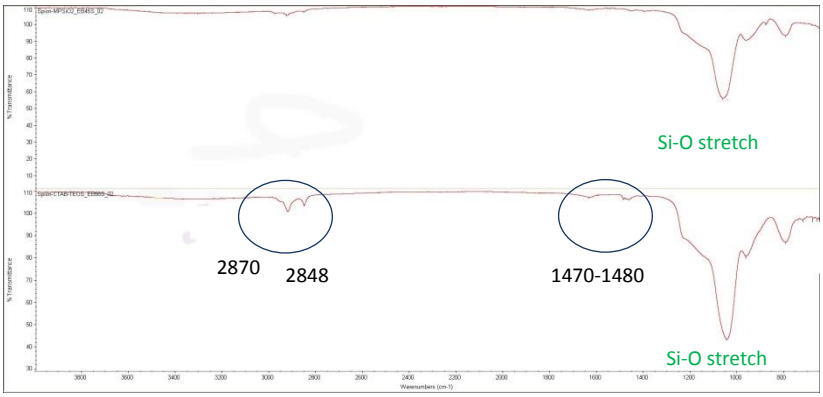

Figure 10*. FT-IR spectra after and before extraction: after and before extraction- in the second one are clear the picks from CTAB (2870 cm^{-1}, 2848 cm^{-1}, and around 1470-1480 cm^{-1}), but after the extraction (twice) there are just the signal from Si-O stretching.*

To obtain good results, other important factors were the amount of CH_3COOEt and the sequence of addition. It was found to be fundamental to add the solvent CH_3COOEt after TEOS (slowly addition) in order to leave the time to the silane to start the polymerization.

The morphology of Fe_3O_4@mSiO_2 NPs was characterized by JEM-2100F field emission transmission electron microscope (TEM) operating at an accelerating voltage of 200 KeV. During the study of reaction condition optimization, different results were obtained by small experimental changes. In the following *Figure* different samples of nanoparticles are reported, obtained by changing the amounts of TEOS and solvent.

Picture **a** shows the presence of aggregates, caused by the big amount of silane and the wrong amount of ethyl acetate; in **b** the nanoparticles are better separate but there are numerous particles without core. In picture **c** there are nanoparticles not completely coated with silica, so it means that the amount of TEOS was too low to cover all the nanoparticles. In picture **d** nanoparticles are composed by a fine structure core-shell but there are some connections between nanoparticles. A possible explanation of this phenomena is the addition of the wrong amount of ethyl acetate. Figure **e** shows a decrease of bridges between nanoparticles. Last, picture **f** evidences that the perfect amount of TEOS and ethyl acetate was found. Also the addition time and the sequence of addition influenced the result.

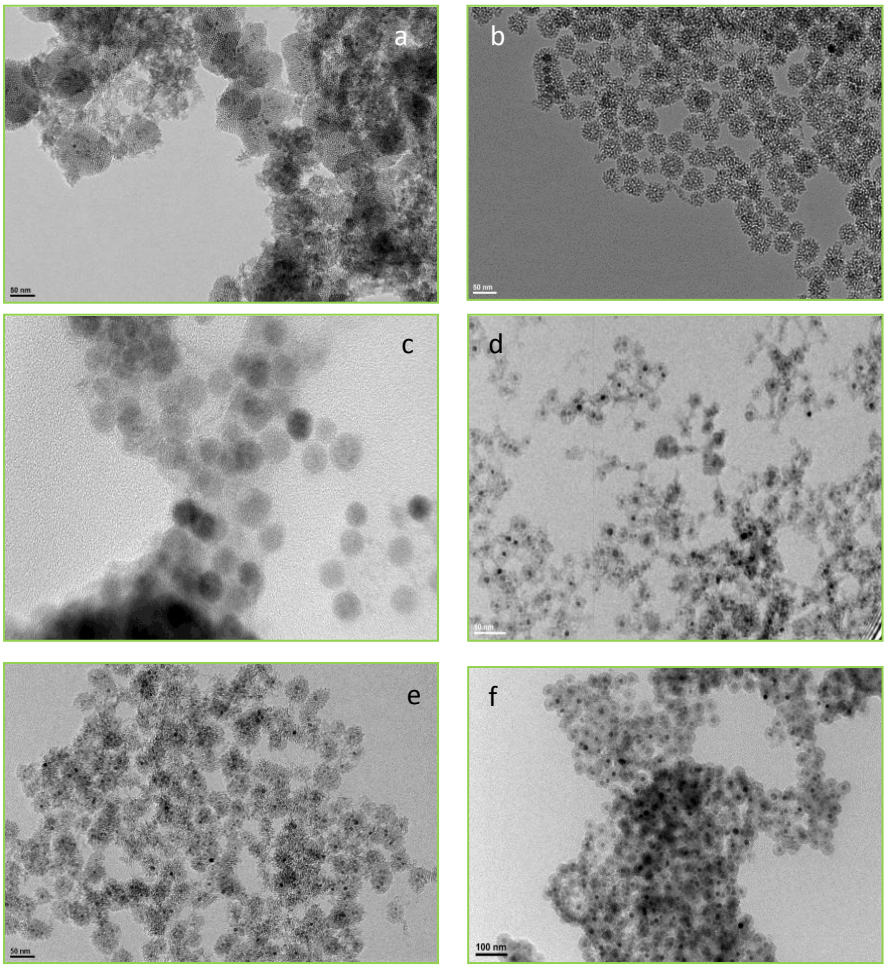

Figure 12. *TEM pictures describe the different results obtained by playing with parameters, before fond a good procedure.*

In *Figure 13* two different samples are shown, one having single core and one multiple core. It was possible obtaine nanoparticles with multiple core that can be interesting for future study. In fact higher amount of magnetite could increase the hyperthermia properties.

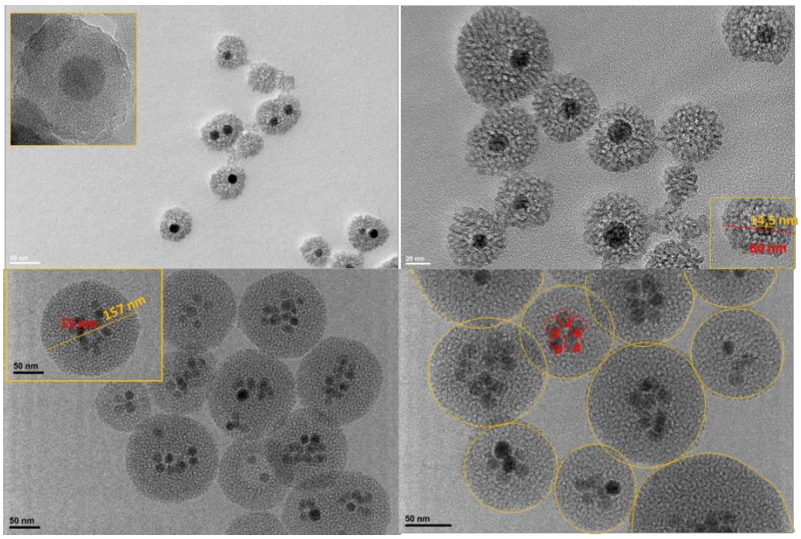

Figure 13. *TEM pictures of core-shell nanoparticles with single core and multiple core.*

Hyperthermia study was performed on nanoparticles with a single core at IMEM -CNR in Parma [Albertini's Group].

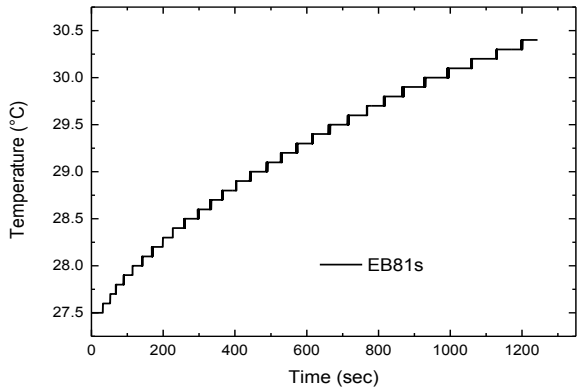

Figure 14: *Temperature vs time it shows the increase of solution temperature (H_2O)of 6 mg/ml core-shell nanoparticles under magnetic stimulation.*

SAR calculation gave the value of 15.98 W/g. Also in this case ICP analysis was required in order to know the weight of magnetic part to have a SAR value normalized.

Z potential analysis was performed, giving a value of -39.96 that evidenced the stability of the nanoparticles and a negative charge on their surface.

To explore the possible application of these nanoparticles in drug delivery, I studied have the possibility to incapsulate a drug inside the pores and deliver it.

STUDY ON DRUG ADSORBTION/DESORBTION

To explore the ability of the nanoparticles with a mesoprous shell to incapsulate and then to release a drug, such as a chemiotherapic, I choose to use Indomethacin[5] as model compound. Indeed, in the literature this molecule is often employed for absorption in mesopores.

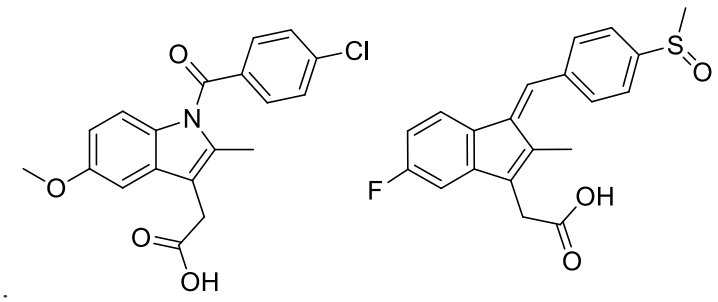

Figure 15. *Structure of Indometachin (antibacterial)(left) and of Sulindoc (anticancer)(right)*

Indometachin (Fig. 8, left) is known to have antibacterial effects, and it is often used as model molecule. I choose this compound because its structure presents some analogy (dimensions and skeleton) with the structure of Sulindoc, an anticancer drug. Sulindoc was known for antibacterial properties and during the last years became famous for anticancer properties because this drug is absorbed from the cells and it can create an interaction with DNA (DNA denaturation). I studied the absorption of Indometachin by nanoparticles described above. To

facilitate the absorption, I decided to operate in EtOH solution due to high drug solubility.

As regards the delivery, I studied the release in PBS solution (commercial one), employing the dialysis tubes in a large volume of PBS solution. The study was accomplished using UV-Vis Spectroscopy.

Indomethacin absorption was obtained suspending the nanoparticles in a highly concentrated Indometachin solution in ethanol. Then, the nanoparticles were centrifuged and washed several times with EtOH and water, in order to remove the Indometachin residue on the surface, and dried.

To examine the Indomethacin release, nanoparticles suspension were dispersed in small amount of PBS solution and transferred into a dialysis tube. The tube was put inside a large amount of PBS and heat at 37 °C. The release was followed by UV-Vis Spectroscopy.

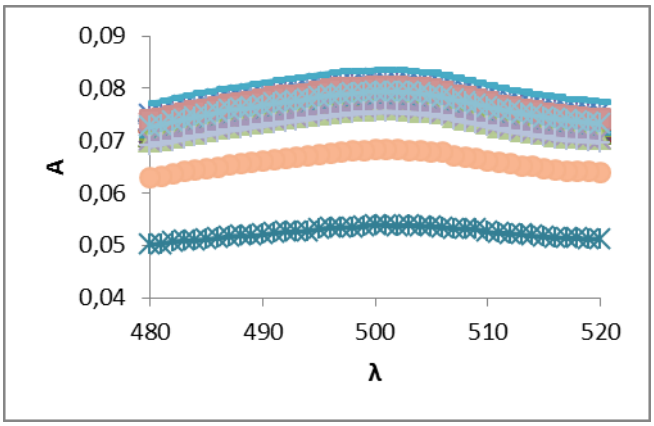

Figure 16. *UV-Vis analysis*

In the previous picture the UV-Vis spectra at different time is reported. The release started quickly and after one hour the delivery became slow and gradual, until the achievement of a plateau, it is a preliminary result (*Figure 17*). This analysis will repeat.

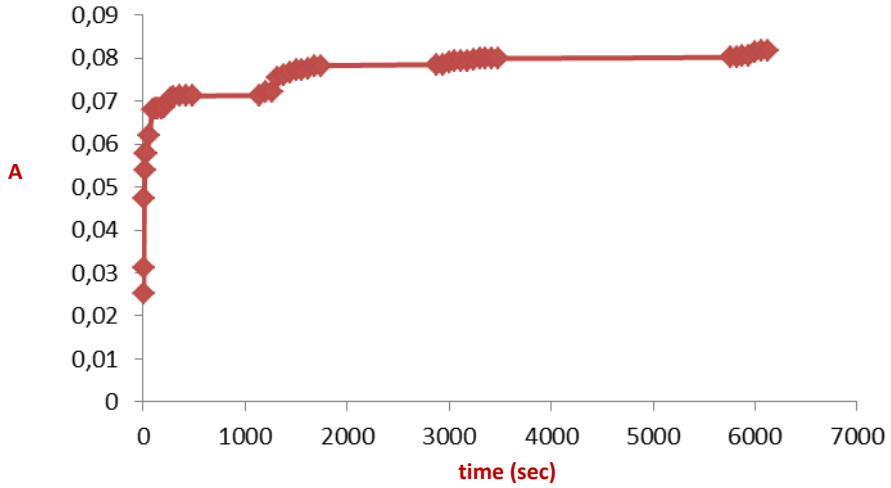

Figure 17. *Absorbance vs time (drug delivery)*

After 3 days the total release is 97% of total amount that was adsorbed (nmol/mg).

Considering the ability shown by the Fe_3O_4/m-SiO_2 nanoparticles to adsorb and release the Indomethacin, in the future the release of a specific drug will be studied for anti-cancer therapy.

Fe_3O_4 –mSiO_2 Conjugation with TCPP:

Starting from the interest to study the effect of these larger nanoparticles in biological systems, as previously performed by the KTH group using smaller NPs[6], I decided to bind a porphyrin to the silica shell of the nanoparticles as fluorescent and photosensitizer agent for *in vitro* study.On the basis of the experience acquired in nanowire functionalization, I planned to join the two components of the hybrid system by amide bond. Therefore it was necessary the functionalization of the nanoparticles surface with amino groups by APTES.

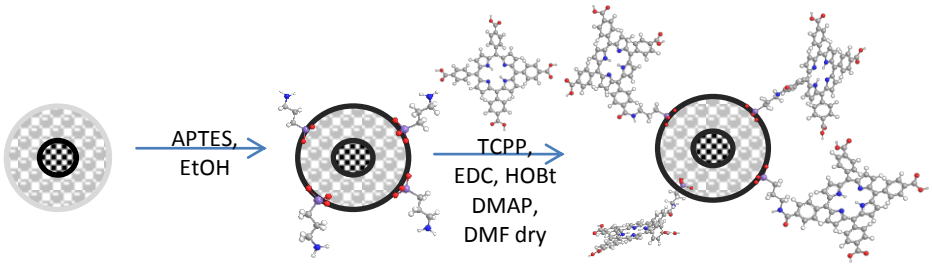

Scheme 5. *Synthetic Scheme for coating nanoparticles with H2TCPP*

APTES was slowly added under magnetic stirring to nanoparticles in ethanol. After the washing step (in order to remove the unreacted APTES), TCPP was pre-activated by using coupling reagents, then added to a nanoparticles suspension in dry solvent.
After thorough washing, the change of color evidenced that nanoparticles were decorated with porphyrin.

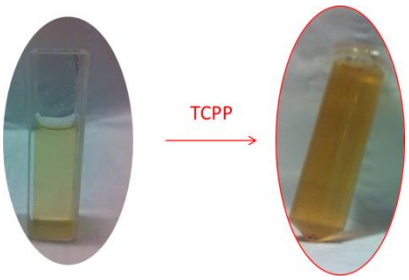

Figure 18.

UV-Vis spectra confirmed our prognostic, showing the presence of B Band and the four Q Bands typical for porphyrin (as described in Porphyrin Chapter).

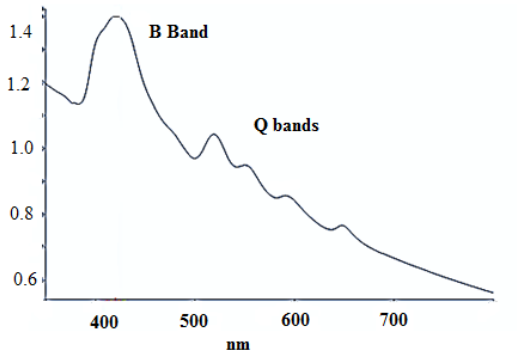

Figure 19. *Uv Vis Spectra of nanoparticles coated with H2TCPP, it is easy to see diagnostic bands for porphyrins (Q Bands and B Band)*

Nanoparticles were coated also with VivoTag® following a protocol reported on web for this molecule[7], in order to obtain nanoparticles to be used for in Vivo analysis (e.g. to study where they will be accumulate).
Nanoparticles previously functionalized with APTES were suspended in a solvent and stirred at room temperature in a solution of VivoTag®, in a flask covered from light. The study of these nanoparticles by UV-Vis Spectroscopy is in progress. After the functionalization the nanoparticles showed a blue color, the same of the free drug.
Study *in vitro* and *in vivo* are in progress at Karoliska Institute in Stockholm (Sweden).

Experimental Section

Synthesis of Fe_3O_4 NPs (d=15 nm)[8]

Synthesis of metal-oleate complex: the metal-oleate complex was prepared by reaction of $FeCl_3 \cdot 6H_2O$ (2 mmol) and 2024 mg of sodium oleate (6.6 mmol), was dissolved in a mixture of solvent composed by 3 ml di H_2O, 4 ml of EtOH and 7 ml Hexane. The resulting solution was heated to 70 °C and kept at this temperature for eight hours. When the reaction was completed, the upper organic layer containing the iron-oleate complex was washed three times with 30 ml distilled water in a separatory funnel. After washing, hexane was evaporated by rotating evaporator and then dry overnight under high vacuum.

36 g (40 mmol) of the iron-oleate complex synthesized as described above and 5.7 g of oleic acid (20 mmol) were dissolved in 200 g of 1-octadecene at room temperature. The reaction mixture was heated to 320 °C with a constant heating rate of 3.3 °C min–1, and then kept at that temperature for 30 min. When the reaction temperature reached 320 °C, a severe reaction occurred and the initial transparent solution became turbid and brownish black. The resulting solution containing the nanocrystals was then cooled to room temperature, and 500 ml of ethanol was added to the solution to precipitate the nanocrystals. The nanocrystals were separated by centrifugation with EtOH and dissolved in $CHCl_3$.

Synthesis of mesoporous shell of SiO_2 on Fe_3O_4 NPs

Oleic acid-capped Fe_3O_4 NPs in $CHCl_3$ (13 mg/ml) were transferred to water by mixing the particles with 10 ml of cetyltrimethyl ammonium bromide solution (0.0345 M), and heated at 65°C for 30’ and then chloroform was evaporated. The solution was left overnight for precipitate the nanoparticles that are not soluble anymore (decantation process).

To create an m-SiO_2 coating layer on Fe_3O_4-CTAB NPS, the water solution (3.3 ml) was diluted with water (7.7 ml) and the pH was adjusted to pH 12 by the addition of NaOH (50 µl of a solution 2 M). After the temperature of the reaction solution had reached 72 °C and tetraethyl orthosilicate (TEOS, 200 µl) and ethyl acetate (EtOAc, 1 ml) were slowly added in sequence. The reaction was left stirred for 2 hours, after that the core shell nanoparticles were collected by centrifugation and washed with EtOH twice.

To transform the SiO_2 in m-SiO_2 was necessary extract CTAB from mesopore channel by washing with a solution (10 mg/ml) of NH_4NO_3 twice at 60 °C for 30'.[9]

Indomethacin absorption:

4.5 mg of nanoparticles were stirred in a 10 ml flask overnight with a high concentration solution of Indometachin in ethanol. Nanoparticles were centrifuged and washed several times in pure EtOH and water and dry.

Indomethacin release:

4.5 mg of core-shell nanoparticles were dissolved in 10 ml of standard PBS solution, and transferred inside a dialysis tube. The amount of PBS solution for release is 2 l, the system was magnetically stirred at 37°C, and the analysis was done using a small amount (2 ml) of solutions that I take

Synthesis of core-shell nanoparticles conjugated with porphyrin

To an ethanol suspension of core-shell nanoparticles (4 mg), magnetically stirred, was added 2.5µl of APTES and left overnight at room temperature under magnetic stirrer. The nanoparticles were separated from non-reactive reagent by centrifugation and wash twice with EtOH. A solution of TCPP (2 mg, 2.5 µmol), EDC (2.4 mg, 15 µmol), HOBt (2.3 mg, 15 µmol) and DMF (2ml) was magnetically stirred for 30', and then a solution of nanoparticles (~3.8 mg) in DMF

(1 ml) with DMAP (1.9 mg, 15 µl) was added drop by drop and vigorously stirred overnight at room temperature. The nanoparticles were precipitated by centrifugation and then washed several times with DMF, water, acetone.

Synthesis of core-shell nanoparticles conjugated with VivoTag®

To an ethanol suspension of core-shell nanoparticles (4 mg), magnetically stirred, was added 2.5µl of APTES and left overnight at room temperature under magnetic stirrer. The nanoparticles were separated from non-reactive reagent by centrifugation and wash twice with EtOH.

3.8 mg of nanoparticles were suspended in DMSO and a solution of VivoTag® was added. The flask was totally covered from light and the nanoparticles were left stirrer overnight at room temperature. The suspension was centrifuged and nanoparticles were washed several times.

References

[1] K. Chatterjee, S. Sarkar, K. J. Rao, S. Paria *Advances in Colloid and Interface Science* 209, 8–39 (**2014**).

[2] A. H. Latham, M. E. Williams, *Account of Chemical research* 41, 3, 411 (**2008**).

[3] N. Wu, L. Fu, M. Asam, K. C. Wong, V. P. Dravid, *Nano Letters 4,2, 383* (**2004**).

[4] L. M. Bronstein, X. Huang, J. Retrum, A. Schmucker, M. Pink, B. D. stein, B. Dragnea, *Chem*. *Mater*., 19, 3624 (**2007**)**.**

[5] Piaoping Yang, Shili Gai, Jun Lin, *Chem*. *Soc*. *Rev*., 41, 3674-3698 (**2012**).

[6] C. M. Vogt, M. Toprak, J. Shi, N. F. Torres, B. Fadeel, S. Laurent, J.L. Bridot, R. N. Müller, M. Muhammed (Mater. Res. Soc. Symp. Proc. Volume 1140, Warrendale, PA, **2009**), DOI: 10.1557/PROC-1140- HH01-04; C.Vogt, M. S. Toprak, S. Laurent, J.-L. Bridot, R.t N. Müller, M. Muhammed, Journal of Nanoparticle Research, DOI: 10.1007/s11051-009- 9661-7.

[7] http://webcache.googleusercontent.com/search?q=cache:2j5OwtZY8IwJ:www.perkinelmer.com/CMSResources/Images/44-47856APP_010811_01_ABR_VivoTag-S.pdf+&cd=1&hl=it&ct=clnk&gl=it.

[8] J. Park, K. An, Y. Hwang, J.Park, H.J Noh, J.Y. Kim, J.H. Park, N.M. Hwang, T. Hyeon; *Nat Mater*. 12:891-5.(**2004**).

[9] F. Ye, S. Laurent, A. Fornara, L. Astolfi, J. Qin, A. Roch, A. Martini, M. S. Toprak, R. N. Muller and M. Muhammed, *Contrast Media Mol*. *Imaging*, **7** 460-468, (**2012**).

Conclusions

During my PhD thesis I successfully prepared novel hybrid nanosystems for possible application in nanomedicine, with particular emphasis on cancer treatments by hyperthermia induced by radiofrequency magnetic fields and photodynamic therapy induced by highly energetic X-rays.

The results study can be summarized in three topics.

1) *Synthesis of nanosystem composed by nanowires decorated with SPIONs (superparamagnetic iron oxide nanoparticles) for hyperthermia properties*.
First, I synthesized superparamagnetic nanoparticles with different size, shape and properties. In all the cases the Fe_3O_4 nanoparticles were in highly crystalline and pure form, with sharp size distribution.
The nanoparticles were completely characterized (TEM, DLS, FT-IR, TGA, magnetic characterization), and their biocompatibility was assessed, thanks to the collaboration with other groups.

I developed a synthetic strategy to join the nanoparticles with core-shell SiC/SiO_x nanowires by covalent bond.
The biocompatibility of the SiC/SiO_2 was also assessed and the results have been recently published (*Nano Lett*., **2014**, 14 (8), 4368–4375).
The magnetite NPs were functionalized introducing carbon-carbon triple bond functional groups in the stabilizing shell and then were bound to the SiC/SiO_x nanowires, previously functionalized with (3-azidopropyl)trialkoxysilane to introduce the complementary reactive group. Using the Cu-catalyzed 1,3-dipolar cycloaddition (click-reaction). I obtained the nanowires decorated with the nanoparticles, with uniform coverage as evidenced by TEM spectroscopy.

2) *Synthesis of hybrid nanosystem composed by nanowires conjugated with porphyrins for PDT*.
I synthesized and characterized four different types of porphyrins for possible application in PDT (photodynamic therapy), widely used approach for the treatment of superficial tumors.

Also in this case, I developed a strategy to anchor the porphyrin on the core-shell SiC/SiO_x nanowires. The aim was to have energy transfer from the nanowires to the photosensitizer under X-ray irradiation, and thus the production of singlet oxygen, toxic for cells. Porphyrin derivatives bearing terminal carbon-carbon triple bond were synthetized. In particular, the derivative of H_2TCPP (tetra-4-carboxyphenylporphyrin) was reacted with the SiC/SiO_x nanowires, previously functionalized with alkylazide groups by thermal azide-alkyne 1,3-dipolar cycloaddition. The hybrid nanosystem (nanowires + porphyrin) was characterized and its activity was studied, in collaboration with other groups. It was first evidenced the ability to produce singlet oxygen, cytotoxic to the cells, in response to irradiation with energetic X-rays and then in vitro experiments in cancer cell lines were performed, demonstrating that our approach is very efficient to enhance radiation therapy effects for cancer treatments. Important advantages are the reduction of dose and time of irradiation, also the possibility to do the treatmet just only one time, with the consequent reduction of collateral effect from both a physical point of view that psychological.
Thus, the potential use of this new nanosystem in Photodynamic Therapy was highlighted. The results have just been published in *Scientific Reports* (Nature Magazine Group) (published on 05 Jan 2015, doi:10.1038/srep07606).

3) Synthesis of Fe_3O_4-mSiO_2 core shell nanoparticles for drug release and imaging.

During my visiting period in Stockholm (April- August 2014) at the Functional NanoMaterial (FNM) Group of KTH, Royal Institute of Technology I synthesized larger nanoparticles of magnetite (abt.15 nm), and found a good method to coated them with a mesoporous shell of silica oxide. I fully characterized the nanoparticles before and after the silica coating using, but the magnetic characterization was performed in collaboration with IMEM. I studied the absorption and delivery of a model drug. Moreover, I functionalized the nanoparticles with porphyrin and VivoTag® for possible imaging studies in vitro.

The results obtained during my PhD work produced two published papers and two manuscripts are in preparation.

Future works

These results presented in my PhD thesis confirm the $^1O_2$ production by the conjugated NW-porphyrin system, occuring through the self-lighted photodynamic process, and demonstrated that our approach is very efficient to enhance radiation therapy effects for cancer treatments.
To increase the cellular uptake of the nonsystem, we have designed to functionalize the porphyrin with hydrophilic chains, such as polyethylene glycol type, and studies are in progress.
On the basis the experience acquired, the preparation of a three-component nanosystems will be performed.
The coupling of porphyrinated NWs with superparamagnetic nanoparticles will combine the SLPDT property with hyperthermia effect induced by radiofrequency magnetic fields.
The resulting triple system could rapresent a new generation of nanomaterials for treatments of the tumors.
Last, but not least, we have planned to study the nanosystem internalization by *in vitro* and *in vivo* experiments, in collaboration with Karolinka Hospital.

The second project that I have started to study, in collaboration with Parmas's Hospital, is the formation of **smart system**, able to deliver an anticancer drug under magnetic stimulation. The release of a drug included in the pores of the F_3O_4-mSiO_2 nanoparticles could be favored under a magnetic field. My idea is that under magnetic radio frequency field (hyperthermia effect) there will be an extra effect in releasing process. This field can change the temperature of nanoparticles and transfer the energy from the loop to nanoparticles. In that case, the particles have enough energy to break the interaction between nanoparticle and drug, and increasing the release of the drug. The increase of temperature increase the Brownian movements so the drugs should be free to move and free to be release.

Acknowledgements

First of all I would like thank my supervisor, Prof. Franca Bigi to give me the opportunity to learn all of this notions in this years of my PhD, to teach me too much and to help me many-many times. For me these years were an amazing experience. Thanks to her and to this project I formed my character and have gained a lot in chemically point of view and in character. I have to thanks to much Antoine that teach me a lot during the first year and help me in lab and also he is a very good colleague; Veronica that shows me a real friendship in and outside the lab. Thanks also to Ray for the support during this three years, and for all the satirical writings that you put on my hood. Thanks to Prof. Sartori for jokes and also always stimulate me to do better. Thanks to students in lab starting from my favourite Tiziana, the best student ever, Andre, Federico, Giammi, Luca and again Francesco, Matteo, Nicolò, Mizar, Giovanni and all the other that spent time with us. Thanks to Emanuele that very patiently had to endure in recent months. Thanks to Francesco that spent with us some months and bring with him to much happiness, we learned to much from you. Thanks to employees in chemistry department (Miki, Paola, Dona, Andrea, Marco D., Marco G., Beppe, Sara, Luca and so on), thanks because whenever I needed helps you always left everything to help me (la vostra dottoranda preferita).
Thanks to the people that spent time with me in Chemistry department (for lunch: always with smile or for my amazing porta-party), I can't forget.

I would like to thanks Dott. Giancarlo Salviati for BioNiMed Project, Dott. Francesca Rossi in particular for help me several time and for the estimation that you always show me. Thanks to Dott. Valentina Chiesi and Dott. Roberta Ciprian for magnetic analysis. Thanks to Dott. Marco Campanini, for TEM analysis and for the support that you showed in this project. Thanks to Dott. Attolini, Dott. Marco Negri e Dott. Paola Lagonegro for a fruitfull collaboration. Thanks to Dott. Tiziano Rimoldi and Prof. Cristofolini, Physics Department, for fluorescence analysis. Thanks to Professor Mutti and his group: Prof. Matteo Goldoni, Dott. Silvana Pinelli, Dott. Rossella Alinovi; a real

and special thanks for teach me a lot of thinks in biomedical field but in particular in live and research, but also for the incredible estimate that you have always shown me. Thanks to Professor Petronini and Dott. Marikla Galetti (Pharmaceutic Department), Dott. Cacchioli e Dott. Ravanetti for profit collaboration.

I would like to thanks Professor Toprak and Professor Muhammed for give me the opportunity to work in your laboratory, and also for give me the chance to learn as much I can. Thanks to the people that work in FNM group, in particular to Dott. Wubeshet Sahle for teach me TEM, and Dott. Ye and Dott. Vogt for help me in chemistry lab. Thanks to all the group for making me feel at home.

Bedogni Elena

08/12/1987	Born Reggio Emilia (Italy)
06/2006	I.T.A.S Zanelli High School, Reggio Emilia, Italy 100/100
25/09/2009	Bachelor Degree in Industrilal Chemistry , University of Parma, Parma, Italy 107/110
28/10/2011	Master in Industrial Chemistry University of Parma, Parma, Italy 110/110
03/2014-09/2014	Visiting Student at KTH, Royal Institute of Technology (FNM group; Prof. M.S. Toprak and Prof. M. Mohammed), Stockholm (Sweden)
01/2012-12/2014	PhD Student with Prof. F. Bigi, University of Parma (Italy)